

Spatiotemporal Analyses of Groundwater and Shoreline Cr(VI) Concentrations in the 100 Areas at Hanford

September 2020

ML Rockhold
X Song
ZF Zhang
NP Qafoku
MA Jensen
JL Downs
JD Tagestad
RD Mackley

DISCLAIMER

This report was prepared as an account of work sponsored by an agency of the United States Government. Neither the United States Government nor any agency thereof, nor Battelle Memorial Institute, nor any of their employees, makes **any warranty, express or implied, or assumes any legal liability or responsibility for the accuracy, completeness, or usefulness of any information, apparatus, product, or process disclosed, or represents that its use would not infringe privately owned rights.** Reference herein to any specific commercial product, process, or service by trade name, trademark, manufacturer, or otherwise does not necessarily constitute or imply its endorsement, recommendation, or favoring by the United States Government or any agency thereof, or Battelle Memorial Institute. The views and opinions of authors expressed herein do not necessarily state or reflect those of the United States Government or any agency thereof.

PACIFIC NORTHWEST NATIONAL LABORATORY
operated by
BATTELLE
for the
UNITED STATES DEPARTMENT OF ENERGY
under Contract DE-AC05-76RL01830

Printed in the United States of America

Available to DOE and DOE contractors from the
Office of Scientific and Technical Information,
P.O. Box 62, Oak Ridge, TN 37831-0062;
ph: (865) 576-8401
fax: (865) 576-5728
email: reports@adonis.osti.gov

Available to the public from the National Technical Information Service
5301 Shawnee Rd., Alexandria, VA 22312
ph: (800) 553-NTIS (6847)
email: orders@ntis.gov <<https://www.ntis.gov/about>>
Online ordering: <http://www.ntis.gov>

Spatiotemporal Analyses of Groundwater and Shoreline Cr(VI) Concentrations in the 100 Areas at Hanford

September 2020

ML Rockhold
X Song
ZF Zhang
NP Qafoku
MA Jensen
JL Downs
JD Tagestad
RD Mackley

Prepared for
the US Department of Energy
under Contract DE-AC05-76RL01830

Pacific Northwest National Laboratory
Richland, Washington 99354

Summary

Cleanup efforts have been ongoing since the late 1990s to remediate contaminated waste sites and groundwater in the 100 Areas at the U.S. Department of Energy (DOE) Hanford Site. One of the primary contaminants of concern is hexavalent chromium (Cr(VI)), which was used as a corrosion inhibitor in cooling water for nuclear reactors that formerly operated along the shoreline of the Columbia River. Cleanup efforts have included 1) removal, treatment (as needed), and disposal of contaminated sediments; 2) in situ redox manipulation as a permeable reactive barrier; 3) pump-and-treat; 4) soil flushing; and 5) monitored natural attenuation. DOE's annual groundwater monitoring reports document the significant reductions in Cr(VI) plume areas that have occurred over the past 10 years or more as a result of these cleanup efforts. The Record of Decision for the 100-HR-3 operable unit specified a cleanup level (CUL) for Cr(VI) in groundwater of 48 µg/L to protect human receptors, and a surface water CUL of 10 µg/L to protect aquatic organisms in the Columbia River. The Record of Decision did not specify point-of-compliance locations for the surface water CUL.

Data for 2019 from the six groundwater operable units (OUs) in the 100 Areas indicate that the 48 µg/L groundwater CUL has been achieved in 100% of the wells in the 100-BC and 100-NR OUs, and in 89-97% of the wells in the other OUs (100-KR, 100-HR-D, 100-HR-H, 100-FR). Data for 2019 indicate that 100% of the aquifer tubes monitored for Cr(VI) in the 100 Areas have concentrations below the 48 µg/L groundwater CUL. However, the 10 µg/L standard has not yet been consistently achieved for both inland groundwater monitoring wells and shoreline aquifer tubes.

This report describes a series of data analyses performed to identify consistent relationships, if any, between inland well and shoreline Cr(VI) concentrations within the 100 Areas. To this end, select monitoring data for Cr(VI) measured in groundwater and aquifer tubes at the 100 Areas were analyzed for a 10-year period—2010 to 2019. Relationships between inland groundwater plumes and surface-water points of discharge in and along the Columbia River were examined through several analyses that included inland well and aquifer tube concentrations as a function of distance from the shoreline, evaluation of cumulative probability plots, trend analysis, correlation analysis, cluster analysis, and identification of plume trajectories for each of the 100 Areas.

The analyses did not identify consistent relationships between inland groundwater Cr(VI) concentrations and shoreline concentrations within the 100 Areas due to several confounding factors influencing groundwater flow directions and Cr(VI) concentrations. The proximity of groundwater Cr(VI) plumes to the river, and the highly dynamic nature of the river, influence the transport behavior of the plumes and create challenges for quantifying attenuation of Cr(VI) between the inland monitoring wells and shoreline concentrations. Other factors contributing to temporal and spatial Cr(VI) concentrations, as supported by some of the data analyses, include the presence of vadose zone sources, variable sorption behavior, and complexities associated with Cr(VI) mass transfer between the upper and lower aquifers and their interactions with the river. Hence, monitoring to assess compliance with target CULs will need to be determined for each area individually since several factors influence Cr(VI) concentrations in the 100 Areas.

Acknowledgments

This document was prepared by the Deep Vadose Zone – Applied Field Research Initiative at Pacific Northwest National Laboratory. Funding for this work was provided by the US Department of Energy (DOE) Richland Operations Office. We thank Mary Hartman and Margo Aye of CH2M Hill Plateau Remediation Company (CHPRC) for their assistance in providing the most current information regarding chromium groundwater plumes and water table elevations. We thank Vicky Freedman and Mike Truex for project management and independent technical reviews, and Matt Wilburn for editorial assistance.

Acronyms and Abbreviations

AWLN	automated water-level network
CERCLA	Comprehensive Environmental Response, Compensation, and Liability Act
COC	contaminant of concern
CUL	cleanup level
DOE	U.S. Department of Energy
DTW	dynamic time warping
EPA	U.S. Environmental Protection Agency
EU	Euclidean distance
GW	groundwater
HEIS	Hanford Environmental Information System
HRS	high river stage
ISRM	in situ redox manipulation
K_d	distribution coefficient
KW	K West
LRS	low river stage
MAE	mean absolute error
M-K	Mann-Kendall
MNA	monitored natural attenuation
NQAP	Nuclear Quality Assurance Program
OU	operable unit
P&T	pump-and treat
PRB	permeable reactive barrier
PRZ	periodically rewetted zone
RMSE	root mean squared error
ROD	Record of Decision
RTD	removal, treatment, and disposal
RUM	Ringold Upper Mud
SW	surface water
TPH-D	total petroleum hydrocarbons-diesel range
USGS	U.S. Geological Survey

Contents

Summary	ii
Acknowledgments.....	iii
Acronyms and Abbreviations	iv
Contents	v
1.0 Introduction.....	1.1
2.0 Background.....	2.1
2.1 History of Site Operations	2.1
2.2 Basis for 10 µg/L Cr(VI) Aquatic Water Quality Standard.....	2.1
2.3 Factors Affecting Cr(VI) Plume Attenuation	2.2
2.3.1 Dam Operations.....	2.3
2.3.2 Hydrogeology	2.7
2.3.3 Geochemistry.....	2.12
2.4 Site Remediation Activities	2.14
2.4.1 GW P&T.....	2.14
2.4.2 ISRM – Permeable Reactive Barrier	2.17
2.4.3 Removal, Treatment, and Disposal.....	2.17
2.4.4 Soil Flushing.....	2.18
2.4.5 Natural Attenuation	2.19
2.5 Monitoring	2.19
2.5.1 Aqueous Chemistry	2.24
2.5.2 GW Levels.....	2.25
2.6 Modeling.....	2.25
3.0 Analysis of GW Monitoring Data.....	3.1
3.1 Correlations.....	3.2
3.2 Concentrations Versus Distance to Shoreline.....	3.7
3.2.1 HEIS Data.....	3.7
3.2.2 Data from Interpreted Plume Maps	3.16
3.3 Plume Trajectories	3.22
3.4 Cluster Analysis.....	3.26
3.5 Trends	3.49
3.6 Cumulative Probabilities.....	3.53
4.0 Summary and Recommendations	4.1
5.0 Quality Assurance.....	5.1
6.0 References.....	6.1
Appendix A.....	A.1

Figures

Figure 1.1.	2018 GW Contaminant Plumes in the River Corridor at the 100 Area	1.1
Figure 1.2.	Temporal Variations in Plume Areas for Contaminants of Concern in the Hanford River Corridor	1.3
Figure 1.3.	GW Cr(VI) Plumes at LRS and HRS for 2010 (upper panels) and 2018 (lower panels).....	1.4
Figure 2.1.	Conceptual Model of 100 Area Waste Sites Showing Relative Locations of GW Monitoring Wells and Aquifer Sampling tubes, and the Zones Influenced by River Stage Fluctuations	2.3
Figure 2.2.	USGS River Gauging Station 12472800 is Located at Latitude 46°37'44" and Longitude 119°51'49," Downstream of the Priest Rapids Dam.....	2.4
Figure 2.3.	Daily Average River Stage at the 100-D Area in 2018.....	2.5
Figure 2.4.	Monthly Average River stage at the Station 12472800 (shown in Figure 2.2), Downstream of the Priest Rapids Dam, (a) from 2000 to 2019 and (b) Average over 10 Years with One Standard Deviation	2.6
Figure 2.5.	Annual Average River Stage at the Station 12472800 (shown in Figure 2.2), Downstream of the Priest Rapids Dam	2.7
Figure 2.6.	r(VI) and Water Levels in Wells 199-B3-47 and 199-B4-14 in 100-BC Area.....	2.8
Figure 2.7.	Generalized Representation of the Hydrogeologic Units in the 100 Areas	2.9
Figure 2.8.	Hydraulic Conductivity Distribution for Layer 1 of the Calibrated 100 Area GW Flow and Transport Model	2.11
Figure 2.9.	Hydraulic Conductivity Distribution for Layer 2 of the Calibrated 100 Area GW Flow and Transport Model	2.11
Figure 2.10.	Important Chromium Species and Biogeochemical Reactions.....	2.13
Figure 2.11.	Map Showing P&T Wells in the 100 Areas that Operated Between Jan. 2014 and Feb. 2020	2.14
Figure 2.12.	Layout of 100-HR-3 OU P&T System	2.15
Figure 2.13.	100-HR-3 P&T Cr(VI) Annual Mass Removal	2.16
Figure 2.14.	Tier III Excavation at 100-D-104 Looking West.....	2.18
Figure 2.15.	Map Showing Locations of GW Monitoring Wells (829) and Aquifer Tubes (365) in the Hanford 100 Areas from Which Cr(VI) Concentration Data were Collected Between Jan. 2010 and Feb. 2020	2.20
Figure 2.16.	Types and Numbers of Samples for Aquifer Tubes and Wells in 100-BC OU	2.21
Figure 2.17.	Types and Numbers of Samples for Aquifer Tubes and Wells in 100-KR OU	2.22
Figure 2.18.	Types and Numbers of Samples for Aquifer Tubes and Wells in 100-NR OU	2.22
Figure 2.19.	Types and Numbers of Samples for Aquifer Tubes and Wells in 100-HR-D OU.....	2.23
Figure 2.20.	Types and Numbers of Samples for Aquifer Tubes and Wells in 100-HR-H OU.....	2.23
Figure 2.21.	Types and Numbers of Samples for Aquifer Tubes and Wells in 100-FR OU.....	2.24
Figure 2.22.	Hanford Site Water Table (blue lines) and Directions (orange arrowed lines) of GW Flow in 2018	2.25

Figure 2.23.	Assessment of the Length of Shoreline Protected from Further Discharges of Chromium along the 100-H Area, together with Mapped Extent of Chromium Contamination above 10 µg/L	2.28
Figure 2.24.	Simulated (Left) and Mapped (Right) Fall 2012 Cr(VI) Top of Unconfined Aquifer Plume for 100-B/C	29
Figure 2.25.	Maximum Simulated Cr(VI) Concentration for No Further Action Case by Model Layer over 125 Years for 100-B./C	30
Figure 3.1.	Time Series Data for Hexavalent Chromium and Specific Conductance Measured in Aquifer Tubes from the 100-BC OU in 2014-2015	3.4
Figure 3.2.	Coefficient of Variation (Standard Deviation/Mean) of Hexavalent Chromium and Specific Conductance Data from Aquifer Tubes in the 100-BC OU for 2014-2015	3.5
Figure 3.3.	Specific Conductance Data from 100-BC for Years 2010 to 2019.....	3.5
Figure 3.4.	Specific Conductance Data by Day of Year for 100-BC for Years 2010 through 2019	3.6
Figure 3.5.	Variations in Specific Conductance Measurements with Distance from Shoreline in 100-BC.....	3.7
Figure 3.6.	Cr(VI) Concentration Data from 2010 (top) and 2019 (bottom) Versus Distance from the Columbia River Shoreline for the 100-BC OU	3.8
Figure 3.7.	Cr(VI) Concentration Data from 2010 (top) and 2019 (bottom) Versus Distance from the Columbia River Shoreline for the 100-KR OU.....	3.10
Figure 3.8.	Cr(VI) Concentration Data from 2010 (top) and 2019 (bottom) Versus Distance from the Columbia River Shoreline for the 100-NR OU.....	3.11
Figure 3.9.	Cr(VI) Concentration Data from 2010 (top) and 2019 (bottom) Versus Distance from the Columbia River Shoreline for the 100-NR OU.....	3.12
Figure 3.10.	Cr(VI) Concentration Data from 2010 (top) and 2019 (bottom) Versus Distance from the Columbia River Shoreline for the 100-HR-H OU.....	3.14
Figure 3.11.	Cr(VI) Concentration Data from 2010 (top) and 2019 (bottom) Versus Distance from the Columbia River Shoreline for the 100-FR OU	3.15
Figure 3.12.	Maximum Spatial Extent of Distinct Large Cr(VI) Plumes in the 100 Areas	3.17
Figure 3.13.	Concentration Versus Distance to Shoreline Computed from GW Cr(VI) Plume Maps Associated with the 100-B/C Area.....	3.18
Figure 3.14.	Concentration Versus Distance to Shoreline Computed from GW Cr(VI) Plume Maps for the Southwestern Plume Associated with the 100-K Area.....	3.18
Figure 3.15.	Concentration Versus Distance to Shoreline Computed from GW Cr(VI) Plume Maps for the Northeastern Plume Associated with the 100-K Area.....	3.19
Figure 3.16.	Concentration Versus Distance to Shoreline Computed from GW Cr(VI) Plume Maps for the Southwestern Plume Associated with the 100-N Area.....	3.19
Figure 3.17.	Concentration Versus Distance to Shoreline Computed from GW Cr(VI) Plume Maps for the Northeastern Plume Associated with the 100-N Area.....	3.20
Figure 3.18.	Concentration Versus Distance to Shoreline Computed from GW Cr(VI) Plume Maps Associated with the 100-D Area	3.20
Figure 3.19.	Concentration Versus Distance to Shoreline Computed from GW Cr(VI) Plume Maps Associated with the 100-H Area	3.21

Figure 3.20.	Concentration Versus Distance to Shoreline Computed from GW Cr(VI) Plume Maps Associated with the 100-F Area.....	3.21
Figure 3.21.	Calculated Trajectory of Plume 1	3.22
Figure 3.22.	Calculated Trajectories of Plumes 2 and 3 Associated with the 100-K Area	3.23
Figure 3.23.	Calculated Trajectories of Plumes 4 and 5 Associated with 100-N Area	3.24
Figure 3.24.	Calculated Trajectories of Plume 6 Associated with 100-D Area	3.24
Figure 3.25.	Calculated Trajectories of Plume 7 Associated with 100-H Area	3.25
Figure 3.26.	Calculated Trajectories of Plume 8 Associated with 100-F Area	3.25
Figure 3.27.	Dendogram of Clustering Results for Cr(VI) Concentration Data from 100-B/C.....	3.27
Figure 3.28.	Map Showing Well and Aquifer Tube Clustering Results for 100-BC with Overlay of 2018 Cr(VI) Plume Map at LRS.....	3.28
Figure 3.29.	Time Series of Cr(VI) Concentration Data from Wells in Cluster 0 for 100-BC	3.29
Figure 3.30.	Time Series of Cr(VI) Concentration Data from Wells and Aquifer Tubes in Cluster 1 for 100-BC.....	3.29
Figure 3.31.	Time Series of Cr(VI) Concentration Data from Wells and Aquifer Tubes in Cluster 2 for 100-B/C	3.30
Figure 3.32.	Time Series of Cr(VI) Concentration Data from Wells and Aquifer Tubes in Cluster 3 for 100-B/C	3.30
Figure 3.33.	Time Series of Cr(VI) Concentration Data from Wells and Aquifer Tubes in Cluster 4 for 100-B/C	3.31
Figure 3.34.	Time Series of Cr(VI) Concentration Data from Wells and Aquifer Tubes in Cluster 5 for 100-B/C	3.31
Figure 3.35.	Time Series of Cr(VI) Concentration Data from Wells and Aquifer Tubes in Cluster 6 for 100-B/C	3.32
Figure 3.36.	Time Series Cr(VI) Concentration Data from Wells and Aquifer Tubes in Clusters 2 and 3 for 100-B/C	3.32
Figure 3.37.	Map Showing Well and Aquifer Tubes Locations for Clusters 2 and 3 in the 100-BC Area with Overlay of 2010 Cr(VI) Plume Map at LRS.....	3.33
Figure 3.38.	Map Showing Well and Aquifer Tubes Locations for Clusters 2 and 3 in the 100-BC Area with Overlay of 2014 Cr(VI) Plume Map at LRS.....	3.34
Figure 3.39.	Map Showing Well and Aquifer Tubes Locations for Clusters 2 and 3 in the 100-BC Area with Overlay of 2018 Cr(VI) Plume Map at LRS.....	3.35
Figure 3.40.	Dendogram of Clustering Results for Cr(VI) Concentration Data from 100-KR.....	3.36
Figure 3.41.	Map Showing Well and Aquifer Tube Clustering Results for 100-KR with Overlay of 2018 Cr(VI) Plume Map at LRS.....	3.36
Figure 3.42.	Time Series of Cr(VI) Concentration Data from Wells in Cluster 0 for 100-KR.....	3.37
Figure 3.43.	Time Series of Cr(VI) Concentration Data from Wells in Cluster 1 for 100-KR.....	3.37
Figure 3.44.	Time Series of Cr(VI) Concentration Data from Wells in Cluster 2 for 100-KR.....	3.38
Figure 3.45.	Time Series of Cr(VI) Concentration Data from Wells in Cluster 3 for 100-KR.....	3.38
Figure 3.46.	Time Series of Cr(VI) Concentration Data from Wells in Cluster 4 for 100-KR.....	3.39
Figure 3.47.	Time Series of Cr(VI) Concentration Data from Wells in Cluster 5 for 100-KR.....	3.39
Figure 3.48.	Time Series of Cr(VI) Concentration Data from Wells in Cluster 6 for 100-KR.....	3.40

Figure 3.49.	Dendrogram of Clustering Results for Cr(VI) Concentration Data from 100-HR-D.....	3.40
Figure 3.50.	Map Showing Well and Aquifer Tube Clustering Results for 100-HR-D with Overlay of 2018 Cr(VI) Plume Map at LRS.....	3.41
Figure 3.51.	Time Series of Cr(VI) Concentration Data from Wells in Cluster 0 for 100-HR-D.....	3.41
Figure 3.52.	Time Series of Cr(VI) Concentration Data from Wells in Cluster 1 for 100-HR-D.....	3.42
Figure 3.53.	Time Series of Cr(VI) Concentration Data from Wells in Cluster 2 for 100-HR-D.....	3.42
Figure 3.54.	Time Series of Cr(VI) Concentration Data from Wells in Cluster 3 for 100-HR-D.....	3.43
Figure 3.55.	Time Series of Cr(VI) Concentration Data from Wells in Cluster 4 for 100-HR-D.....	3.43
Figure 3.56.	Time Series of Cr(VI) Concentration Data from Wells in Cluster 5 for 100-HR-D.....	3.44
Figure 3.57.	Time Series of Cr(VI) Concentration Data from Wells in Cluster 6 for 100-HR-D.....	3.44
Figure 3.58.	Dendrogram of Clustering Results for Cr(VI) Concentration Data from 100-HR-H.....	3.45
Figure 3.59.	Map Showing Well and Aquifer Tube Clustering Results for 100-HR-H with Overlay of 2018 Cr(VI) Plume Map at LRS.....	3.46
Figure 3.60.	Time Series of Cr(VI) Concentration Data from Wells in Cluster 1 for 100-HR-H.....	3.47
Figure 3.61.	Time Series of Cr(VI) Concentration Data from Wells in Cluster 2 for 100-HR-H.....	3.47
Figure 3.62.	Time Series of Cr(VI) Concentration Data from Wells in Cluster 3 for 100-HR-H.....	3.48
Figure 3.63.	Time Series of Cr(VI) Concentration Data from Wells in Cluster 4 for 100-HR-H.....	3.48
Figure 3.64.	Time Series of Cr(VI) Concentration Data from Wells in Cluster 5 for 100-HR-H.....	3.49
Figure 3.65.	Time Series of Cr(VI) Concentration Data from Wells in Cluster 6 for 100-HR-H.....	3.49
Figure 3.66.	Mann-Kendall Trend Analysis Results for Cr(VI) in the 100 Areas at LRS	3.51
Figure 3.67.	Mann-Kendall Trend Analysis Results for Cr(VI) in the 100 Areas at HRS.....	3.52
Figure 3.68.	Cumulative Probability Distributions for Cr(VI) Sample Data from GW Monitoring Wells (a) and Aquifer Tubes (b) in the 100-BC OU.....	3.53
Figure 3.69.	Cumulative Probability Distributions for Cr(VI) Sample Data from GW Monitoring	3.53
Figure 3.70.	Cumulative Probability Distributions of Cr(VI) Sample Data from (a) GW Monitoring Wells and (b) Aquifer Tubes in the 100-NR OU.....	3.54
Figure 3.71.	Cumulative Probability Distributions of Cr(VI) Sample Data from (a) GW Monitoring Wells and (b) Aquifer Tubes in the 100-HR-D OU.....	3.54
Figure 3.72.	Cumulative Probability Distributions of Cr(VI) Sample Data for (a) GW Monitoring Wells and (b) Aquifer Tubes in the 100-HR-H OU.....	3.54
Figure 3.73.	Cumulative Probability Distributions of Cr(VI) Sample Data from (a) GW Monitoring Wells and (b) Aquifer Tubes in the 100-FR OU	3.55

Tables

Table 1.1.	Summary of CERCLA GW Remediation in the 100 Areas.....	1.2
Table 2.1.	Average Hydraulic Conductivity Values for Geologic Units in the 100 Areas	2.10
Table 2.2.	GW Sampling Trips in 2018	2.20
Table 3.1.	Percentage of Monitoring Wells with Cr(VI) Concentrations Below Target CULs in 2010 and 2019.....	3.55
Table 3.2.	Percentage of Aquifer Tubes with Cr(VI) Concentrations Below Target CULs in 2010 and 2019.....	3.55

1.0 Introduction

Significant progress has been made in cleaning up contaminated groundwater (GW) at the Hanford Site (DOE-RL 2019a). According to the *2018 Hanford Groundwater Monitoring Report* (DOE-RL 2019a), about 94% of the waste sites in the river corridor (100 and 300 areas) have been remediated or determined to not require remediation. Remedial action decisions are in progress for the remaining 6% of the waste sites. As shown in Table 1.1, one of the primary contaminants of concern (COCs) in GW is chromate (CrO_4^{2-}) [a.k.a., Cr(VI) or hexavalent chromium] for each of the 100 Area GW operable units (OUs). Remediation of GW Cr(VI) contamination in the 100 Areas is the primary subject of this report.

The spatial extent of the Cr(VI) GW contamination is shown in Figure 1.1, which depicts the GW plumes along the Columbia River corridor where concentrations exceeded target cleanup levels (CULs) for different COCs in 2018. Figure 1.1 shows the decrease in the Cr(VI) aggregate plume area as well as the reductions in aggregate plume areas over time for other GW COCs in the river corridor (DOE-RL 2019a).

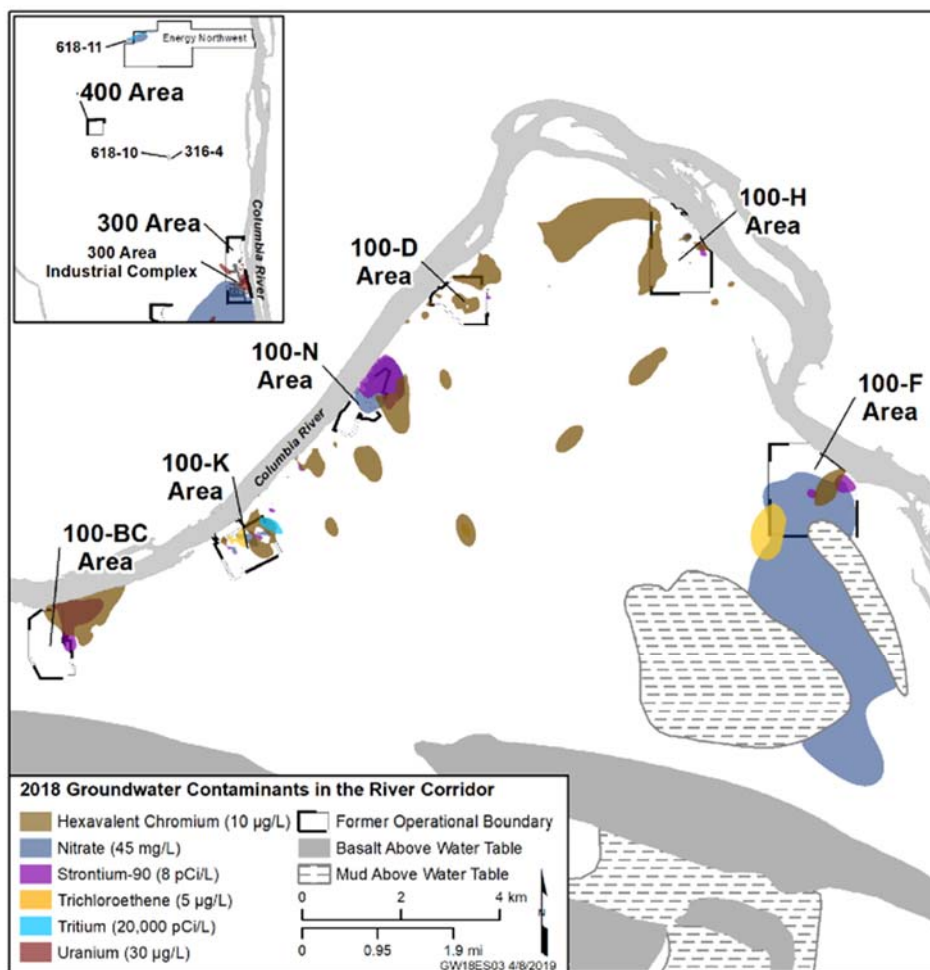


Figure 1.1. 2018 GW Contaminant Plumes in the River Corridor at the 100 Area (after Fig. ES-3 of DOE-RL 2019a)

Table 1.1. Summary of CERCLA GW Remediation in the 100 Areas (after DOE-RL-2019-33, Rev. 0)

GW Operable Unit	CERCLA Decision Status	GW Contaminants of (Potential) Concern ^(a)	Current GW Remediation ^(b)	Mass Removed
100-BC-5	Rev. 0 RI/FS report and proposed plan in 2019	Cr(VI), strontium-90, TCE, tritium	No interim action required; final action pending	Not applicable
100-FR-3	ROD for final action signed in 2014	Cr(VI), nitrate, strontium-90, TCE	Monitored natural attenuation	Not applicable
100-HR-3	ROD for final action signed in 2018	Cr(VI), total chromium, nitrate, strontium-90	Pump-and-treat (P&T) from 1997-2018 and monitored natural attenuation	Cr(VI) 2018: 55.9 kg Total: 2,460 kg
100-KR-4	Interim ROD; Draft B RI and Draft A FS report in progress	Cr(VI), total chromium, carbon-14, nitrate, strontium-90, TCE, tritium	Interim action P&T for Cr(VI) from 1997-2018	Cr(VI) 2018: 35.0 kg Total: 939 kg
100-NR-2	Draft B RI/FS report in progress	Strontium-90, TPH-D, nitrate, Cr(VI), total chromium, tritium	Interim action permeable reactive barrier for strontium-90; removal of TPH-D	Strontium-90: not applicable; TPH-D 2018: 2.05 kg; TPH-D total: 19 kg

(a) Contaminants of concern are listed for OUs with RODs for final action. The primary contaminants of potential concern are listed for the other OUs.

(b) The July 2018 ROD (EPA et al. 2018) selected continued P&T as the remedy for total chromium and Cr(VI); monitored natural attenuation is the selected remedy for nitrate and strontium-90.

CERCLA = Comprehensive Environmental Response, Compensation, and Liability Act of 1980
Cr(VI) = hexavalent chromium
RI/FS = remedial investigation/feasibility study
ROD = Record of Decision
TCE = trichloroethene
TPH-D = total petroleum hydrocarbons-diesel range

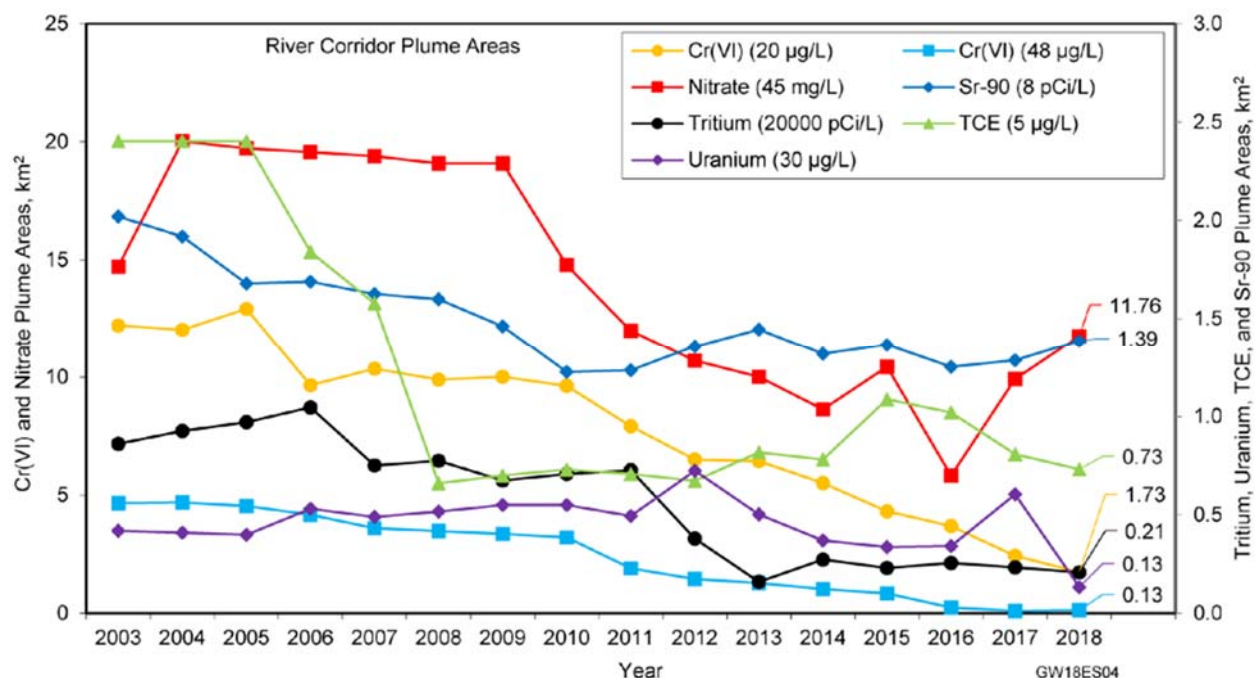


Figure 1.2. Temporal Variations in Plume Areas for Contaminants of Concern in the Hanford River Corridor (after Fig. ES-4 of DOE-RL 2019a)

Extensive efforts have been made to cleanup Cr(VI) and other GW contaminants in the 100 Area since the late 1990s, including source zone removal (WCH 2015, 2012a,b), injection of permeable reactive barriers (Fruchter et al. 1996, 2000; Vermeul et al. 2002), and GW P&T (DOE/RL-2017-67, Rev. 0). Significant progress has been made in cleaning up Cr(VI), and the decrease in the spatial extent and concentration of Cr(VI) GW plumes from 2010 to 2018 at both low river stage (LRS) and high river stage (HRS) is shown in Figure 1.3. Decreased plume areas and concentrations are particularly evident for the 100-D and 100-H Areas. In addition, Figure 1.3 indicates that at HRS in 2018, Cr(VI) concentrations in GW in the 100-B/C and 100-F Areas, which do not have P&T systems but are instead monitored for natural attenuation, were mostly less than 10 µg/L.

Remediation efforts in the 100 Areas are ongoing, subject to the applicable regulatory criteria. The CERCLA final ROD (EPA 2018) for GW cleanup in the 100-HR-3 GW OUs mandated an inland GW CUL of 48 mg/L for Cr(VI) and 100 mg/L for total Cr for human receptors. Figure 1.3 suggests that the 48 µg/L Cr(VI) GW CUL has largely been achieved. However, injection and extraction wells will need to be shut down to perform rebound studies to more fully assess cleanup progress. In addition, the ROD specified a CUL of 10 µg/L for Cr(VI) and 65 µg/L for total Cr in surface water (SW) to protect ecological receptors in the Columbia River. The ROD was less prescriptive in specifying point-of-compliance locations for the SW CUL.

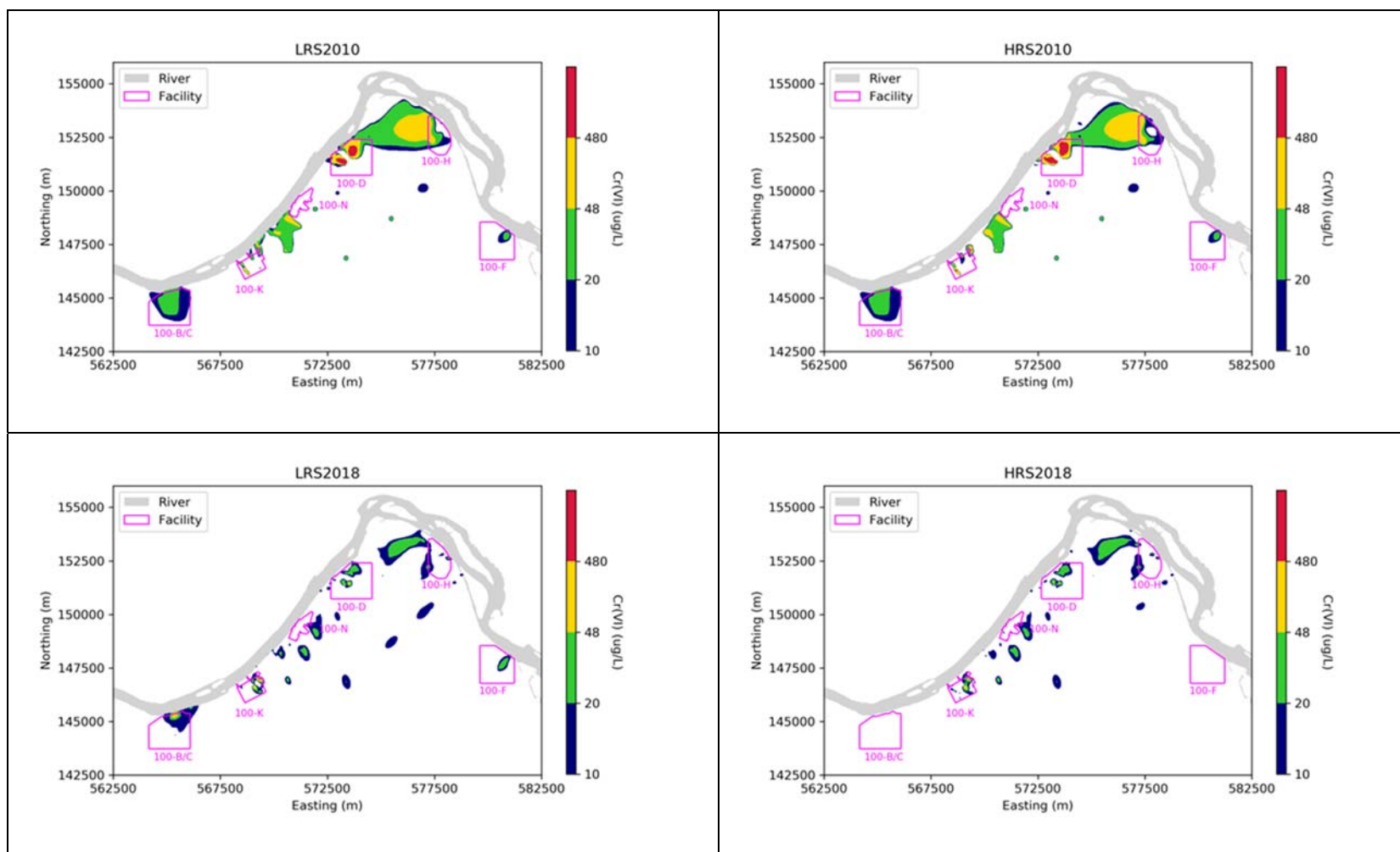


Figure 1.3. GW Cr(VI) Plumes at LRS and HRS for 2010 (upper panels) and 2018 (lower panels) (reproduced from DOE/RL 2019a; DOE/RL 2011)

The proximity of GW Cr(VI) plumes to the river, and the highly dynamic nature of the river, influence the transport behavior of the plumes and create challenges for monitoring and interpretation of Cr(VI) fate and transport. Understanding the controlling processes, the spatial and temporal relationships between inland GW and SW Cr(VI) concentrations, and the effects of ongoing remediation efforts is critical to establishing technically defensible compliance monitoring for SW and GW CULs.

This report collates information on Cr(VI) GW and remediation in the Hanford 100 Areas and presents the results of several analyses that examined relationships between inland and shoreline concentrations. Available data and selected past work on Cr(VI) GW contamination and remediation efforts in these areas are reviewed and summarized. Key controlling processes responsible for changes in Cr(VI) concentrations as GW disperses, mixes, and interacts with river water are also reviewed. Relationships between inland GW plumes and surface-water points of discharge in and along the Columbia River are also examined to identify a technical basis supporting selection of appropriate and representative compliance monitoring for Cr(VI) CULs in GW and SW.

The report is organized as follows. Section 2.0 provides a summary of historical operations in the 100 Areas that led to Cr(VI) GW contamination, factors that affect plume attenuation, and an overview of selected GW monitoring, remediation, and modeling activities. The basis for the 10 µg/L Cr(VI) SW quality CUL is also described. Section 3.0 examines relationships between Cr(VI) aqueous concentration data in GW monitoring wells and aquifer tubes located in riverbed sediments, plume metrics over time, and correlations with other variables, and the influence of other processes such as dilution in contributing to Cr(VI) plume attenuation. Section 4.0 provides a summary and recommendations. Appendix A provides additional details on the data analysis methods in this report.

2.0 Background

This section discusses the basis for the 10 µg/L Cr(VI) CUL, provides a summary of information on the history of site operations that led to the Cr(VI) GW contamination in the Hanford 100 Areas, and describes factors that affect Cr(VI) plume mobility and attenuation. Data collection activities for monitoring GW contamination and remedy performance are summarized, along with an overview of site remedial actions influencing Cr(VI) concentrations. Selected site modeling efforts are also presented within this context.

2.1 History of Site Operations

The Hanford 100 Areas (100-B/C, 100-D/DR, 100-F, 100-H, 100-K, 100-N; Figure 1.1) are located along the Columbia River corridor in the northern portion of the Hanford Site. A series of nuclear reactors were built in the 100 Areas starting in the early 1940s to produce plutonium for nuclear weapons. Operation of these reactors produced various COCs in GW, including Cr(VI).

The origin of the Cr(VI) contamination in the 100 Area is provided in the report by Dresel et al. (2008), which is summarized here. GW chromium contamination originated as sodium dichromate ($\text{Na}_2\text{Cr}_2\text{O}_7 \times 2\text{H}_2\text{O}$), which was used at all the reactor sites as a corrosion inhibitor in reactor cooling water. A typical concentration of 2.0 mg/L (0.7 mg/L as Cr) was used (Foster 1957). Until approximately 1953, the sodium dichromate solutions were made up in a batch system using 100-lb bags of granular dichromate manually hopped into large (~3600 gal) tanks to obtain a final solution concentration of 15% $\text{Na}_2\text{Cr}_2\text{O}_7$ by weight (Whipple 1953). After 1953, concentrated stock solutions of 70% $\text{Na}_2\text{Cr}_2\text{O}_7$ by weight were delivered to the site, stored in large tanks, and diluted (Schroeder 1966). The concentrated stock solutions were delivered to the reactor sites in rail cars, tanker trucks, barrels, and local pipelines. After passing through the reactors, cooling water containing the chromate was transported through large-diameter underground pipes to retention basins for thermal and radioactive cooling prior to release to the Columbia River (Dresel et al. 2008). Chromate was discharged intentionally to the ground through surface or near-surface disposal cribs, or accidentally released by spills during handling or from pipeline leaks (Dresel et al. 2008).

The exact pH of the chromate stock solutions that were used is not well known. However, a 10% $\text{Na}_2\text{Cr}_2\text{O}_7$ (0.82 mol L⁻¹ Cr) solution has a pH of 3.5, and a 70% $\text{Na}_2\text{Cr}_2\text{O}_7$ (8.96 mol L⁻¹ Cr) solution will have an even lower pH (~1.5 to 2) (Dresel et al. 2008). Additional chromate was discharged to the environment from decontamination operations, likely after mixing with sulfuric acid to form chromic acid (Peterson et al. 1996). Therefore, the chromate discharged to the ground is assumed to have been acidic. The pH, buffering capacity, and counter-ion concentrations of the disposed aqueous solutions of $\text{Na}_2\text{Cr}_2\text{O}_7$, determine the bulk solution chemistry and associated sorption and transport behavior of Cr(VI) in the vadose zone and underlying aquifer sediments.

2.2 Basis for 10 µg/L Cr(VI) Aquatic Water Quality Standard

In natural waters, trivalent chromium, Cr(III), and hexavalent chromium, Cr(VI), are the main forms present. The U.S. Environmental Protection Agency (EPA) and the State of Washington both limit the amount of chromium in SWs and the limiting criteria for freshwater are expressed in terms of the dissolved metal in the water column for both chronic and acute effects. Acute effects include short-term effects such as survival and growth, whereas chronic effects include longer-term effects such as reproduction. !

The Washington State limit for *chronic exposure* to hexavalent chromium concentrations in the Columbia River is 10 µg/L as listed in [WAC 173-201A-240](#), “Water Quality Standards for Surface Waters of the State of Washington,” “Toxic Substances,” Table 240(3). The 10 µg/L standard represents the chronic toxicity level to aquatic life (lowest observed effect level, LOAL) determined by the EPA (EPA 1986). EPA’s water quality criteria for the protection of aquatic organisms for hexavalent chromium is 11 µg/L (EPA 1996).¹ Trivalent chromium toxicity depends on water hardness and is determined using an algorithm where chronic exposure is limited by the continuous criterion concentration² (CCC) $\leq (0.860)(e^{(0.8190[\ln(\text{hardness})] + 1.561)})$. Plume maps (Figure 1.3), aquifer tube data, and riverbed sampling indicate that aqueous Cr(VI) concentrations in sediments underlying the riverbed are, in many cases, nearly as large as inland GW plume concentrations (DOE/RL 2019a; SGW 2015). Thus, it is important to understand the relationship between inland plumes and discharge to the river.

2.3 Factors Affecting Cr(VI) Plume Attenuation

The chemistry of the disposed chromate solutions and geochemical processes in the subsurface, including precipitation/dissolution reactions, aqueous speciation, and sorption, affect the transport of Cr(VI) through both the vadose zone and aquifer systems. Mixing of surface and GWs and hydrodynamic dispersion also have controlling effects on Cr(VI) concentrations between the inland GW plumes and points of discharge at GW-SW interfaces. These processes are controlled in part by the physical, hydraulic, and geochemical properties of the geologic materials. Fluctuations in river stage, resulting from dam operations on the Columbia River, also have a significant effect on the transport and fate of Cr(VI). Figure 2.1 shows a conceptual model of GW-SW interaction zones at 100 Area sites along the Columbia River, and the relative locations of waste disposal sites and the GW monitoring wells and aquifer sampling tubes that are used to assess the extent of GW contamination. The effects of Columbia River dam operations on river stage, the hydrogeologic characteristics of the 100 Areas, and the local geochemistry affecting Cr(VI) GW plumes are discussed in more detail in the following subsections.

¹ EPA National Recommended Water Quality Criteria – Aquatic Life Criteria, <https://www.epa.gov/wqc/national-recommended-water-quality-criteria-aquatic-life-criteria-table>

² A 4-day average concentration not to be exceeded more than once every 3 years on the average.

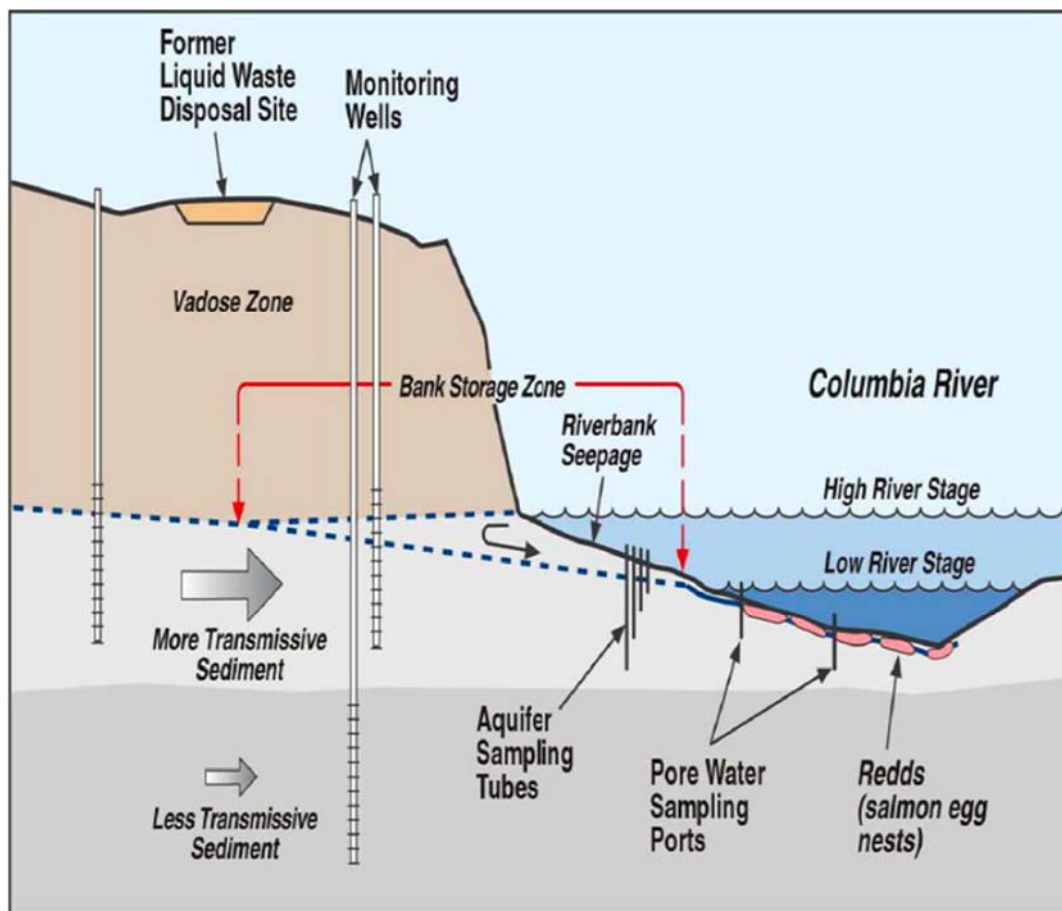


Figure 2.1. Conceptual Model of 100 Area Waste Sites Showing Relative Locations of GW Monitoring Wells and Aquifer Sampling tubes, and the Zones Influenced by River Stage Fluctuations (from Peterson and Connelly 2001)

2.3.1 Dam Operations

Dam operations are influenced by hydroelectric power demand and ecological considerations associated primarily with maintaining specified river flows during the seasonal migration and spawning of salmon. The rise and fall of the river create a zone of interaction between SW and GW (a.k.a. the bank storage zone; Figure 2.1), with GW flowing toward the river during LRS, and with river water flowing inland during HRS.

River stage along the Hanford Reach is controlled by 1) water outflow from the upstream Priest Rapids Dam; 2) the bathymetry of the river channel; and 3) for the lower portions of the Hanford Reach (e.g., 300 Area), the forebay elevation at the downstream McNary Dam. Columbia River stage varies over both short (e.g., hourly) and long (e.g., seasonal) time scales in response to seasonal precipitation and snow melt patterns, upstream reservoir storage conditions, and dam operations. River stage is usually the highest in the summer (~June-July) and lowest in the fall (Oct-Nov).

The stage of the Columbia River is monitored at several locations along the Hanford Reach by the U.S. Geological Survey (USGS). For example, Station 12472800 is located in the upper reach of the Hanford Site (Figure 2.1). Observational data from this and other river gauging stations is available from the

USGS National Water Information System.¹ River stage at different locations and times also can be estimated from regression analysis (CH2M 2019), or from the Modular Aquatic Simulation System 1D (MASS1) model (Richmond et al. 2000). Calibration of MASS1, and comparisons of observed and simulated river stage, are described by Waichler et al. (2005). Daily river stage fluctuations of ~0.5 m (± 0.25 m) and annual fluctuations of 3-4 m (± 1.5 -2 m) are common (Figure 2.3 – Figure 2.5).

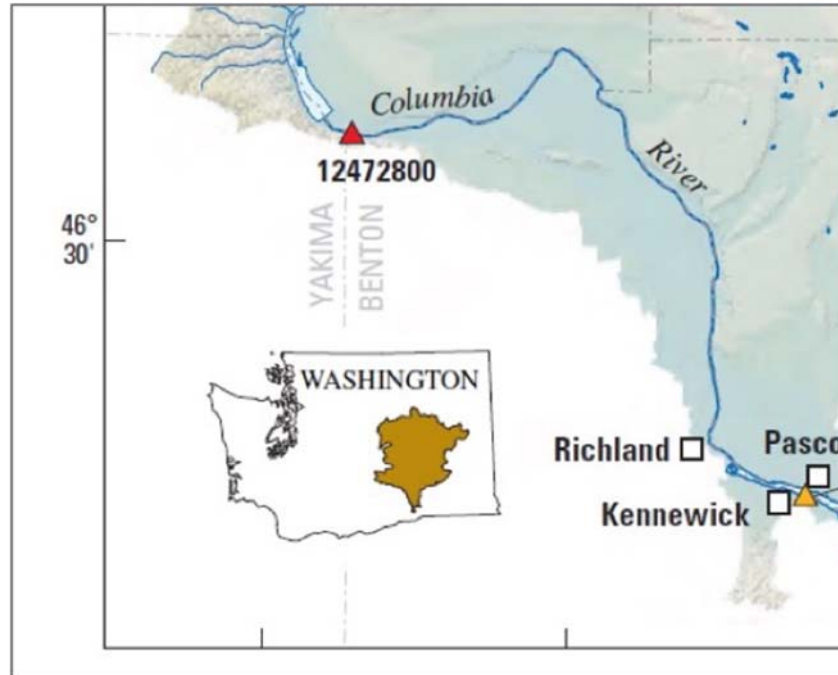


Figure 2.2. USGS River Gauging Station 12472800 is Located at Latitude 46°37'44" and Longitude 119°51'49," Downstream of the Priest Rapids Dam (https://wa.water.usgs.gov/data/realtime/adr/interactive/maps/CentralColumbiaSC_basin.pdf; accessed 27-Sep-2020)

¹ https://waterdata.usgs.gov/wa/nwis/dv?referred_module=sw&site_no=12472800

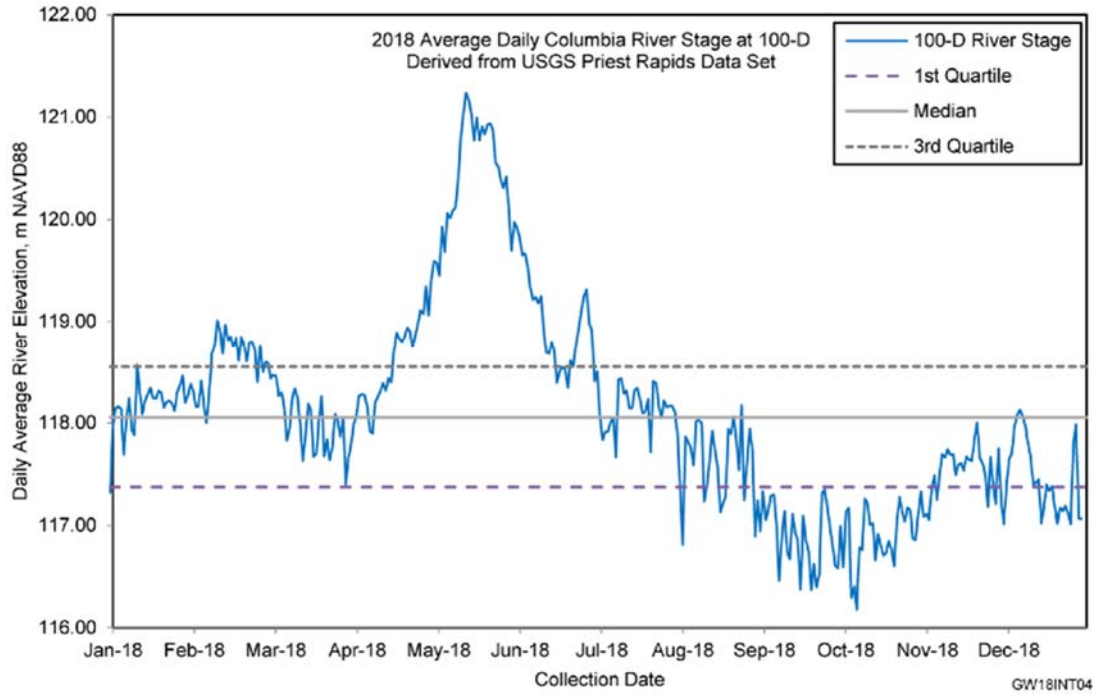


Figure 2.3. Daily Average River Stage at the 100-D Area in 2018 (after Fig. 1-6 of DOE-RL 2019a)

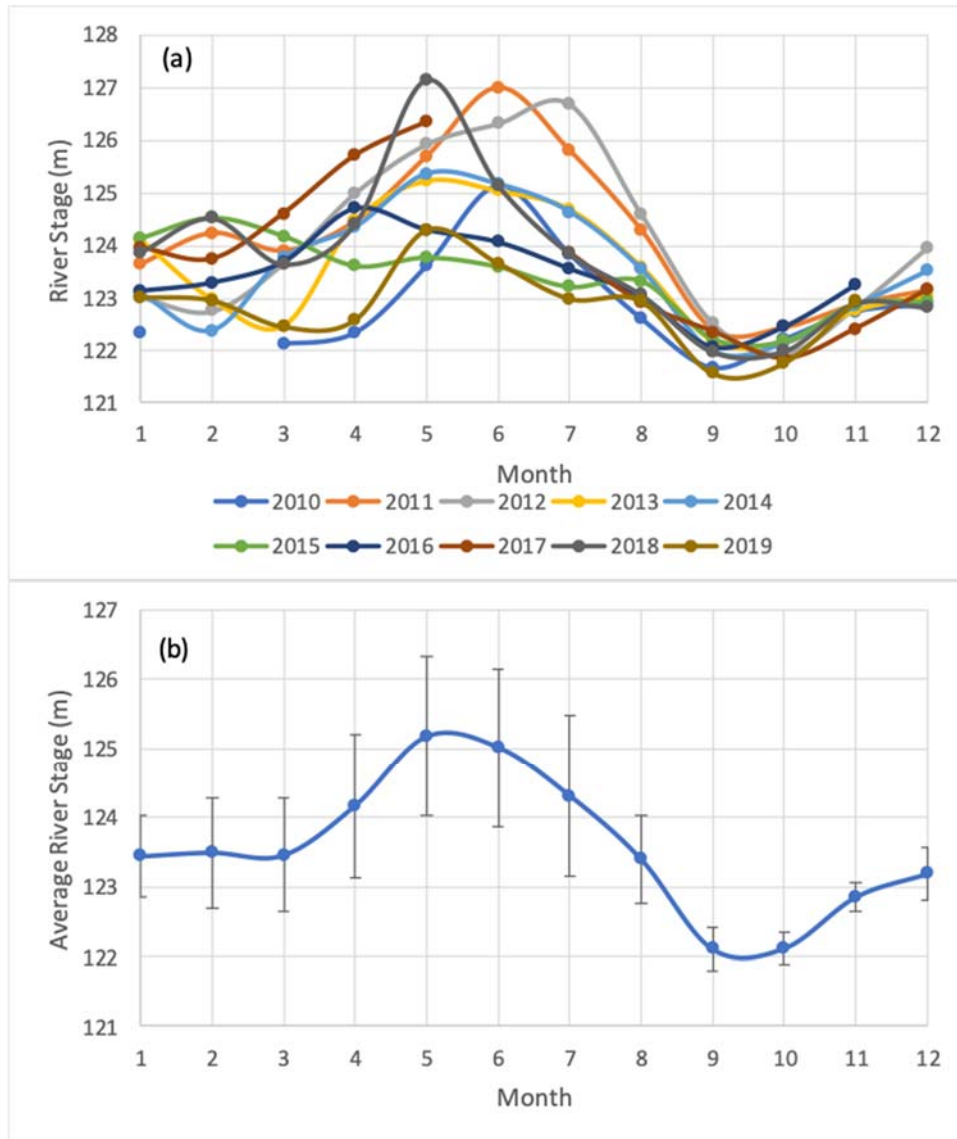


Figure 2.4. Monthly Average River stage at the Station 12472800 (shown in Figure 2.2), Downstream of the Priest Rapids Dam, (a) from 2000 to 2019 and (b) Average over 10 Years with One Standard Deviation

GW Cr(VI) concentrations can vary due to changes in both horizontal and vertical gradients and associated river or GW incursion into regions previously occupied by water of different origin. The response of Cr(VI) concentrations to river stage fluctuations, as determined from well and aquifer tube samples, depends on proximity to the river, the location of the well screen (e.g., whether it is in the unconfined or confined aquifer), the nature of the sediments surrounding the well/tube, and whether or not continuing sources of Cr(VI) exist in the vicinity of the sampling device.

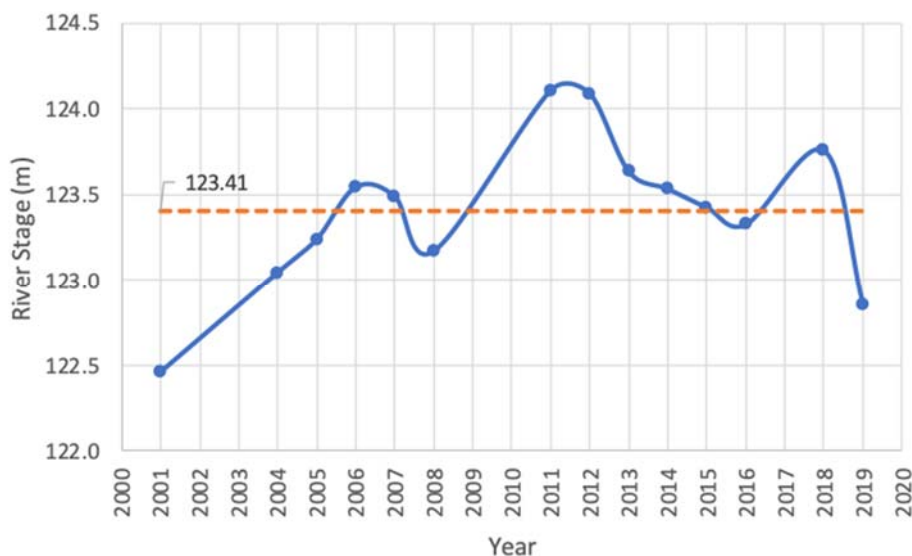


Figure 2.5. Annual Average River Stage at the Station 12472800 (shown in Figure 2.2), Downstream of the Priest Rapids Dam

The frequency and schedule of GW sampling do not always clearly define the seasonal variability, but river dilution effects have been observed in some instances. For example, in the 100-B/C Area, the low Cr(VI) result in well 199-B3-47 (located ~100 m from the shoreline) in June 2011 (top panel of Figure 2.6) was accompanied by HRS and low specific conductance, which indicates river water incursion into the aquifer (DOE-RL 2019b). On the other hand, Cr(VI) concentrations vary inversely with water level in well 199-B4-14 (bottom panel of Figure 2.6), which is about 1 km away from the river. It is clear that the fluctuations in Cr(VI) concentrations at this location are not due to dilution with river water. The shallow Cr(VI) plume in this area is thin, and concentrations are affected by the vertical hydraulic gradient. Variations also occur locally at each of the former reactor sites owing to their different locations along the river corridor, and to variability in the hydrogeology and associated aquifer properties at each site.

2.3.2 Hydrogeology

The vadose zone within the 100 Areas can be divided into two primary hydrostratigraphic units: 1) the gravel-dominated facies association of the Hanford formation and 2) the conglomeratic member of Wooded Island, Unit E, of the Ringold Formation (Last et al. 2006). The Ringold E unit makes up the lower portion of the vadose zone at the 100-K, 100-N, and the 100-D Areas. It is only partially present in the 100-B/C and 100-H Areas and is absent from the 100-F Areas. The Hanford formation extends from the ground surface to just above the water table when the Ringold Formation is present. The Hanford formation extends beneath the water table and makes up the unconfined aquifer in the 100-H and 100-F Areas (Last et al. 2006). As indicated by Figure 2.7, ground surface elevations are higher in the 100-B/C, -K, -N, and -D Areas, so the vadose zone is thicker in those areas, relative to the 100-H Area and the area between the 100-D and -H Areas known as the “Horn.”

The Hanford formation and Ringold E unit (where present) are underlain by paleosols and overbank flood deposits of the Ringold Upper Mud (RUM) unit, which overlies lacustrine deposits of the Ringold Lower Mud (Figure 2.7). The fluvial sand- and gravel-dominated Ringold A unit may be present locally at the base of the lower Ringold mud unit, overlying the basalt. The fluvial sand- and gravel-dominated Ringold B and C units may also be present locally at the base and within the RUM unit, respectively.

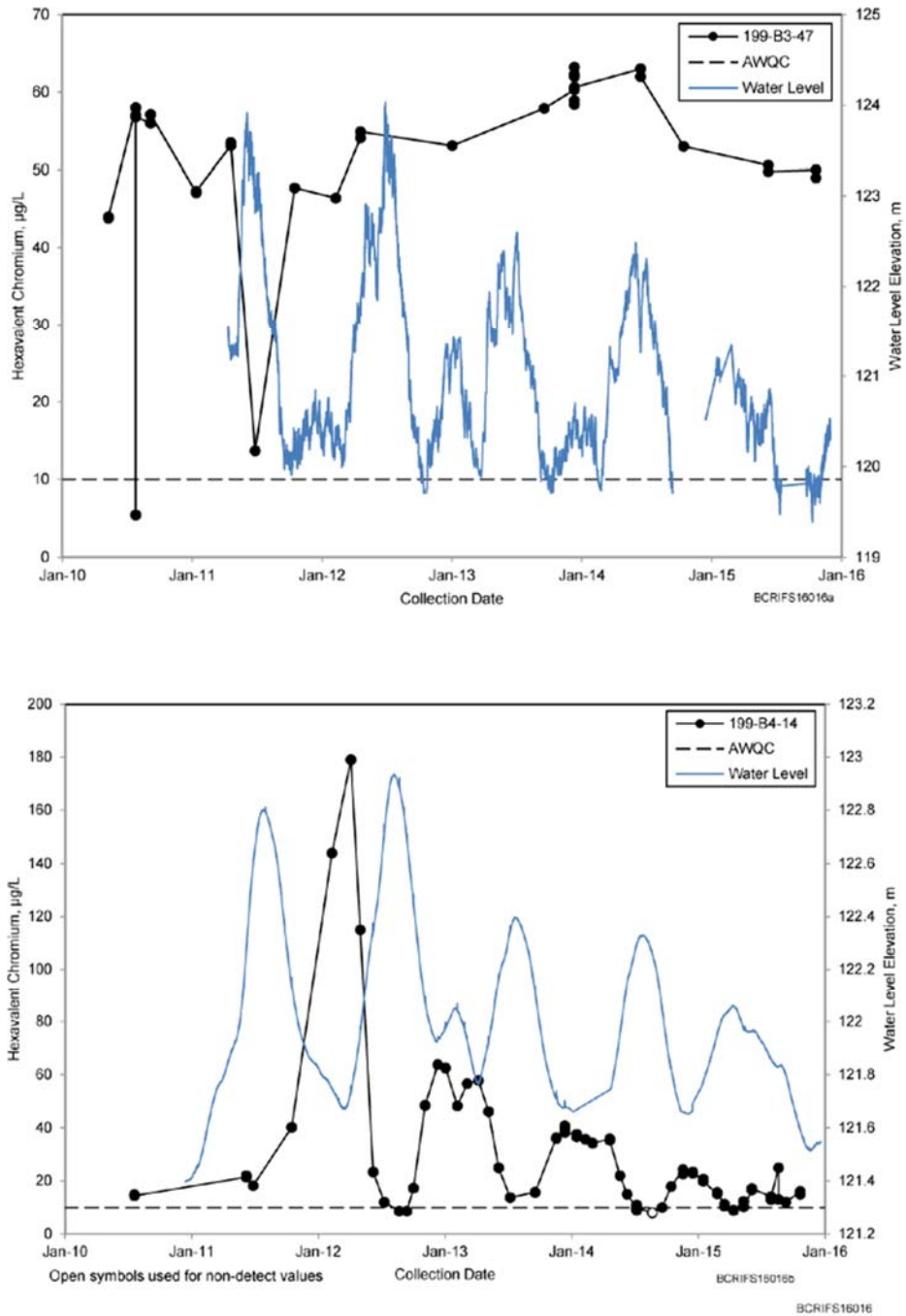
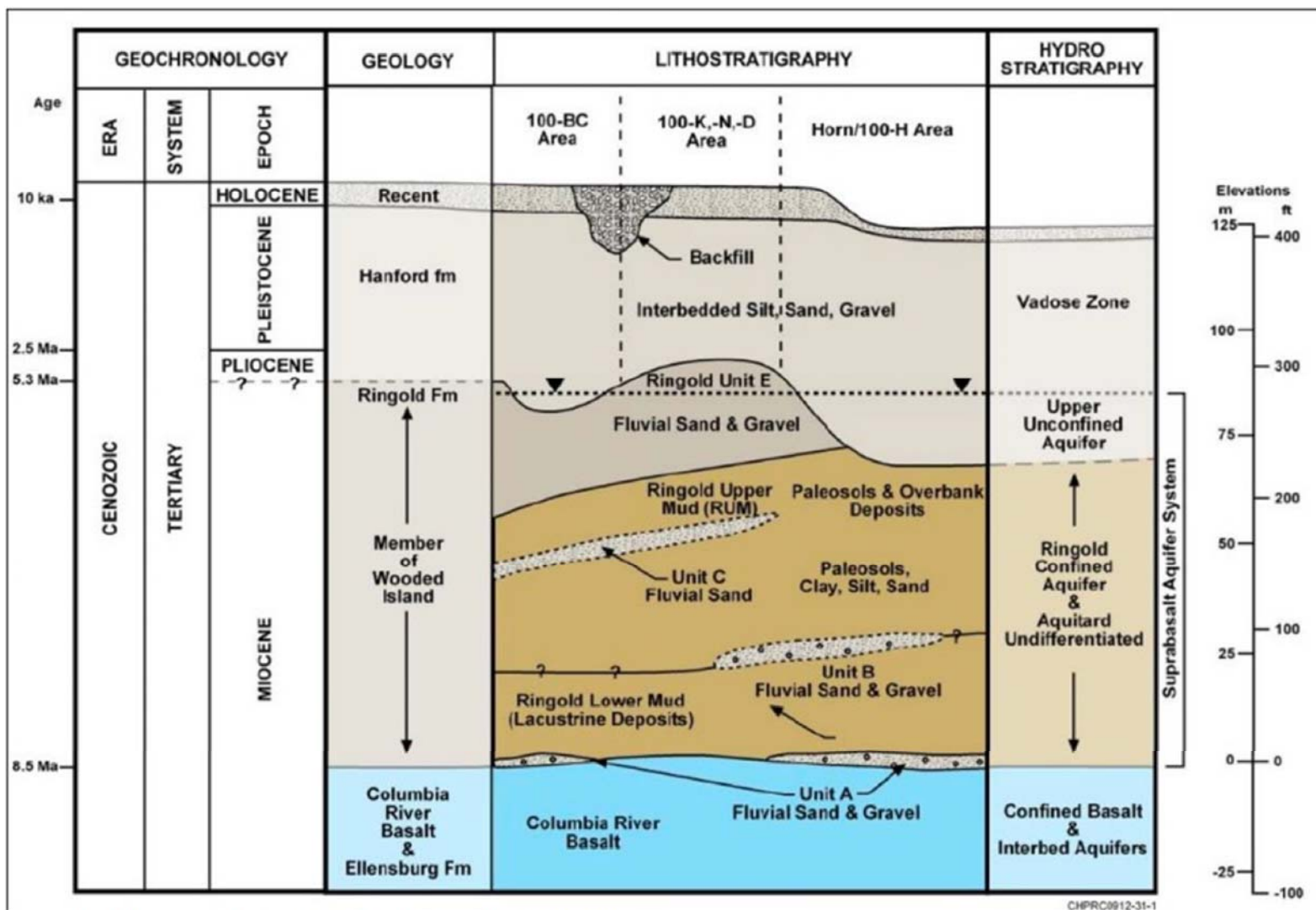


Figure 2.6. Cr(VI) and Water Levels in Wells 199-B3-47 and 199-B4-14 in 100-BC Area (after Fig. 4-39 of DOE-RL 2019b)



Source: SGW-44022, *Geohydrologic Data Package in Support of 100-BC-5 Modeling*.

Figure 2.7. Generalized Representation of the Hydrogeologic Units in the 100 Areas (Khaleel and Williams 2011)

Hydraulic conductivities, effective porosities, and storage properties of the hydrogeologic units in the 100 Areas have been estimated from core samples, aquifer testing, and numerical flow and transport modeling (DOE/RL 2019b). Table 2.1 lists the average values of hydraulic conductivity that were estimated for the major hydrogeologic units in a calibrated flow and transport model of the aggregate 100 Areas, referred to as the 100 Area Groundwater Model (100AGWM) (CH2M 2016).

As indicated by Table 2.1, the hydraulic conductivity of the Hanford formation is about 1 to 2 orders of magnitude larger than that of the RUM unit. The 100AGWM is a four-layer model with spatially variable properties within each model layer. Figure 2.8 and Figure 2.9 show the spatial distribution of hydraulic conductivities for model layers 1 and 2. Constant values for effective porosity and specific yield of 0.18 and 0.1, respectively, were estimated by model calibration, and a constant value for specific storage of 5×10^{-6} day⁻¹ was assumed for the entire model (CH2M 2016). Additional details about the 100AGWM and other 100 Area modeling efforts are provided later in this report.

Table 2.1. Average Hydraulic Conductivity Values for Geologic Units in the 100 Areas (from CH2M 2016)

Operable Unit	Geologic Unit	Hydraulic Conductivity (m/d)
All	Hanford	88
100-K	Reworked Ringold E	25
100-D and 100-H	Reworked Ringold E	35
100-B	Ringold E	6.9
100-K	Ringold E	17.3
100-D, 100-H, and 100-F	Ringold E	28.7
100-K	Reworked RUM	2
100-D and 100-H	Reworked RUM	5
100-B	High conductivity paleochannel	1,251

m/d = meters per day
RUM = Ringold Upper Mud (unit)

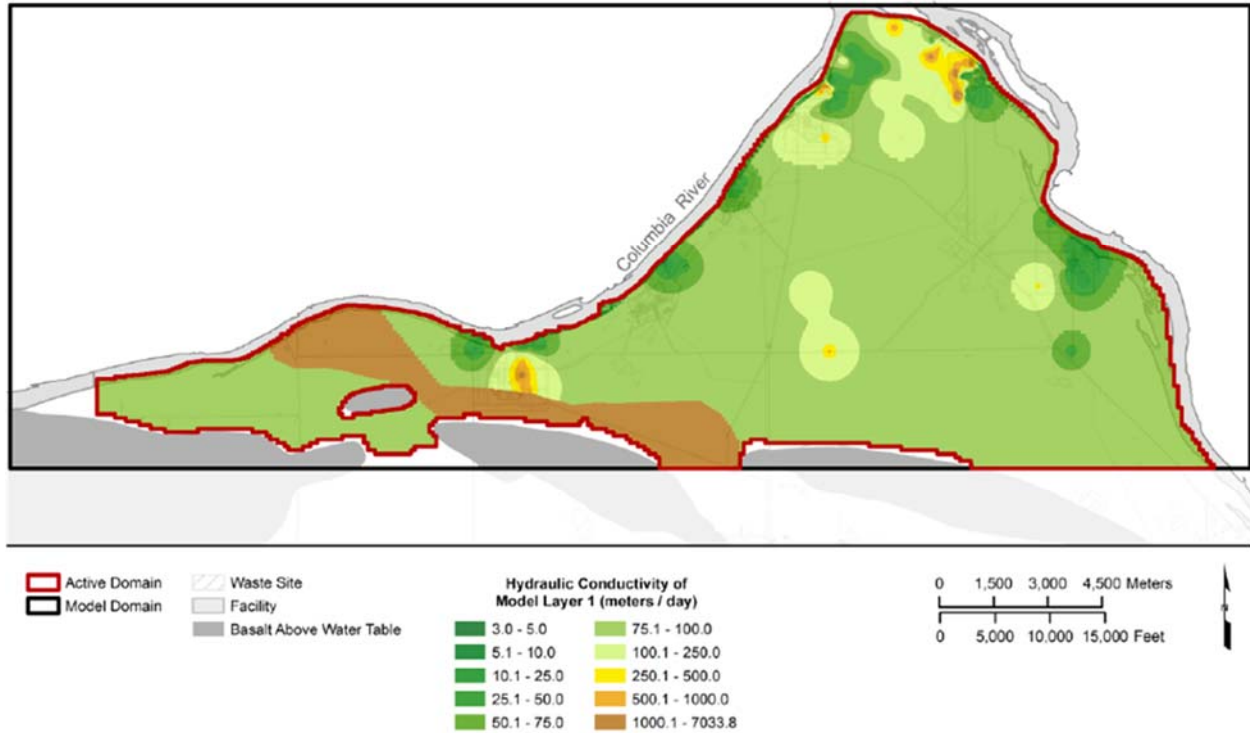


Figure 2.8. Hydraulic Conductivity Distribution for Layer 1 of the Calibrated 100 Area GW Flow and Transport Model (from CH2M 2016)

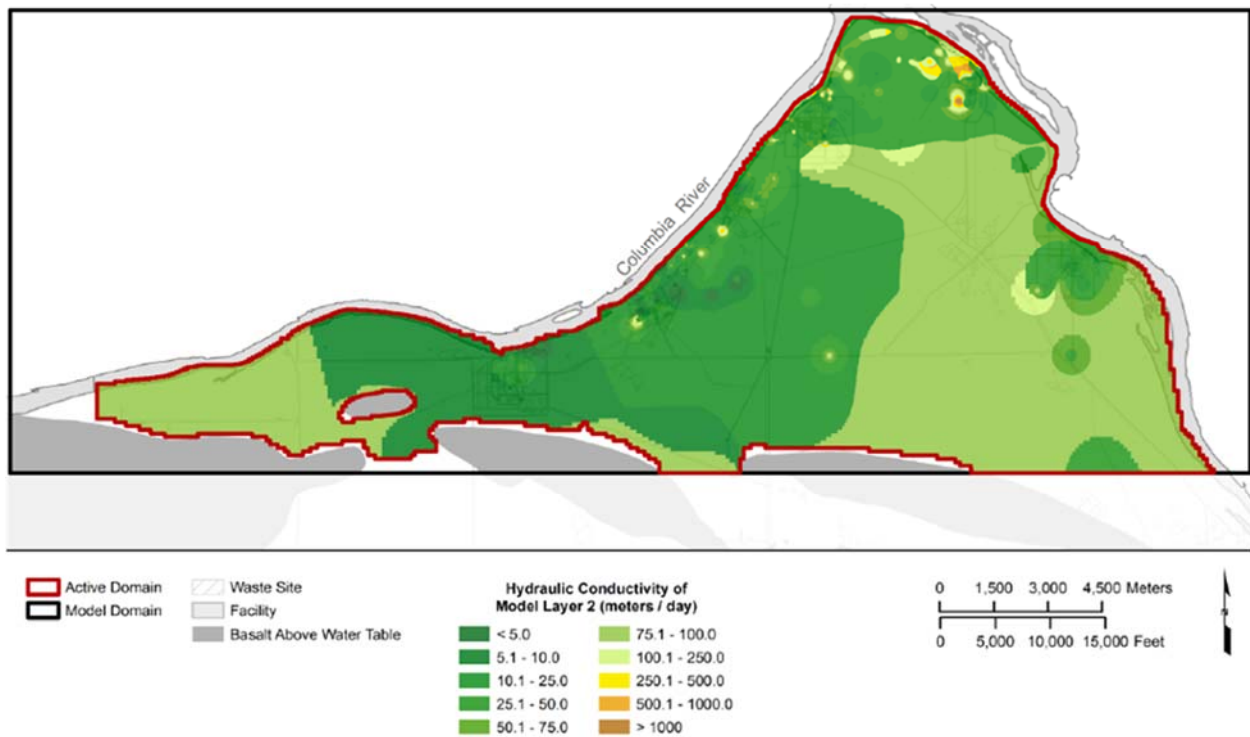


Figure 2.9. Hydraulic Conductivity Distribution for Layer 2 of the Calibrated 100 Area GW Flow and Transport Model (from CH2M 2016)

2.3.3 Geochemistry

Important Cr species and biogeochemical reaction paths relevant to the subsurface in the Hanford 100 Areas are illustrated in Figure 2.10. Aqueous speciation studies on 100 Area sediments have shown that Cr in the aqueous phase is dominated by chromate and dichromate species (Qafoku et al. 2009; Szecsody et al. 2019). Both of these anionic species are relatively mobile in the subsurface at the near-neutral pH and low ionic strength conditions that are prevalent in 100 Area vadose zone and aquifer sediments. As shown in this figure, Cr may sorb to sediments and/or precipitate as Cr(III) or Cr(VI) species, depending on geochemical conditions. Sorption reactions are typically much faster than precipitation/dissolution reactions.

Sorption of Cr to sediments is an important attenuation mechanism contributing to Cr(VI) removal from the aqueous phase. Early studies with pure mineral phases showed strong sorption on minerals such as gibbsite ($\alpha\text{-Al}_2\text{O}_3$) and amorphous hydrated ferric oxide ($\text{Fe}_2\text{O}_3 \cdot x\text{H}_2\text{O}(\text{am})$) at low to neutral pH values (i.e., pH=2-7), and relatively weak sorption to silica (SiO_2) at all but very low pH values (Griffin et al. 1977; Davis and Leckie 1980). Studies conducted with natural soils and sediments showed that adsorption of Cr(VI) over a range of pH values varied from essentially no adsorption to extensive adsorption (Zachara et al. 1989).

Qafoku et al. (2009) examined sorption in Hanford sediments under slightly alkaline and oxic conditions, which predominate in the Hanford subsurface, and reported Cr in the sediments to be present in multiple fractions: 1) a highly mobile fraction (over 95% of the total Cr); 2) a fraction with a slow and time-dependent release during leaching that was assumed to be held in physically and mineralogically remote sites that provide a longer-term continuing source of contaminant chromium; 3) a reduced immobile fraction of Cr(III) (that may become mobile after Cr(III) oxidation) that is most likely associated with surface-mediated redox reactions of aqueous Cr(VI) and aqueous, sorbed, or structural Fe(II); and 4) Cr(VI) in the form of relatively insoluble BaCrO_4 precipitates that likely do not contribute to the aqueous Cr(VI) in GW. The presence of competing and, less commonly, complexing ions, may significantly alter chromate adsorption. Although sulfate is adsorbed less strongly on amorphous hydrated ferric oxide than CrO_4^{2-} , sulfate may compete for adsorption sites when present in higher concentrations (Leckie et al. 1980).

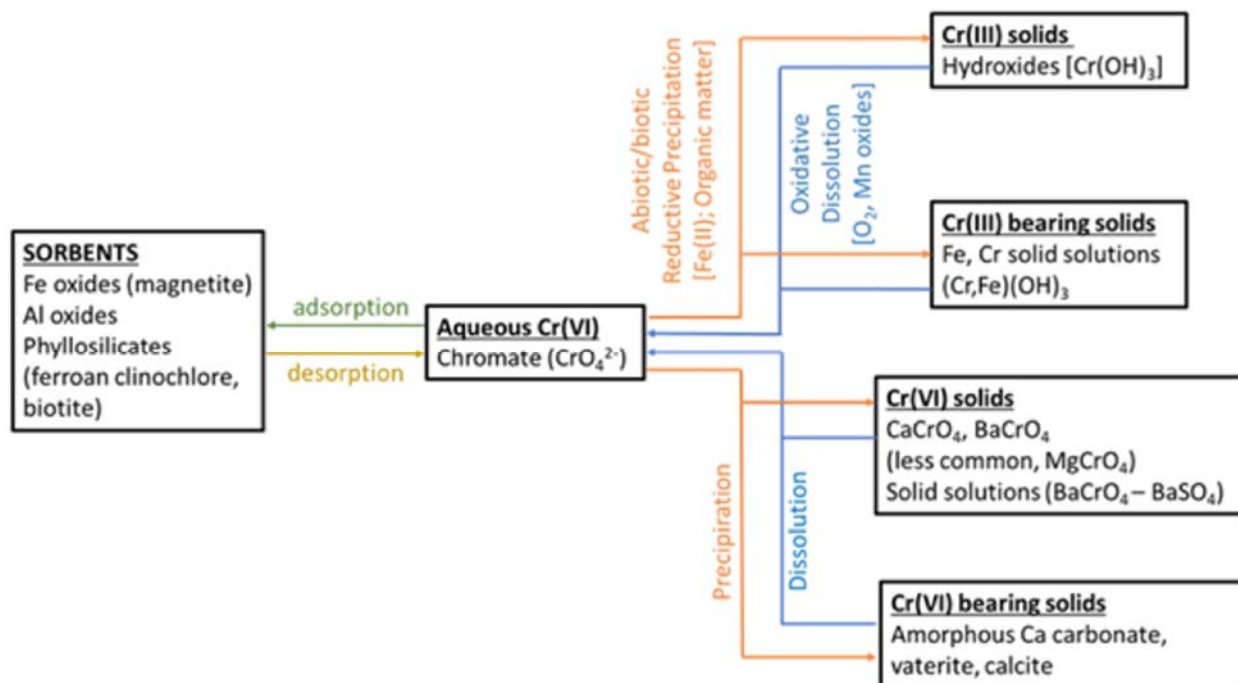


Figure 2.10. Important Chromium Species and Biogeochemical Reactions. Sorption reactions are generally much faster than precipitation/dissolution reactions.

Aquifer sediments underlying 100 Area waste sites generally have been found to contain significantly less Cr(VI) relative to overlying contaminated vadose zone sediments. Cr(VI) was found in vadose zone sediments in the 100-C Area after removal of the process water treatment head house (Dresel et al. 2008) where a zone of yellow, Cr-stained soil was observed below the concrete slab, at a depth of approximately 15 ft below ground surface. In addition, chromate concentrations upgradient of the in situ redox manipulation (ISRM) barrier have remained high since the plume was discovered in 1999, indicating that there are continuing chromate sources in the vadose zone (Dresel et al. 2008). In the 100-D Area, very high chromate concentrations have been measured in GW in the past (DOE-RL 2011), indicating that the chromate was from a source that was more concentrated than reactor cooling water.

Szecsody et al. (2019) performed solid-phase characterization studies on contaminated vadose zone sediments from the 100 Areas that showed the presence of numerous, highly soluble, 1 to 10 μm size CaCrO_4 crystals that readily released Cr at relatively high concentrations. Lesser amounts of unidentified phases containing Ba and Cr in association with weathered pyroxenes and weathered Ca-rich plagioclase were also found. Most (>90%) of the Cr(VI) mass in these vadose zone sediments was readily leached from the sediments during the laboratory column experiments, resulting in concentrations up to 187 mg/L Cr(VI) in the column effluent. The highly soluble dissolving phase was calcium chromate, but less soluble Cr(VI)-bearing phases may have contributed to a slower, prolonged release that was observed over a period of hundreds of hours. The source of Ca and Ba for the Cr(VI) precipitates is believed to be from mineral dissolution associated with historical surface spills of Cr(VI) as an acidic dichromate solution (Szecsody et al. 2019; Dresel et al. 2008). Mineral dissolution may have also triggered the release of Fe(II) from Fe(II)-bearing minerals, which has been observed in other studies conducted with Hanford sediments using simulated waste solutions that were highly alkaline or acidic (Qafoku et al. 2003, 2010, 2011).

2.4 Site Remediation Activities

Past and ongoing remediation activities for the 100 Areas include:

- GW P&T
- ISRM
- Removal, treatment (as required), and disposal (RTD)
- Soil flushing (in combination with P&T)
- Monitored natural attenuation (MNA)

Application of these remedies to sites in the 100 Area is briefly summarized below.

2.4.1 GW P&T

The U.S. Department of Energy (DOE) currently operates and maintains five GW P&T systems along the Columbia River corridor: three P&T systems are located within the 100-KR-4 GW OU and two P&T systems are located within the 100-HR-3 OU (Figure 2.11). Figure 2.12 shows a layout of the 100-HR-3 OU P&T system.

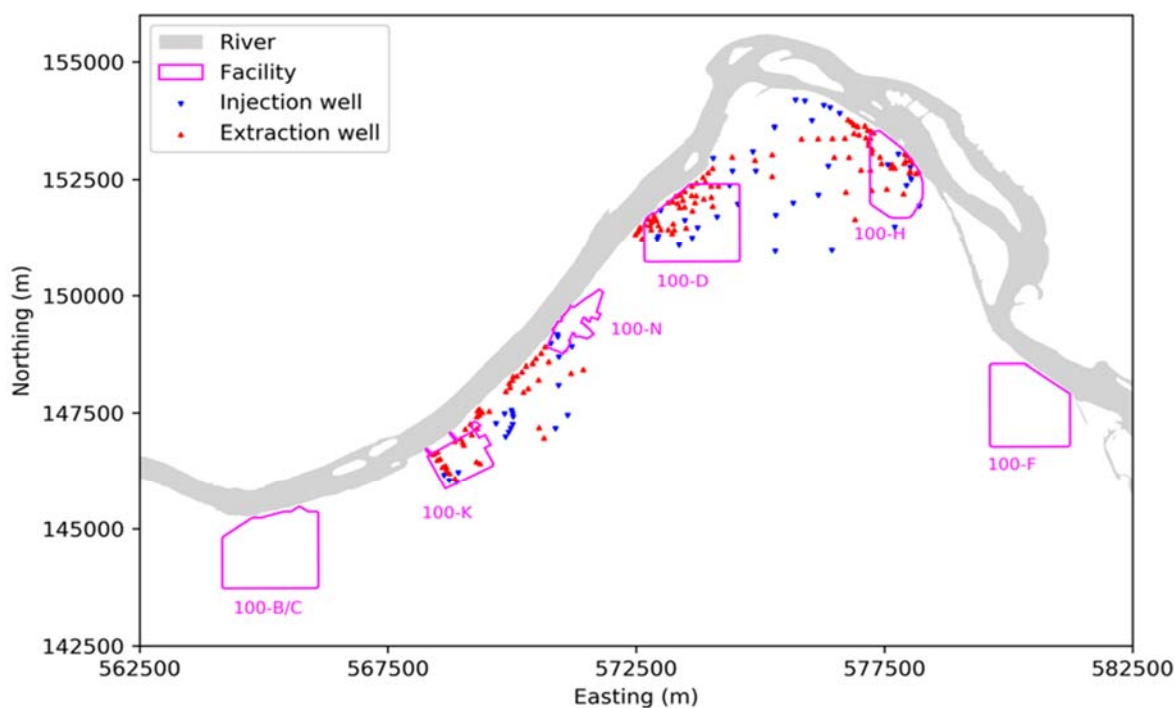


Figure 2.11. Map Showing P&T Wells in the 100 Areas that Operated Between Jan. 2014 and Feb. 2020

Cr(VI) is the primary COC in both the 100-HR-3 and 100-KR-4 OUs (Table 1.1). In the 100-HR-3 OU, Cr(VI) contamination is removed from GW by the DX and HX P&T systems (DOE-RL 2018). Figure 2.13 shows the mass of Cr(VI) removed over time from P&T systems in the 100-HR-3 OU. In the 100-KR-4 OU, Cr(VI) GW contamination is removed by the KR4, KX, and KW P&T systems.

In the 100-NR-2 GW OU, interim remedial actions have been implemented for strontium-90 and total petroleum hydrocarbons as GW COCs (DOE-RL 2018 Table 1). A P&T system developed in the 1990s for removing and treating strontium-90-contaminated GW proved ineffective. The 100-NR-2 P&T system was placed in cold-standby status in March 2006. This system was demolished, excavated, and removed during the period from August through November 2016. Although Cr(Vi) is not the primary COC in the 100-NR-2, early operations of the 100-NR-2 P&T system may have influenced the movement of Cr(VI) in the area.

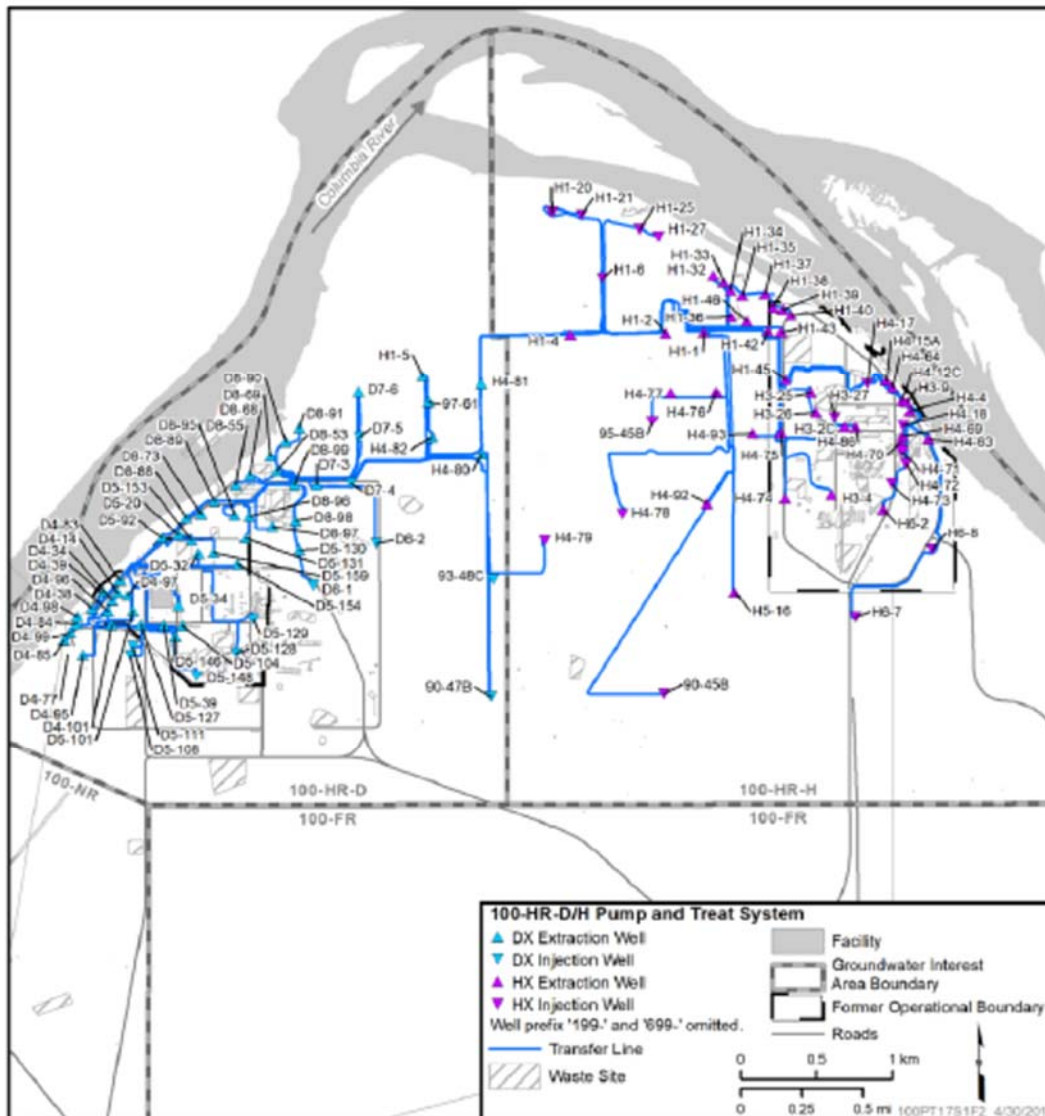


Figure 2.12. Layout of 100-HR-3 OU P&T System (as of December 31, 2017) (DOE/RL-2017-67, Rev. 0)

Waste site remedial actions in 100-D/H began in 1995 under an interim action ROD.¹ GW remediation by P&T was initiated in 1997 under the interim action ROD² with startup of the first P&T system, HR-3. A second P&T system, DR-5, began operating in 2004. Under the 2009 Explanation of Significant

¹ <http://www.epa.gov/superfund/sites/rods/fulltext/r1095126.pdf>

² <http://pdw.hanford.gov/arpir/index.cfm/viewDoc?accession=0078950H>

Differences,¹ these two initial P&T systems (DR-5 and HR-3) were expanded to include additional plume treatment capacity. As part of this expansion, two new ion exchange treatment facilities were constructed, and most of the wells under the HR-3 and DR-5 systems were transitioned to the new systems: HX and DX. The original treatment facilities for HR-3 and DR-5 stopped operating after this transition was complete. The DX and HX P&T systems have continued to operate within the 100-HR-3 OU under the interim action ROD. The treatment capacities have been increased, and numerous wells (injection, extraction, and monitoring) have been constructed. Remediation under the interim action ROD was completed for most of the 100-D/H waste sites by 2017 (DOE-RL 2018).

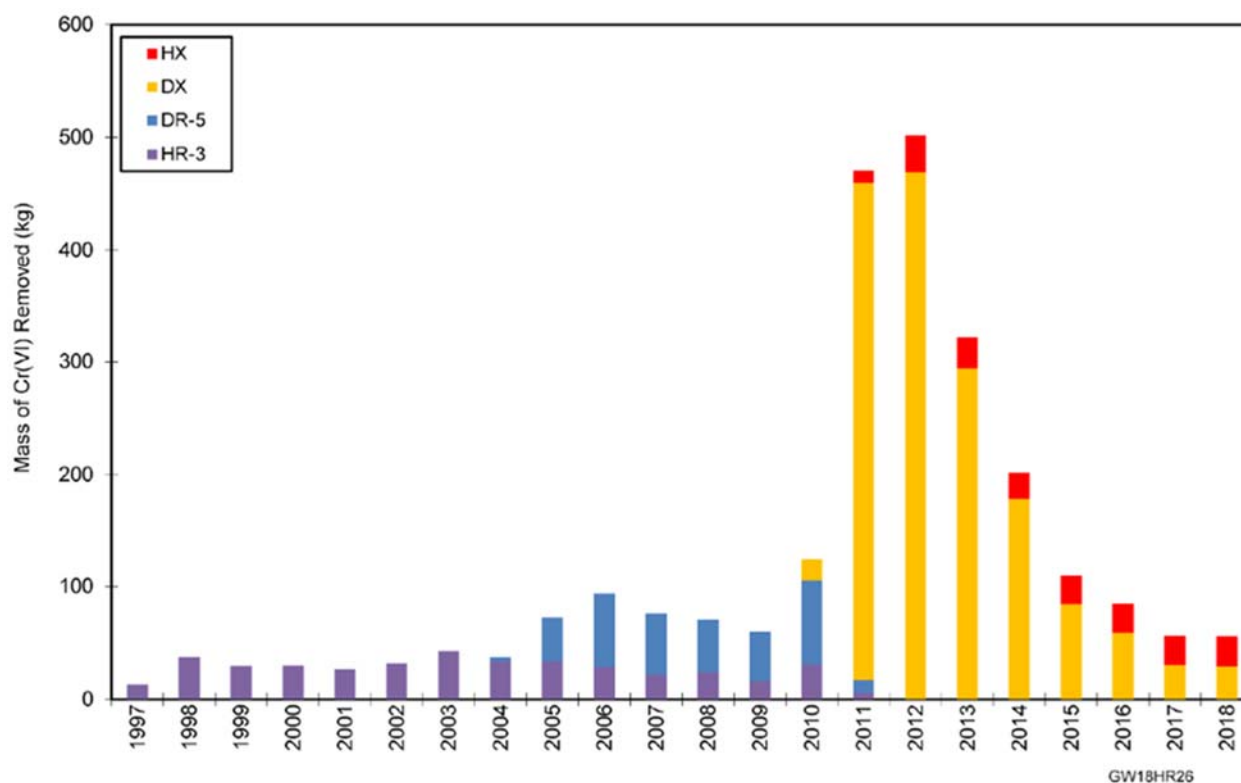


Figure 2.13. 100-HR-3 P&T Cr(VI) Annual Mass Removal (after Fig. 4-23 of DOE-RL 2019a)

From startup to 2018, the 100-HR-3 GW OU P&T systems have treated 23,892 million L (6,308 million gal) of GW and removed 2,546 kg of Cr(VI) (DOE-RL 2019a). Most of the 100-D/H contaminated vadose zone materials have also been removed by excavation and disposal of contaminated soils.

Three P&T systems (KR4, KW, and KX) are operating in the 100-KR-4 GW OU (DOE-RL 2019a). P&T operations at the 100-KR-4 GW OU are ongoing in accordance with the interim action ROD.² The 100-KW Area (KW) P&T system has been operating since 2007 (CH2M 2018). From startup through 2018, the KX, KW, and KR4 P&T systems have treated 26,345 million L (6,955 million gal) of GW and removed 939 kg of Cr(VI) (DOE-RL 2019a). The river protection evaluation for the 100-K Area for 2018 identified that all 4,000 m (13,120 ft) of shoreline affected by chromium-contaminated GW were “protected” or “protected but additional action may be required.” Hydraulic containment improvements provide protection of the 100 m (330 ft) of 100-K Area shoreline previously identified as “not adequately protected” in 2017 but currently designated as “protected but additional action may be required.”

¹ <http://pdw.hanford.gov/arpir/index.cfm/viewDoc?accession=0096029>

² <http://pdw.hanford.gov/arpir/pdf.cfm?accession=D196097243>

Additional details regarding the methods used for determining protection status and interpretations are provided in Section 2.5.

2.4.2 ISRM – Permeable Reactive Barrier

100-D Area: An ISRM barrier was installed as a new technology for treating Cr(VI)-contaminated GW in the 100-D Area under the 1999 interim action ROD amendment¹ and the 2003 ESD.² In 2009, it was determined that breakthrough of Cr(VI) was occurring at the ISRM barrier, and the barrier was not achieving the required level of performance. The Tri-Parties agreed that barrier maintenance could be discontinued because the DX P&T system would provide adequate protection of the river.³

The ISRM permeable reactive barrier (PRB) in the 100-D Area continues to chemically reduce Cr(VI), but river protection is supplemented by the P&T system extraction wells. At the end of 2018, Cr(VI) concentrations at barrier wells ranged from below detection to 38 µg/L, with an overall decrease in concentrations compared to 2017 levels. The observed changes in Cr(VI) concentrations are attributed to a combination of residual chemical reduction by the ISRM PRB, as well as extraction and treatment of contaminated GW in areas where the PRB is no longer effective. Under the 2018 100-D/100-H Areas ROD,⁴ the ISRM barrier is not monitored separately from the P&T remedy (DOE-RL 2019a).

2.4.3 Removal, Treatment, and Disposal

Areas of persistent sources of Cr(VI) contamination have been identified (CH2M 2015). RTD has been used to remediate contaminated soil, structures, and debris (WCH 2012a,b; BHI 2000). Removal is accomplished by excavation and transport of material to the disposal site. If necessary, excavated material is treated to meet disposal facility requirements, protect workers, and prevent unacceptable environmental releases. Waste is then disposed at Hanford's Environmental Restoration Disposal Facility. Remediated sites are backfilled and contoured, and native vegetation reestablished.

100-D/DR and 100-H Areas: RTD actions have been used to address waste sites at 100-DR-1, 100-DR-2, 100-HR-1, and 100-HR-2 OUs. The 100-D/H ROD⁵ (EPA et al. 2018) identified CULs for the shallow zone [depth ≤4.6 m (15 ft) below ground surface] for protection of human health and the environment and for protection of GW and SW. In some cases, removal and disposal of contaminated sediments from just the shallow zone has been found to be insufficient, and additional excavation was required. Figure 2.14 shows an example (referred to as the “big dig”) from the 100-D Area, where extensive excavation was required to remove Cr-contaminated sediments.

¹ <http://pdw.hanford.gov/arpir/index.cfm/viewDoc?accession=D199159580>.

² <http://pdw.hanford.gov/arpir/index.cfm/viewDoc?accession=D1499872>

³ <http://pdw.hanford.gov/arpir/index.cfm/viewDoc?accession=1011290677>

⁴ <https://pdw.hanford.gov/arpir/pdf.cfm?accession=0065047H>.

⁵ <https://pdw.hanford.gov/arpir/index.cfm/viewDoc?accession=0065047H>



Figure 2.14. Tier III Excavation at 100-D-104 Looking West (March 3, 2014) (WCH 2015)

100-B/C Area: Chromium concentrations beneath waste sites in the 100-B/C Area were generally low. However, three waste sites (100-B-27, 100-C-7, and 100-C-7:1) within 100-B/C had more extensive contamination, requiring the entire vadose zone soil column to be excavated to the depth of the water table to remove Cr(VI)-contaminated soil (DOE-RL 2019b). Currently, the remedy for remaining Cr(VI) GW contamination in the 100-B/C area is MNA.

2.4.4 Soil Flushing

A rebound study was performed with the 100-KW P&T system between May 2016 and March 2017 (CH2M 2018). Within weeks following shutdown of the system to assess rebound, hexavalent chromium concentrations nearly tripled in several wells in the study area and later peaked at about 180 $\mu\text{g/L}$ in the upper portion of the unconfined aquifer (CH2M 2018b). The timing of the peaks and locations of impacted wells indicated that hexavalent chromium secondary source materials were present within and near the periodically rewetted zone. The continuing sources likely originated from historical handling, use, and accidental or intentional discharges of sodium dichromate solution that migrated vertically through the vadose zone. The hexavalent chromium in this area continues to be an ongoing source of contamination to the underlying GW and will likely result in longer GW remediation timeframes to achieve CULs protective of human health and aquatic organisms in the Columbia River.

In response to the results of the rebound study, a soil flushing treatability test (DOE-RL 2018) was approved by DOE and EPA to address the secondary source location near the 183.1 KW Headhouse. The

goal of soil flushing is to remove Cr(VI) from the deep portions of the vadose zone by flushing it into GW, and then capture the mobilized Cr(VI) with the active P&T system to remove it from the GW.

The soil flushing test was intended to remove a remaining area of Cr(VI) contamination in the 100 K Area.¹ The soil flushing treatability test started on May 28, 2019. As of August 12, 2019, approximately 26.7 million gallons of KW P&T effluent had been discharged to the ground via the leach field. KW extraction wells 199-K-166 and 199-K-205, and monitoring well 199-K-236, exhibited increased Cr(VI) concentration during the test. A final report on the results from this soil flushing test is scheduled to be published in fall 2020.

2.4.5 Natural Attenuation

Truex et al. (2015) conducted laboratory experiments to evaluate the potential for natural attenuation of Cr(VI) via reduction of aqueous Cr(VI) and co-precipitation and dissolution using 100 Area sediments and GW conditions. They determined that a combination of biotic and abiotic processes likely contributed to the reduction of Cr(VI) to functionally immobile Cr(III) that was observed in their experiments. The reduction process acted as a mechanism for removal of Cr(VI) from the aqueous phase. They also noted that co-precipitation of Cr(VI) with calcium carbonate minerals of moderate solubility could act as a solubility-controlled release mechanism that could slowly release aqueous Cr(VI) for transport through the vadose zone to GW.

2.5 Monitoring

Monitoring data collected from the 100 Area include water levels measured in GW monitoring wells, and aqueous chemistry data determined using samples collected from both monitoring wells and aquifer tubes. Aquifer tubes are small diameter (nominally 0.6 to 1.3 cm), flexible tubes that are screened on one end. Most aquifer tube sites include two or three individual tubes monitoring at different depths, from about 1 to 8 m below ground or riverbed surface. They are not constructed as resource protection wells, as specified in WAC 173-160,² and are therefore not formally used as compliance monitoring locations. However, aquifer tube data inform the development of GW plume maps in locations where plumes are immediately adjacent to the river.

Figure 2.15 shows the locations of GW wells and aquifer tubes that have been monitored in the 100 Areas. Table 2.2 lists the number of wells and aquifer tubes sampled in 2018 in the different GW OUs of the 100 Areas. The frequency of monitoring varies, depending on the type of sampling required to meet regulatory requirements, the history of concentrations for COCs in the wells, and the objectives of any particular study that may have been performed at a site.

¹ https://www.hanford.gov/files.cfm/FINAL_Soil_Flushing_Treatability_Testing.pdf

² <http://apps.leg.wa.gov/wac/default.aspx?cite=173-160>

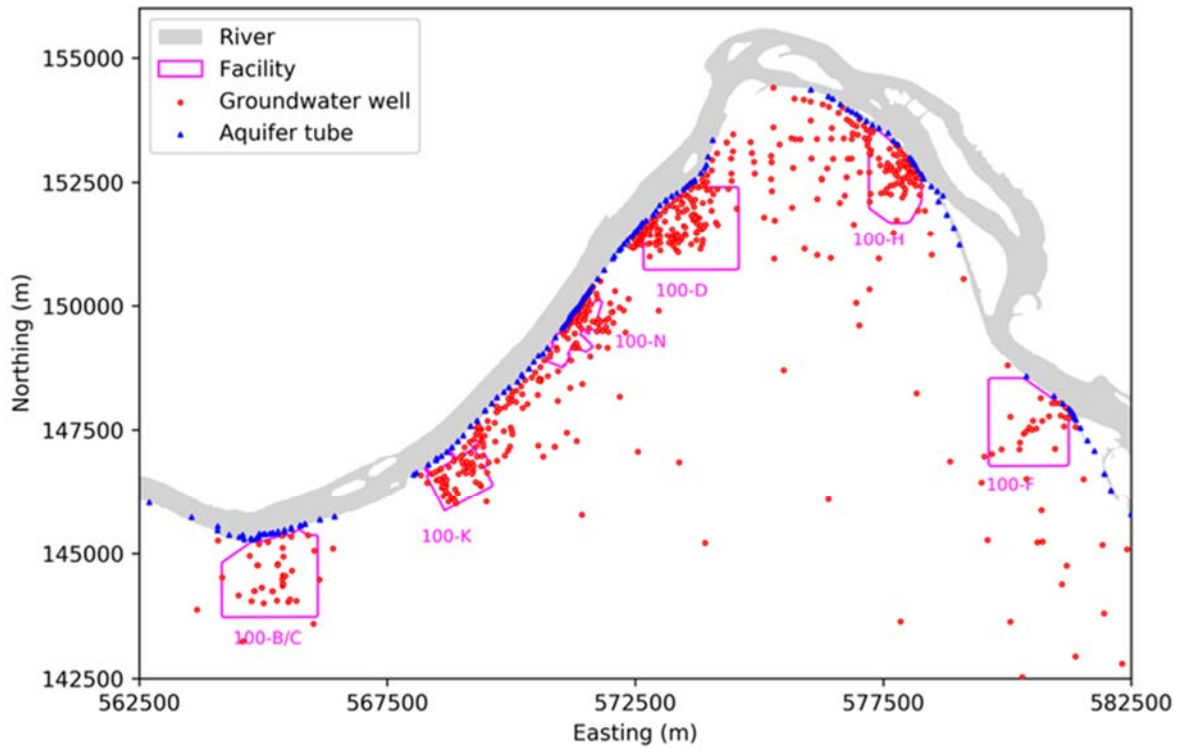


Figure 2.15. Map Showing Locations of GW Monitoring Wells (829) and Aquifer Tubes (365) in the Hanford 100 Areas from Which Cr(VI) Concentration Data were Collected Between Jan. 2010 and Feb. 2020

Table 2.2. GW Sampling Trips in 2018 (after Table 1-2 of DOE-RL 2019a)

Interest Area	Number of Wells Sampled	Number of Successful Well Trips	Number of Aquifer Tubes Sampled	Number of Successful Aquifer Tube Trips
100-BC	32	39	25	30
100-FR	39	78	9	9
100-HR-D	121	743	21	21
100-HR-H	103	688	20	20
100-KR	107	720	54	70
100-NR	100	200	41	64

Figure 2.16 through Figure 2.21 depict some of the variables that are measured and the number of measurements that were made for each of the variables in different wells for all of the 100 Area sites over the 10-year period from 2010-2019. These figures are shown to illustrate the differences in the number of monitoring locations and frequency of monitoring for the different areas. The number of wells and aquifer tubes that are monitored, and monitoring frequency, is higher at sites with active P&T operations (i.e., 100-KR, 100-HR-D, 100-HR-H). Some of the sample data represented in Figure 2.16 through Figure 2.21 were used for analyses reported later in Section 3.0 of this report. In Figure 2.16 through Figure 2.21, “Index” is an integer identifier for each of the wells or aquifer tubes in each OU.

The frequency of aqueous sample collection from GW monitoring wells typically varies from annual to quarterly, depending on site/well history and remediation activities. DOE typically collects GW samples from shoreline seeps and aquifer sampling tubes (Figure 2.1) in the fall when the river stage is low (DOE-RL 2019a). Higher frequency (e.g., monthly) sampling has also been performed at some 100 Area sites for special studies (DOE/RL 2019b; CH2M 2015b).

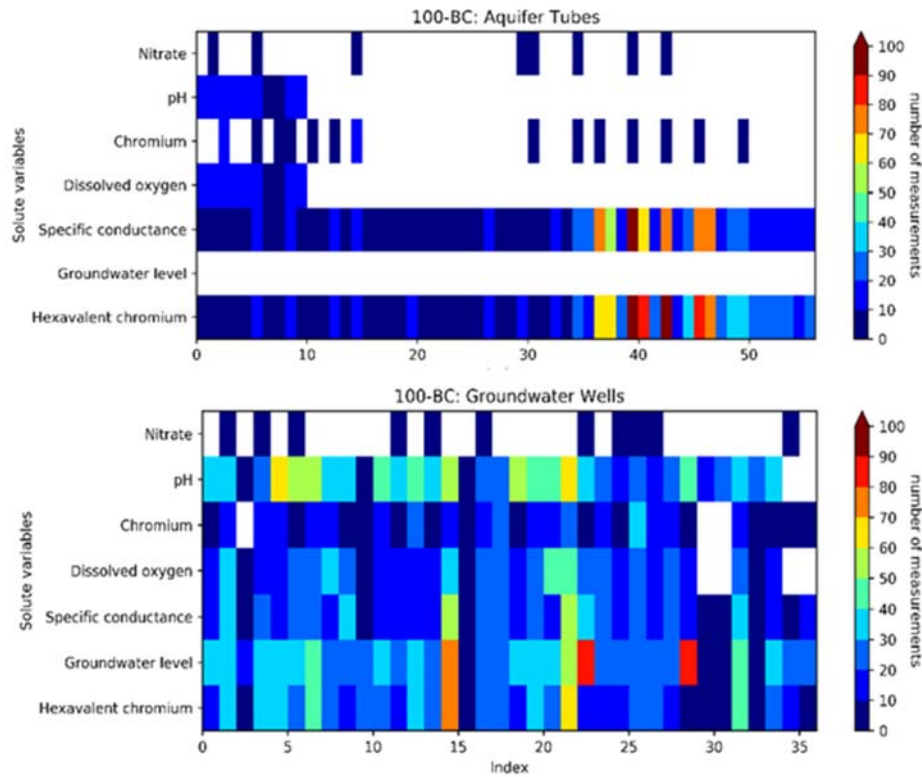


Figure 2.16. Types and Numbers of Samples for Aquifer Tubes and Wells in 100-BC OU. Index is an integer identifier for each well or aquifer tube.

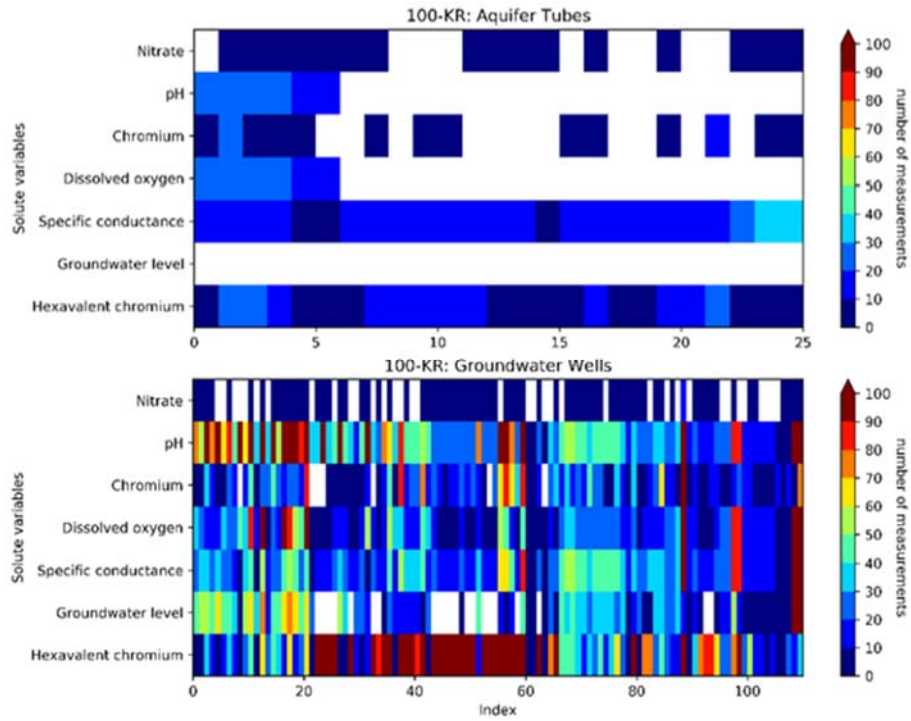


Figure 2.17. Types and Numbers of Samples for Aquifer Tubes and Wells in 100-KR OU. Index is an integer identifier for each well or aquifer tube.

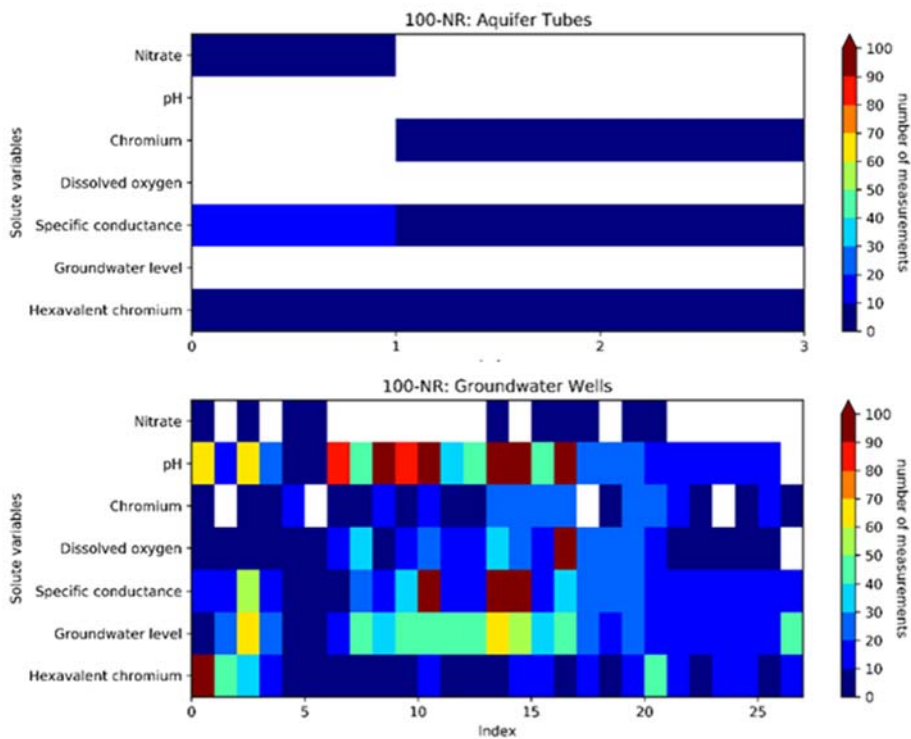


Figure 2.18. Types and Numbers of Samples for Aquifer Tubes and Wells in 100-NR OU. Index is an integer identifier for each well or aquifer tube.

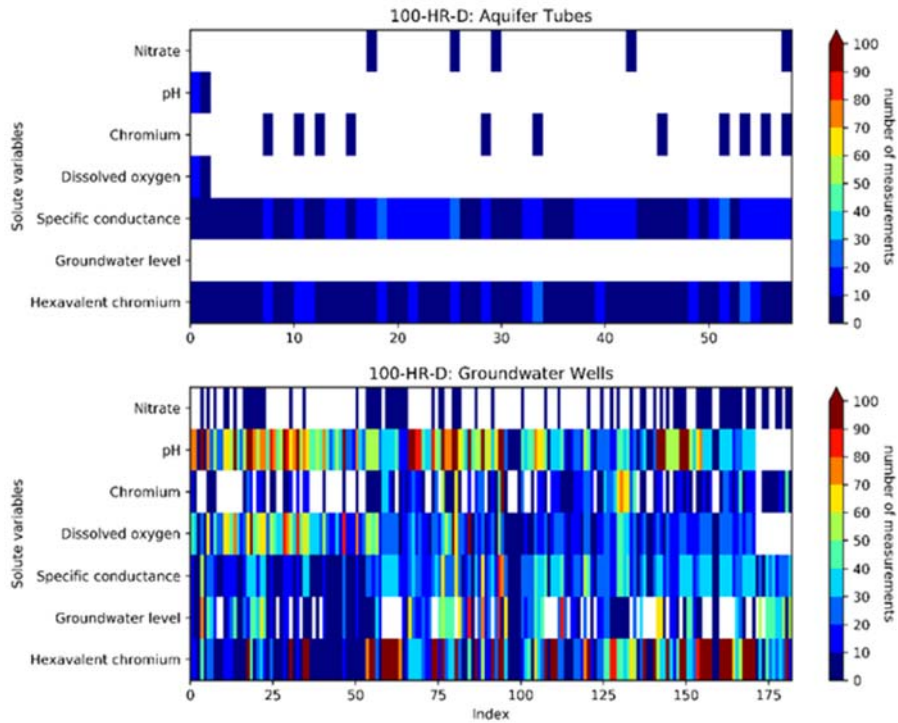


Figure 2.19. Types and Numbers of Samples for Aquifer Tubes and Wells in 100-HR-D OU. Index is an integer identifier for each well or aquifer tube.

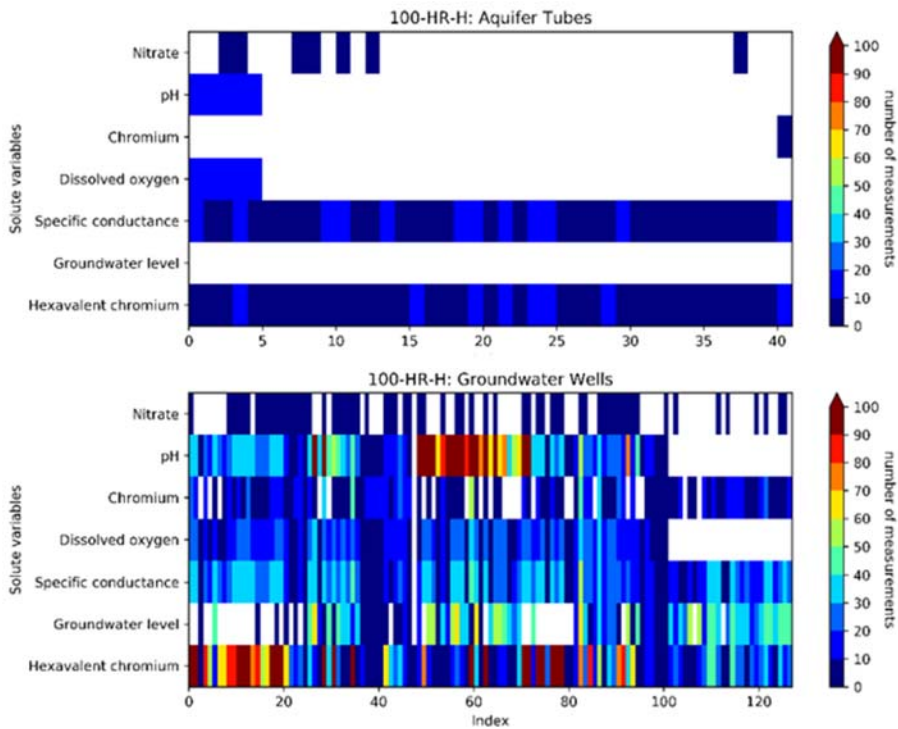


Figure 2.20. Types and Numbers of Samples for Aquifer Tubes and Wells in 100-HR-H OU. Index is an integer identifier for each well or aquifer tube.

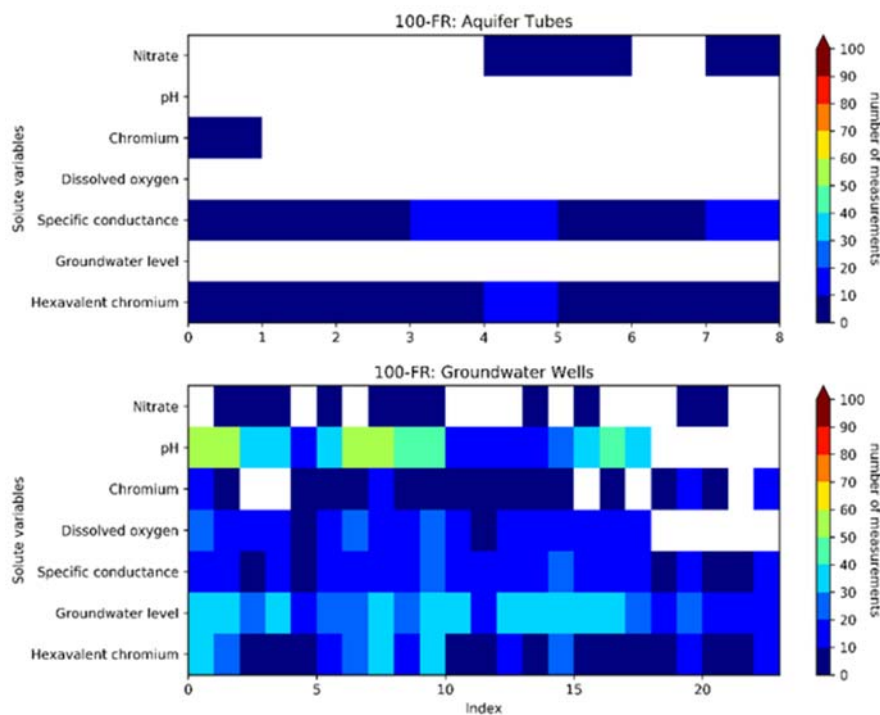


Figure 2.21. Types and Numbers of Samples for Aquifer Tubes and Wells in 100-FR OU. Index is an integer identifier for each well or aquifer tube.

As indicated by Figure 2.16 through Figure 2.21, aqueous Cr(VI) concentration and specific conductance are the two most commonly measured variables for most of the aquifer tubes and wells. Specific conductance is of interest, in part, because the average specific conductance of river water is $\sim 130 \mu\text{S}/\text{cm}$ (DOE-RL 2019b), which is factor of 3 or more lower than typical GW specific conductance values. Therefore, specific conductance can potentially provide an indicator of dilution of GW by river water (Song et al. 2020).

2.5.1 Aqueous Chemistry

Aqueous chemistry data, including all major cations and anions, and COCs, is usually measured on aqueous samples collected from GW monitoring wells. Additional water quality variables such as pH, dissolved oxygen, carbonates, and specific conductance are typically also measured. These data can be used for a variety of purposes, including the evaluation of eH-pH conditions to determine what Cr species are dominant. Cr(VI) has been determined to be the dominant species under the prevailing conditions in the unconfined aquifer, but reducing and anoxic conditions more favorable to Cr(III) may be present at depth in the lower permeability Ringold sediments. Similar data are often measured for samples collected from aquifer tubes, but the measurement frequency differs. Data analysis presented later in this report focuses primarily on Cr(VI), but correlations between Cr(VI) concentrations and specific conductance are also examined.

2.5.2 GW Levels

In March of each year, water levels are measured using an extensive network of wells. In many areas of the Hanford Site, water levels are measured more frequently to evaluate seasonal changes. CH2M (2018) describes the collection and analysis of manual water-level measurements at the Hanford Site. Hartman (2018) describes how the water table map (Figure 2.22) is constructed.

In addition to manual measurements, an automated water-level network (AWLN) is maintained. Data from the AWLN were not used for analyses reported in this document because the high frequency of these data were not needed to establish longer-term trends. These data are very useful in areas where water levels change rapidly to define head gradients and flow directions, and for capture zone analysis (CH2M 2013), and model calibration. The AWLN consists of wells that are typically equipped with pressure transducers, and specific conductance and temperature sensors, connected to dataloggers. AWLN data are typically collected at relatively high frequency (e.g., hourly for wells in the river corridor). The AWLN locations are connected to telemetry network from which data are automatically transferred to a central base station. By the end of December 2018, there were 189 AWLN stations operating at the Hanford Site. Note that Figure 2.16 through Figure 2.21 do not include water-level data from AWLN.

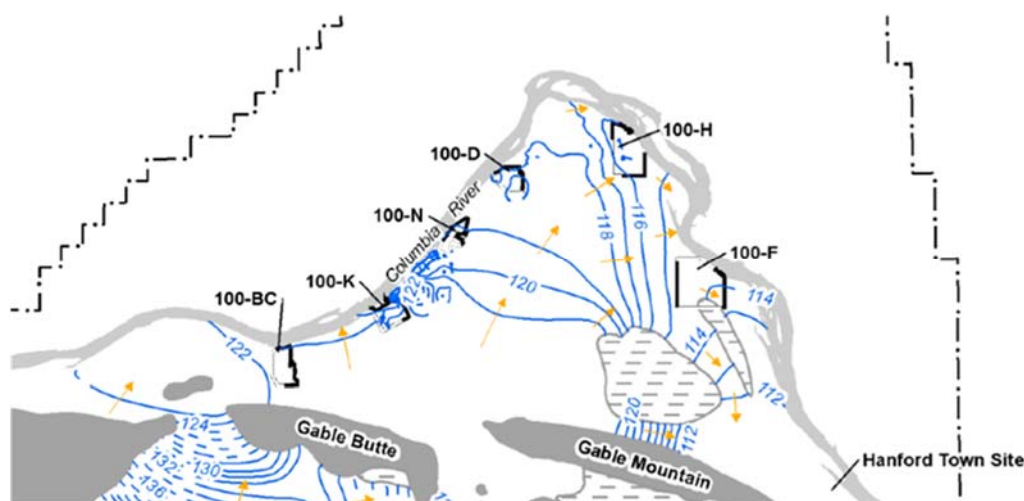


Figure 2.22. Hanford Site Water Table (blue lines) and Directions (orange arrowed lines) of GW Flow in 2018 (Modified after Fig. 1-2 of DOE-RL 2019a). Elevation reference: NAVD88.

2.6 Modeling

A calibrated GW flow and transport model for the aggregate 100 Areas (100AGWM) has been developed to assess and optimize the performance of the P&T remedy in the 100 Areas (ECF-HANFORD-19-0011, Rev. 0). The model is periodically updated and recalibrated to account for new characterization and monitoring data, and an update of the 100AGWM is currently in progress.

CH2M (2013) describes the development of a method for using site monitoring data, and the 100AGWM, for capture frequency analysis to evaluate the protectiveness of the P&T and MNA remedies in preventing Cr(VI) concentrations above the target 10 $\mu\text{g/L}$ SW CUL from entering the Columbia River. The concept of hydraulic containment (capture) was used to develop an integrated assessment of remedy performance and to evaluate the relative protectiveness at different points along the shoreline of each 100 Area GW OU. Point locations were categorized as follows (CH2M, 2013):

1. “Groundwater is contaminated above standards, but inland contamination is hydraulically contained, or groundwater exhibits concentrations below standards such that hydraulic containment is not required. Interpretation: the required River Protection Objective is being met.”
2. “Groundwater is contaminated above standards and inland contamination is not hydraulically contained, however hydraulic gradients and concentration trends suggest there is limited net migration toward the Columbia River such that the river is not threatened by discharge of inland contamination. Interpretation: the required River Protection Objective is being met. However, although the Columbia River is not immediately threatened by contamination, action may be required to ensure that the River Protection Objective is met of the longer-term.”
3. “Groundwater is contaminated above standards and inland contamination is not hydraulically contained, and hydraulic gradients and concentration trends suggest there is the potential for significant net migration toward the Columbia River, such that the river is potentially threatened by discharges of inland contamination. Interpretation: the required River Protection Objective is not being met. If a remedy is in place to achieve the River Protection Objective, the remedy is likely underperforming and additional action is required to achieve the River Protection Objective.”

Figure 2.3 shows some results from this analysis for the 100-H Area for calendar year 2018. This analysis has been applied to all of the 100 Area sites and is repeated periodically to assess the degree to which site remediation activities are protecting the Columbia River.

The 100AGWM represents the aggregate 100 Areas, but local models have also been developed to evaluate the effectiveness of P&T and MNA for specific GW OUs areas, and to forecast the time required to achieve CULs under different scenarios. For example, CH2M (2014) developed a three-dimensional GW flow and transport model of the 100-H Area and used it to assess the time required to meet the 10 µg/L CUL during a 25-year period with active P&T for different scenarios involving upward and downward hydraulic gradients with and without a source of Cr(VI) in the RUM aquitard. The simulation results predicted that with no source of Cr(VI) in the RUM aquitard, and an upward hydraulic gradient, the mean time after implementation of P&T to achieve the 10 µg/L CUL was 9 years. With a source of Cr(VI) in the RUM aquitard, and a downward hydraulic gradient, the predicted mean and maximum times to achieve the 10 µg/L CUL were 19.7 years and 69 years, respectively. CH2M (2016) developed a similar calibrated three-dimensional GW flow and transport model of the 100-B/C Area (Figure 2.4) and used it to forecast the time required to reach the 10 µg/L SW CUL under the current MNA remedy at that site (Figure 2.5). Simulation results suggest that it could take up to 125 years to achieve the 10 µg/L CUL at the 100-BC OU using MNA. While the simulations for both areas addressed Cr(VI) contamination in the aquifer, neither considered possible continuing sources of Cr(VI) from the vadose zone, which could lengthen the time required to achieve target CULs.

Peterson and Connelly (2001) performed two-dimensional simulations of tracer transport in a vertical cross section through the 100-H Area to evaluate flow paths within the zone of GW-river water exchange flows. Their analysis concluded that a dilution factor of 50% (equal parts GW and river water) was a reasonable assumption for the zone of GW-river water interaction. Shuai et al. (2019) developed a GW model for the river corridor of the Hanford Site to evaluate the effects of river stage fluctuations, channel morphology, and subsurface hydrogeology on hydrologic exchange flows across the river-aquifer interface. Results indicate that due to the high hydraulic conductivity of the Hanford formation sediments, river water can penetrate several kilometers inland. Their simulation results also indicated that some river water can flow through the aquifer from the 100-BC Area to the 100-F Area.

Song et al. (2020) developed a more refined model of the area between the 100-D and 100-H Areas, known as the “horn.” Flow fields from the model were used with particle tracking to illustrate the potential impacts of river stage fluctuations and subsurface features on hydrologic exchange flows and

residence times. River fluctuations were found to have the largest impacts on aquifer water compositions in areas dominated by GW upwelling, and the exchange flux was found to be mainly influenced by the thickness of the high permeability Hanford formation. The residence time of particles was shown to be influenced by multiple factors and exhibited complex patterns.

All field-scale modeling efforts for Cr(VI) transport in the 100 Area that have been performed to date have represented sorption as an equilibrium process using the well-known linear Freundlich isotherm (or distribution coefficient [K_d]) model (Domenico and Schwartz 1998). Laboratory experimental studies suggest that a large fraction (up to 95%) of Cr(VI) contamination is readily removable, and the K_d model likely provides a good description of sorption for this fraction. However, laboratory studies also indicate that there are recalcitrant fractions that may not be well represented by a K_d model. A two-site model was shown to provide a good description of Cr(VI) desorption profiles of both aged and freshly contaminated sediments (Dresel et al. 2008). Calculated equilibrium and kinetic site K_d and rate constants were sediment dependent. Observed nonequilibrium Cr(VI) desorption behavior was attributed to mass transfer from poorly accessible domains within the sediment matrix.

Based on the review of modeling performed for P&T optimization and identifying GW and SW interactions, the following general observations are made:

- River water can move several hundred meters or more inland through the higher permeability Hanford formation sediments during prolonged periods of HRS.
- River water incursion is less extensive in the underlying, lower permeability Ringold Formation sediments.
- Cr(VI) contamination in the RUM aquifer may provide a continuing source of Cr(VI) for the overlying unconfined aquifer.
- In spite of RTD of contaminated sediments from known waste disposal sites, residual contamination remains in the vadose zone and periodically rewetted zone (PRZ), as evidenced by locally elevated Cr(VI) concentrations during HRS conditions.
- Remaining vadose zone contamination can provide a continuing source of GW contamination that is accessed and partially mobilized during periods of HRS.

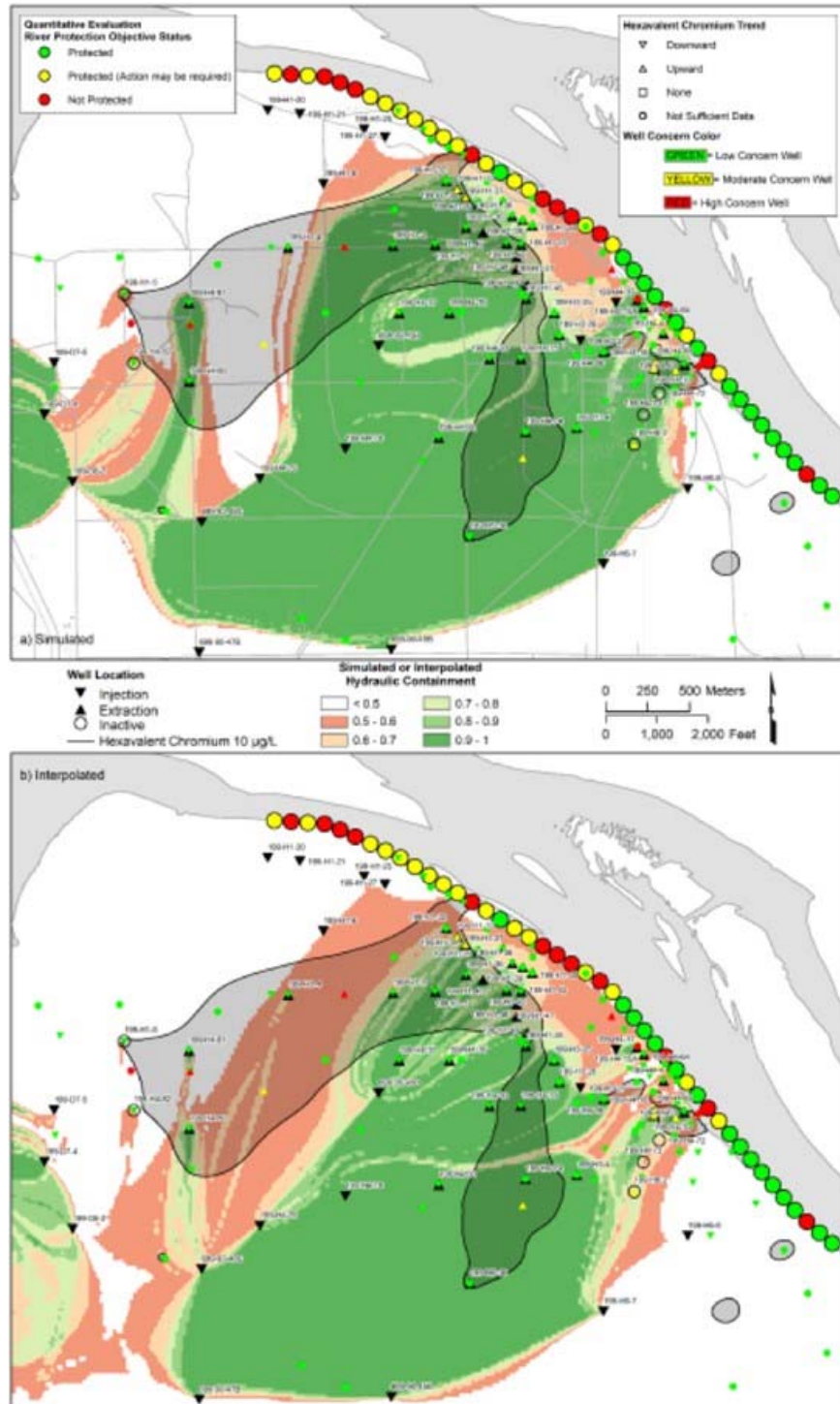


Figure 2.23. Assessment of the Length of Shoreline Protected from Further Discharges of Chromium along the 100-H Area, together with Mapped Extent of Chromium Contamination above 10 µg/L. Results from a Standard Test and Trend Test and an Interpolated Capture Frequency Map (a), and a Simulated Capture Frequency Map (b). (Fig 7.29 from CH2M, 2019)

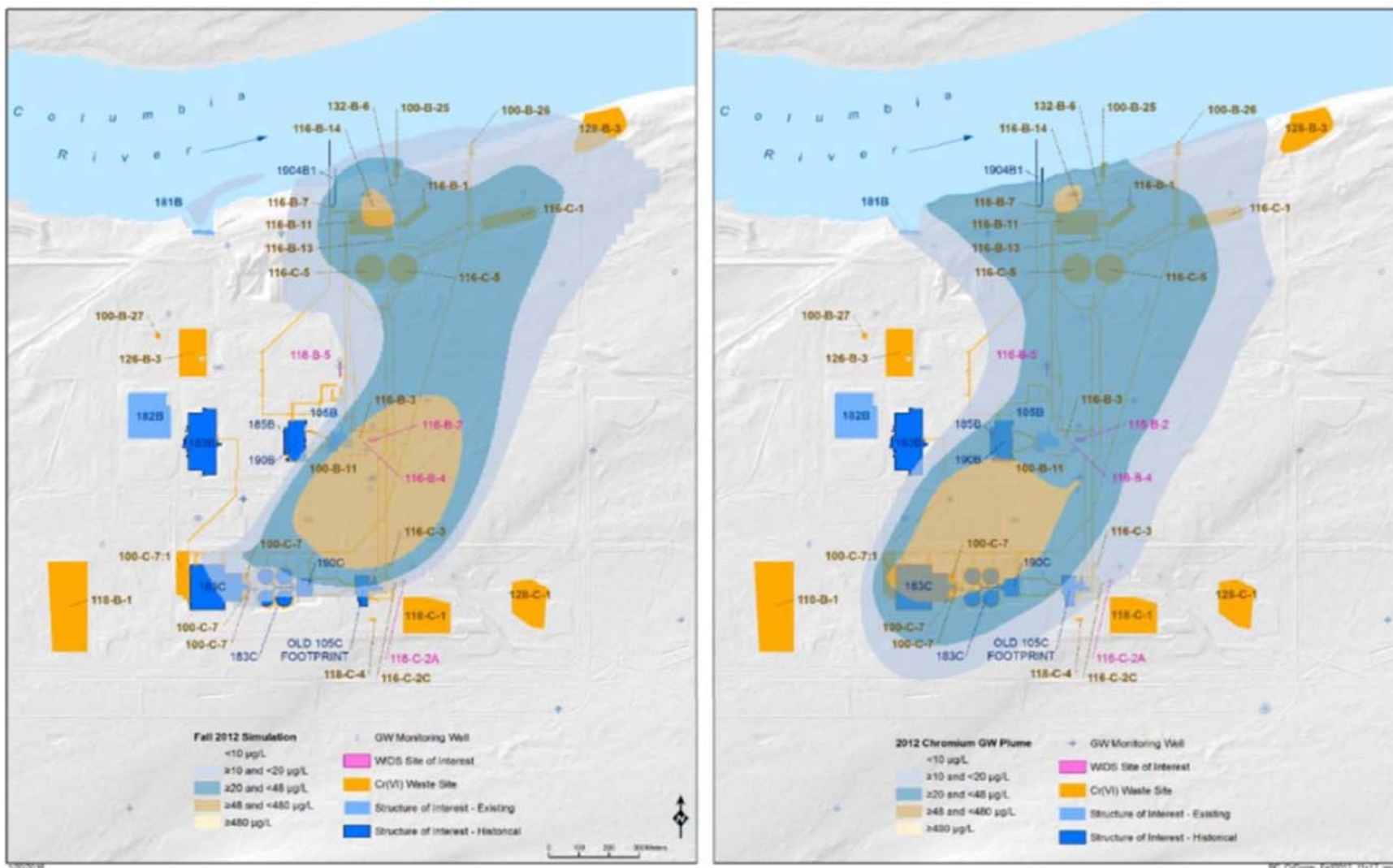


Figure 2.24. Simulated (Left) and Mapped (Right) Fall 2012 Cr(VI) Top of Unconfined Aquifer Plume for 100-B/C (after Fig. 5-12, p. 5-70 in DOE-RL 2019b)

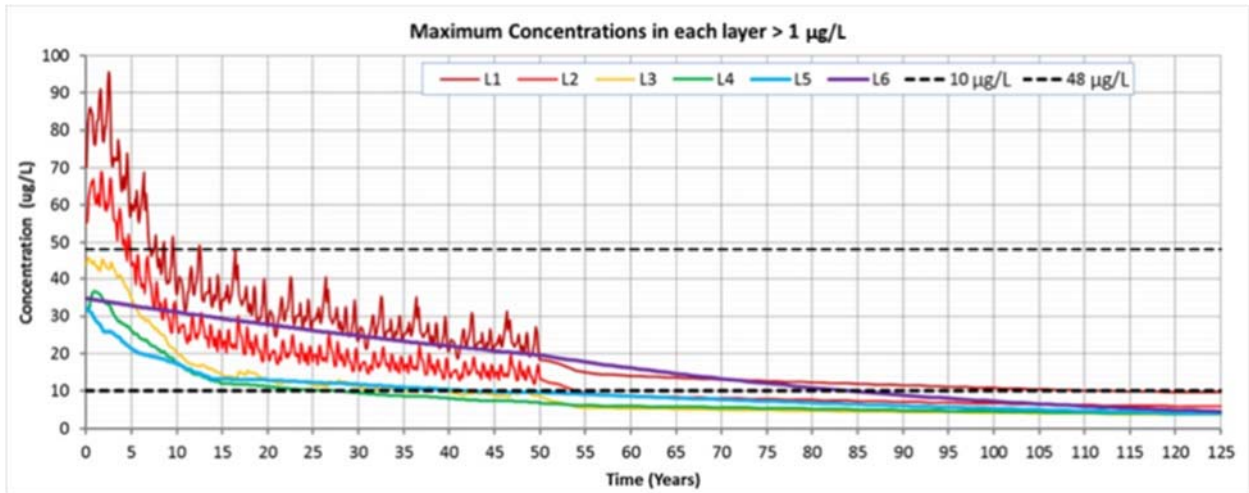


Figure 2.25. Maximum Simulated Cr(VI) Concentration for No Further Action Case by Model Layer over 125 Years for 100-B./C (after Fig. 5-20, p. 5-79, in DOE-RL 2019b)

3.0 Analysis of GW Monitoring Data

The primary objective of this work was to identify possible relationships between Cr(VI) inland and shoreline concentrations. If consistent relationships exist between Cr(VI) concentrations and distance to shoreline, this information can potentially be used as a basis for selecting existing wells, or locating new wells, to monitor compliance with target CULs. Some field observations suggest that there may be relatively little dilution of GW concentrations in the nearshore environment just below the riverbed, especially during LRS when GW discharges to the river. Under these conditions, benthic organisms may be exposed to Cr(VI) concentrations that are nearly as high as in the inland GW plumes. If GW plume concentrations can be reduced to the SW CUL, then concentrations entering the river should be less than the SW CUL, thus protecting the aquatic ecosystem.

Aquifer tubes are typically sampled only in the fall when Cr(VI) concentrations measured from these devices are highest. The fall months happen to be the time period when salmon, a keystone species, are spawning in the Hanford Reach, so focused monitoring only at this time of year is a logical and cost-saving approach relative to more frequent sampling. Logistically, it is also much easier and safer to collect aquifer tube samples in the fall, when the river stage is low. However, the limited sampling of the shallow riverbed sediments raises questions about how well these data represent the actual Cr(VI) concentrations throughout the year.

Additional analyses were also performed to provide a more complete understanding of Cr(VI) plume dynamics and remediation progress. The analysis steps and purpose of each are as follows:

1. Examine correlations between Cr(VI) concentration data and specific conductance data to evaluate dilution effects and representativeness of aquifer tube annual sampling (DOE/RL 2019a). The focus of this analysis was on the 100-BC Area because it has more aquifer tube and hyporheic zone samplers with higher frequency of sampling.
2. Analyze GW and aquifer tube Cr(VI) concentrations versus distance to shoreline within each GW OU to identify possible spatial trends. Data from both Hanford Environmental Information System (HEIS) and interpreted plume maps are used for this analysis.
3. Calculate centers of Cr(VI) plume mass and their changes over time to evaluate plume trajectories as influenced by P&T activities and natural gradients.
4. Perform cluster analysis to evaluate similarities in time series of Cr(VI) concentration data from wells and aquifer tubes to identify possible patterns in the spatial arrangements of well clusters. If consistent relationships exist between Cr(VI) concentrations and distance to shoreline, these relationships should also be evident in the clustering results.
5. Evaluate trends in Cr(VI) concentrations from wells and aquifer tubes to determine monitoring locations showing decreasing or increasing trends or no detectable change. Results may be used to determine potential locations where continuing sources of Cr(VI) contamination may exist in the vadose zone or PRZ, and where other focused remediation efforts like soil flushing may be beneficial.

Two types of data were used for the analyses reported here:

1. Aqueous Cr(VI) concentration and specific conductance data for GW wells, aquifer tubes, and hyporheic zone samplers from the HEIS database (Environmental Dashboard Application; <https://ehs.hanford.gov/eda>; accessed 13-Aug-2020)

2. Interpreted Cr(VI) plume data for LRS and HRS that have been reported in annual Hanford Site-wide GW monitoring reports (DOE/RL 2019a)

In addition to the above analyses, probability density and cumulative probability distributions were computed for the fraction of wells with concentrations below surface and GW CULs. Although these metrics do not directly address spatial concentration distributions, they do quantify collective concentration changes occurring over the 10-year analysis period.

All analyses were based on historical records for a 10-year time period from 2010 through 2019. The locations of the GW monitoring wells and aquifer tubes are shown in Figure 2.17. GW monitoring wells throughout most of the 100 Areas are usually sampled less than 10 times a year, with the exception of some monitoring wells in the 100-KR, 100-HR-D, and 100-HR-H OUs that are sampled more frequently. Aquifer tubes are typically sampled just once a year, in the fall, when concentrations are usually highest. One exception is that some aquifer tubes and hyporheic zone samplers in the 100-BC OU were sampled more frequently (>10 times annually) in 2014-2015 to provide better understanding of natural attenuation processes (DOE/RL-2010-96, Rev. 0; SGW-58308, Rev. 0). Some of the analyses described above have a minimum data requirement (e.g., trend analysis requires at least 10 data points), so the analyses were performed only if sufficient data were available.

3.1 Correlations

As noted in Section 2.4, specific conductance and Cr(VI) were the two most commonly measured variables in both GW wells and aquifer tubes over the 2010-2019 time period. Higher frequency sampling of aquifer tubes and hyporheic zone samplers was done in the 100-BC Area in 2014-2015 to provide better understanding of natural attenuation processes (DOE/RL-2010-96, Rev. 0; SGW-58308, Rev. 0). Results and conclusions from 100-BC are assumed to be more broadly applicable, with the caveat that site-specific details of the hydrogeology, monitoring networks, and the remediation approaches being used at each site differ.

Figure 3.1 shows time series of Cr(VI) and specific conductance data from aquifer tubes and hyporheic zone samplers in the 100-B/C OU in 2014-2015, together with river stage measured at USGS river gauging station 12472800 (located downstream of Priest Rapids Dam). As noted previously, the average specific conductance of Columbia River water is 130 $\mu\text{S}/\text{cm}$ (DOE/RL-2010-96, Rev. 0). Figure 3.1 shows that the specific conductance values measured for samples from these aquifer tubes and hyporheic zone samplers are generally about 2 to 3 times higher than the expected concentrations for river water, indicating that the aquifer tube and hyporheic zone sampler data in this area are more representative of GW concentrations.

The concentration trends for Cr(VI) and specific conductance shown in Figure 3.1 are consistent for many of the aquifer tube and hyporheic zone sampling locations, with Cr(VI) concentrations rising and falling largely in sync with changes in specific conductance. For some of the sampling locations, the changes in Cr(VI) concentrations and specific conductance values are out of phase with the river stage (e.g. C8852, C8856), reflecting some river dilution effects. For other locations, Cr(VI) concentrations and specific conductance values are relatively constant in time (e.g. C8861, C9441), indicating relatively little dilution. Overall, given the generally high specific conductance values measured in the aquifer tubes and hyporheic zone samplers relative to average river water conditions, dilution effects at this site appear to be relatively minor.

The variability in observed behavior for the aquifer tube and hyporheic zone sampling locations at the 100-BC OU illustrates a fundamental challenge in the 100 Areas of determining which sampling locations are most representative of a site or area. If an aquifer tube or hyporheic zone sampler is located in high

permeability sediments of the Hanford formation or Ringold unit E, it will likely exhibit more significant river dilution effects. Otherwise, if it is located in lower permeability sediments, it will not be influenced as much by changes in river stage. Cr(VI) groundwater contamination is known to exist in both unconfined and confined aquifer systems in the 100 Areas, so determining optimal riverbed sampling locations is not straightforward.

The measured specific conductance at a particular well or aquifer tube location and time, the maximum observed specific conductance at that location, and the average specific conductance of river water can potentially be used to estimate river water and GW mixing (Zachara et al. 2020). However, specific conductance represents an integrated measure of the contributions from all ionic solutes present in a water sample, including highly conductive species such as nitrate, and results should be interpreted accordingly.

The magnitude of the specific conductance data shown in Figure 3.1 is approximately a factor of 20 greater than the Cr(VI) data. The two data sets were standardized by calculating their coefficients of variation (standard deviation/mean). The probability density versus coefficient of variation is plotted in Figure 3.2, which provides another way of assessing similarity of these two variables. Although there is not a 1:1 correspondence between the behavior of specific conductance and Cr(VI), further analysis of the specific conductance data is useful for qualitative assessment of potential dilution effects.

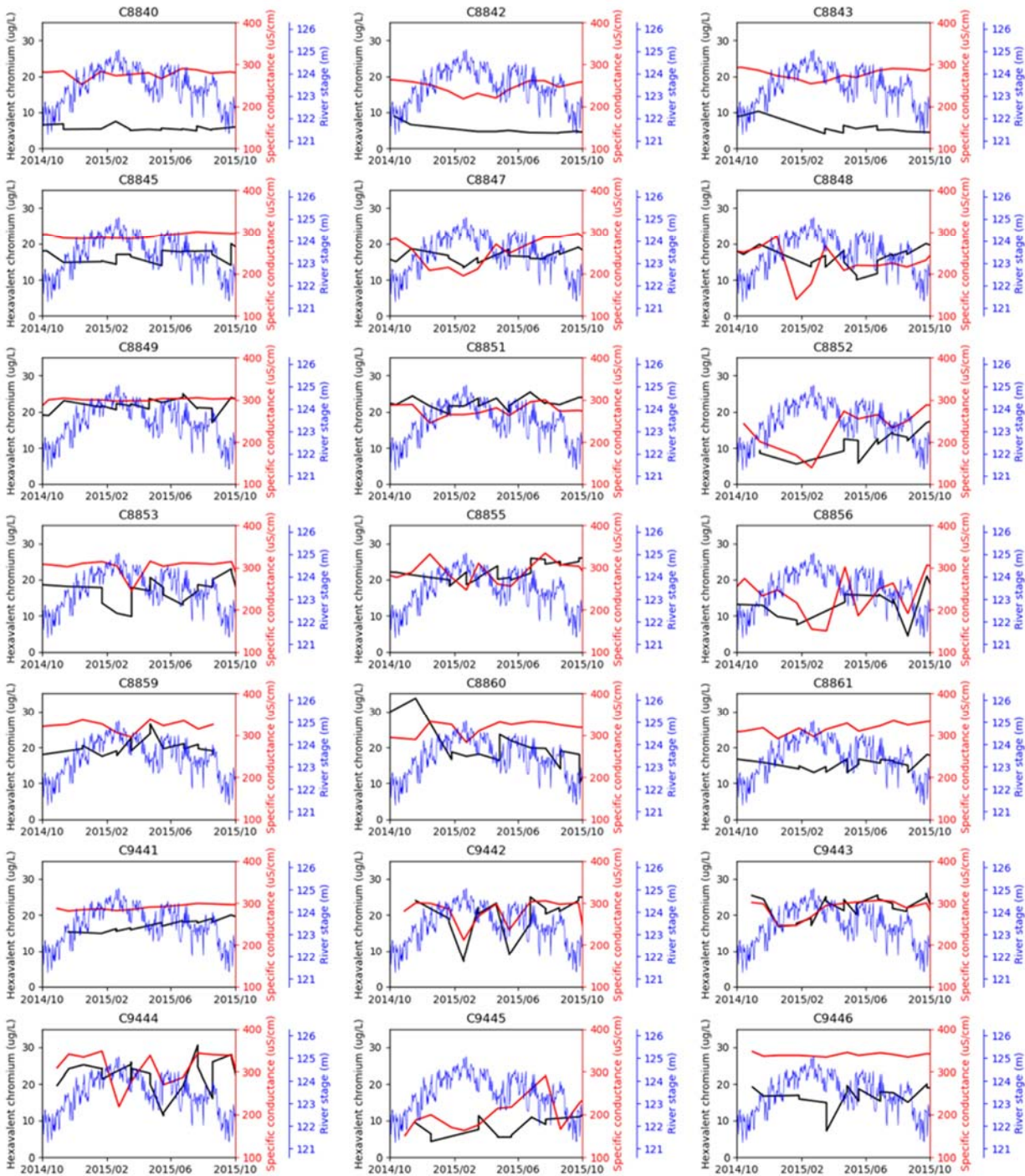


Figure 3.1. Time Series Data for Hexavalent Chromium and Specific Conductance Measured in Aquifer Tubes and Hyporheic Zone Samplers from the 100-BC OU and River Stage at USGS River Gauging Station 12472800 (located downstream of Priest Rapids Dam) in 2014-2015

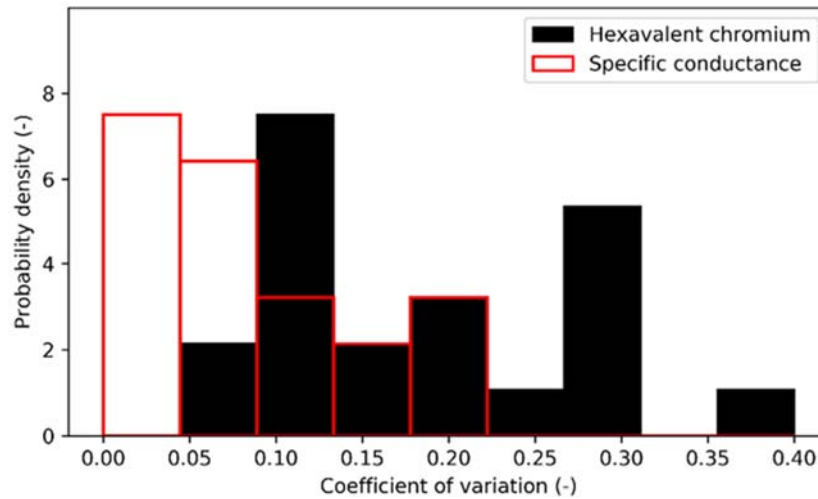


Figure 3.2. Coefficient of Variation (Standard Deviation/Mean) of Hexavalent Chromium and Specific Conductance Data from Aquifer Tubes in the 100-BC OU for 2014-2015

Figure 3.3 shows the discrete measurements of specific conductance that were collected in monitoring wells and aquifer tubes for 100-B/C over the 2010-2019 time period. Specific conductance data potentially provide in indicator of mixing between river and GW, if interference from comingled contaminant plumes in GW is limited. Note the higher frequency data collection during 2014-2015. Figure 3.4 shows the same data by day of year, which highlights the more frequent (roughly monthly) sampling during 2014-2015.

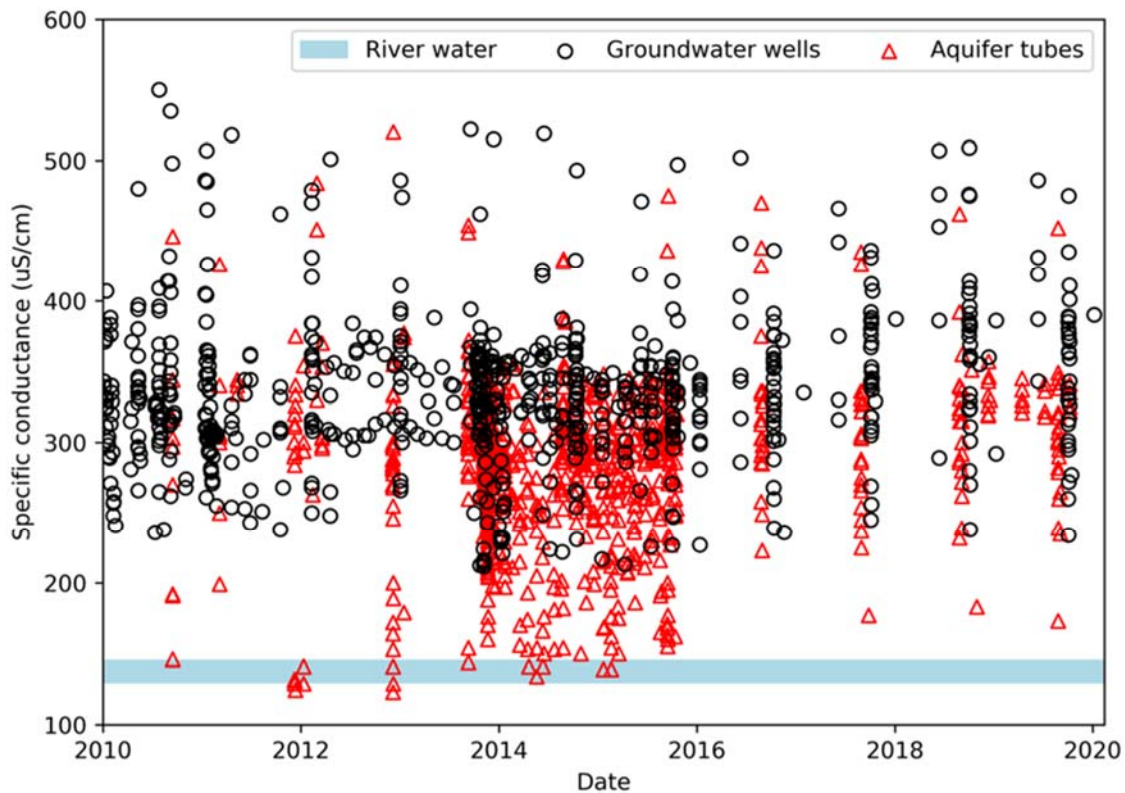


Figure 3.3. Specific Conductance Data from 100-BC for Years 2010 to 2019

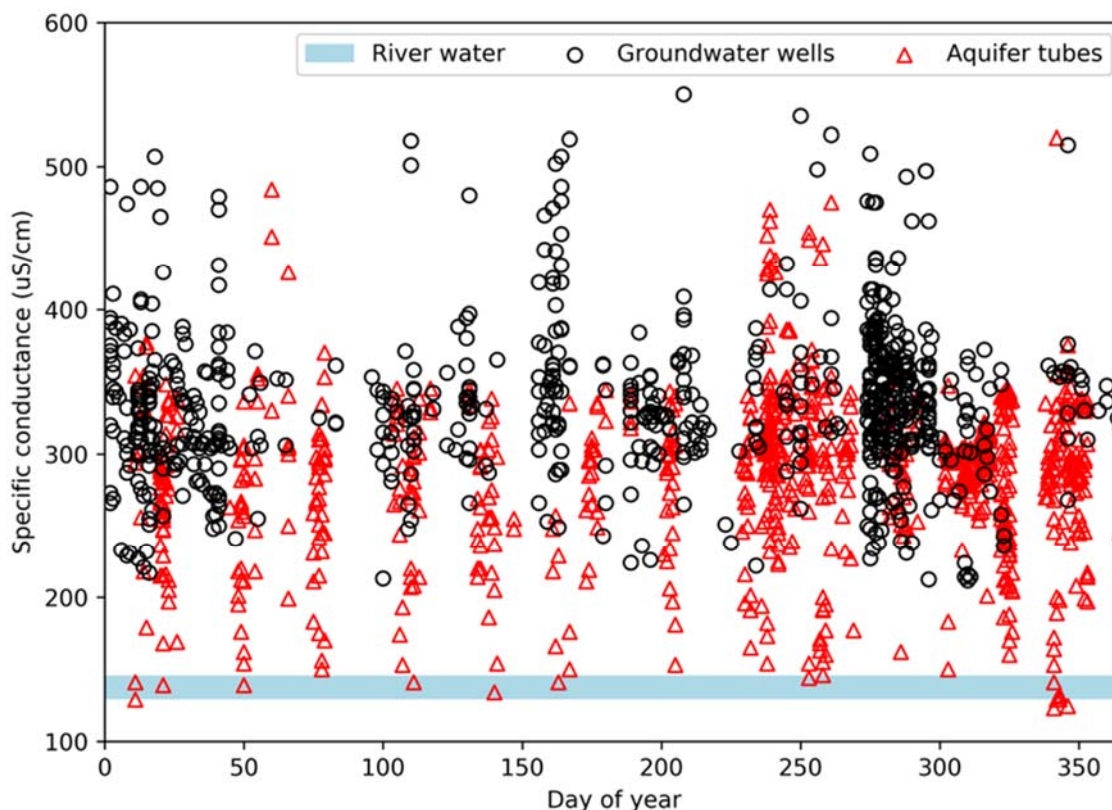


Figure 3.4. Specific Conductance Data by Day of Year for 100-BC for Years 2010 through 2019

Figure 3.3 and Figure 3.4 also show the approximate specific conductance of river water. These high specific conductance data suggest that there is relatively little dilution of GW in the shallow riverbed sediments underlying the river at 100-BC, except during prolonged periods of HRS (also see discussion for Figure 3.1). These results suggest that many of the aquifer tubes and hyporheic zone sampling points off of the 100-BC shoreline are located in relatively low permeability sediments, and these sediments are hydraulically connected to the aquifer and inland Cr(VI) GW plume.

Figure 3.5 shows the same specific conductance data, but as a function of distance to the shoreline, with positive distances representing inland GW monitoring wells and negative distances representing aquifer tubes. Therefore, points located to the left of zero on the x axis of Figure 3.5 represent aquifer tube locations in the river. This plot shows that the highest specific conductance values have been measured in the wells that are the closest to the shoreline. Plume maps for the 100-BC also show that Cr(VI) concentrations are highest in areas immediately adjacent to the river. The notion that Cr(VI) concentrations decrease as the plume approaches the shoreline is clearly not applicable to the 100-BC Area.

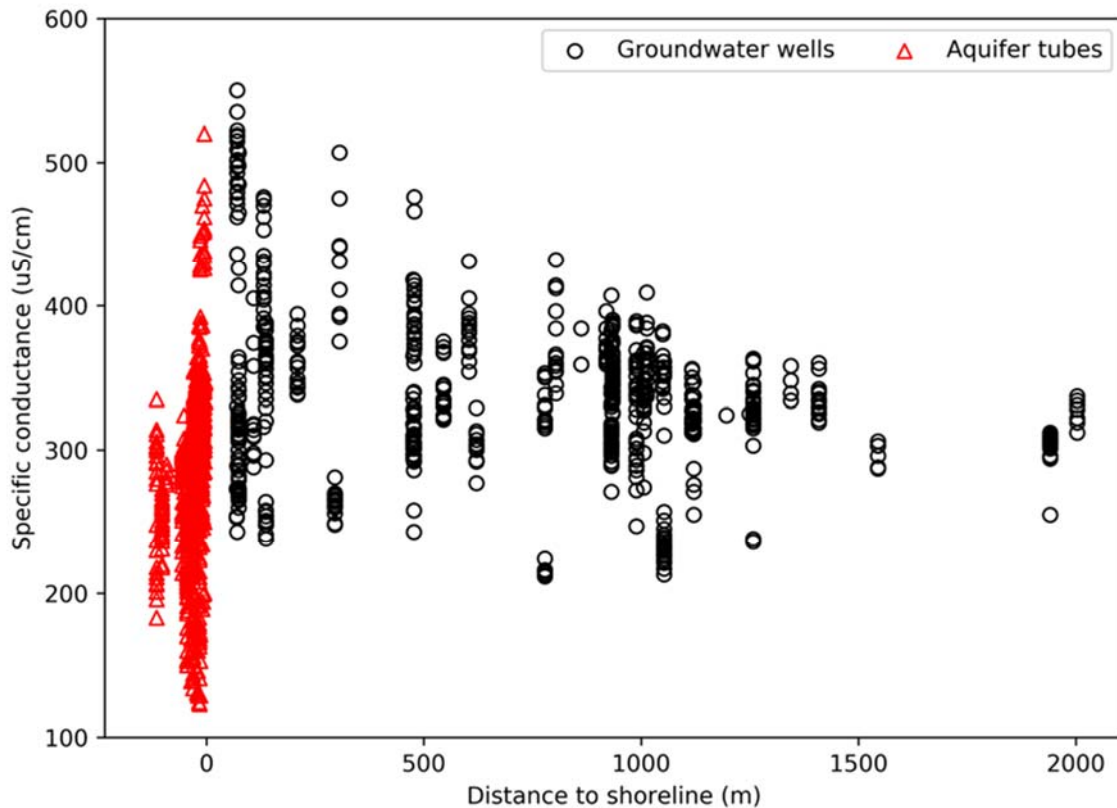


Figure 3.5. Variations in Specific Conductance Measurements with Distance from Shoreline in 100-BC

3.2 Concentrations Versus Distance to Shoreline

The primary objective of identifying relationships, if any, between inland and shoreline Cr(VI) concentrations was carried out using data measured in inland GW monitoring wells and aquifer tubes located in the riverbed.

3.2.1 HEIS Data

In Figure 3.6 through Figure 3.11, Cr(VI) aqueous concentration data from 2010 (top figures) and 2019 (bottom figures) from the HEIS database are plotted versus distance to the shoreline for the 100 Areas.

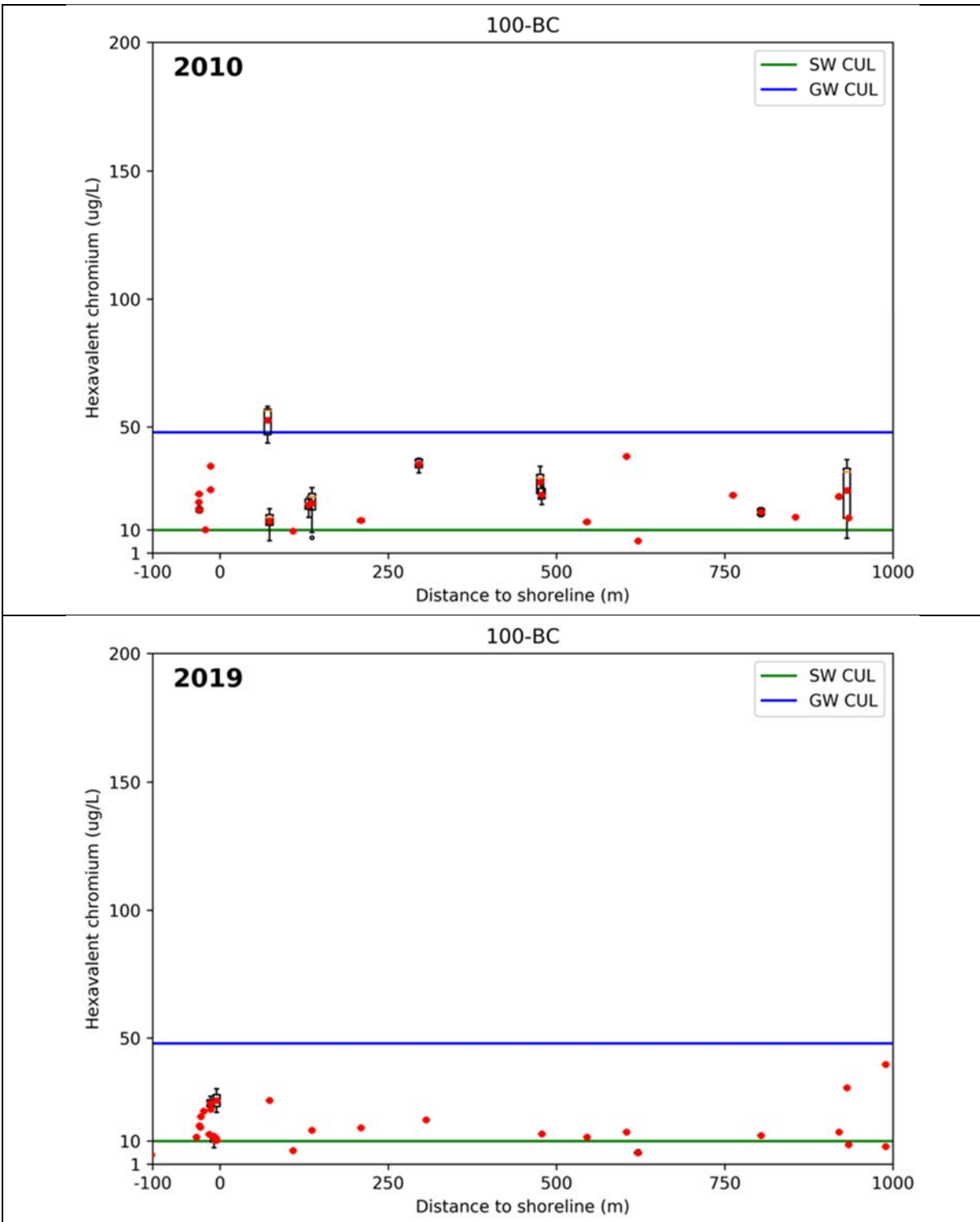


Figure 3.6. Cr(VI) Concentration Data from 2010 (top) and 2019 (bottom) Versus Distance from the Columbia River Shoreline for the 100-BC OU. Red points are mean values; boxes define the 25th and 75th percentiles. The horizontal blue and green lines represent the GW and SW CUL.

The horizontal blue and green lines in these figures represent GW and SW CULs, respectively. Points with negative distances to shoreline represent data from aquifer tubes that are located within the river channel.

Figure 3.6 shows the Cr(VI) aqueous concentration data from the 100-BC OU, which does not have a P&T system. The data indicate that average annual GW Cr(VI) concentrations generally decreased from 2010 to 2019 and were mostly below the GW CUL in both 2010 and 2019. However, average annual Cr(VI) concentrations measured from aquifer tube samples all exceeded the 10 µg/L SW CUL in both 2010 and 2019. There is no clear relationship evident between inland GW and shoreline concentrations for this site, but the relatively high Cr(VI) concentrations measured from aquifer tube and hyporheic zone samples suggests that they sample sediments that are connected to the inland GW plume.

Figure 3.7 shows the Cr(VI) aqueous concentrations data from the 100-KR OU. Concentrations in many GW monitoring wells and aquifer tubes exceeded the GW CUL of 48 µg/L at this site in 2010, but concentrations were reduced significantly by 2019, primarily as a result of P&T. In 2019, GW Cr(VI) concentrations within 400 to 500 m of the shoreline were all below the GW CUL, but concentrations at a number of wells that are further inland were above the GW CUL. Cr(VI) concentrations measured on samples collected from multiple aquifer tubes offshore of the 100-KR OU were above the SW CUL of 10 µg/L in both 2010 and 2019. Interpretation of relationships between inland plume and shoreline concentrations is complicated by the soil flushing activities at this site.

Figure 3.8 shows the Cr(VI) aqueous concentration data from the 100-NR OU. In 2010, Cr(VI) concentrations measured at all but one GW monitoring well were below the GW CUL. In 2019, Cr(VI) concentrations measured in nearly all of the monitoring wells were also below the SW CUL. A few inland wells, located greater than 800 m from the shoreline, had concentrations that exceeded the SW CUL. As shown in Table 1.1, Cr(VI) is a potential COC in the 100-NR OU, but Sr-90 is the primary COC.

Figure 3.9 shows the Cr(VI) aqueous concentration data from the 100-HR-D OU. Like the 100-KR OU, GW Cr(VI) concentrations at most of the monitoring well locations exceeded the GW CUL of 48 µg/L in 2010, but significant reductions in concentrations had occurred by 2019, as a result of P&T. In 2019, only a few wells, all located greater than 600 m from the river, had Cr(VI) concentrations that exceeded the GW CUL. Many aquifer tubes had Cr(VI) concentrations that exceeded both the surface and GW CULs in 2010. Fewer aquifer tubes were monitored in 2019 than in 2010, but concentrations measured at those locations in 2019 were mostly below the SW CUL.

Qualitatively, GW concentrations increase with distance from the shoreline for 100-HR-D. Under the current operating conditions, it appears that GW monitoring for wells located within approximately 50 m of the shoreline are below the CUL. However, GW concentrations greater than the GW CUL were observed at a few wells located greater than 600 m from the shoreline. The predominant GW flow conditions, which are influenced by P&T operations at this site, are such that the GW plume appears to be moving in an easterly direction, away from the shoreline, toward the 100-HR-H OU.

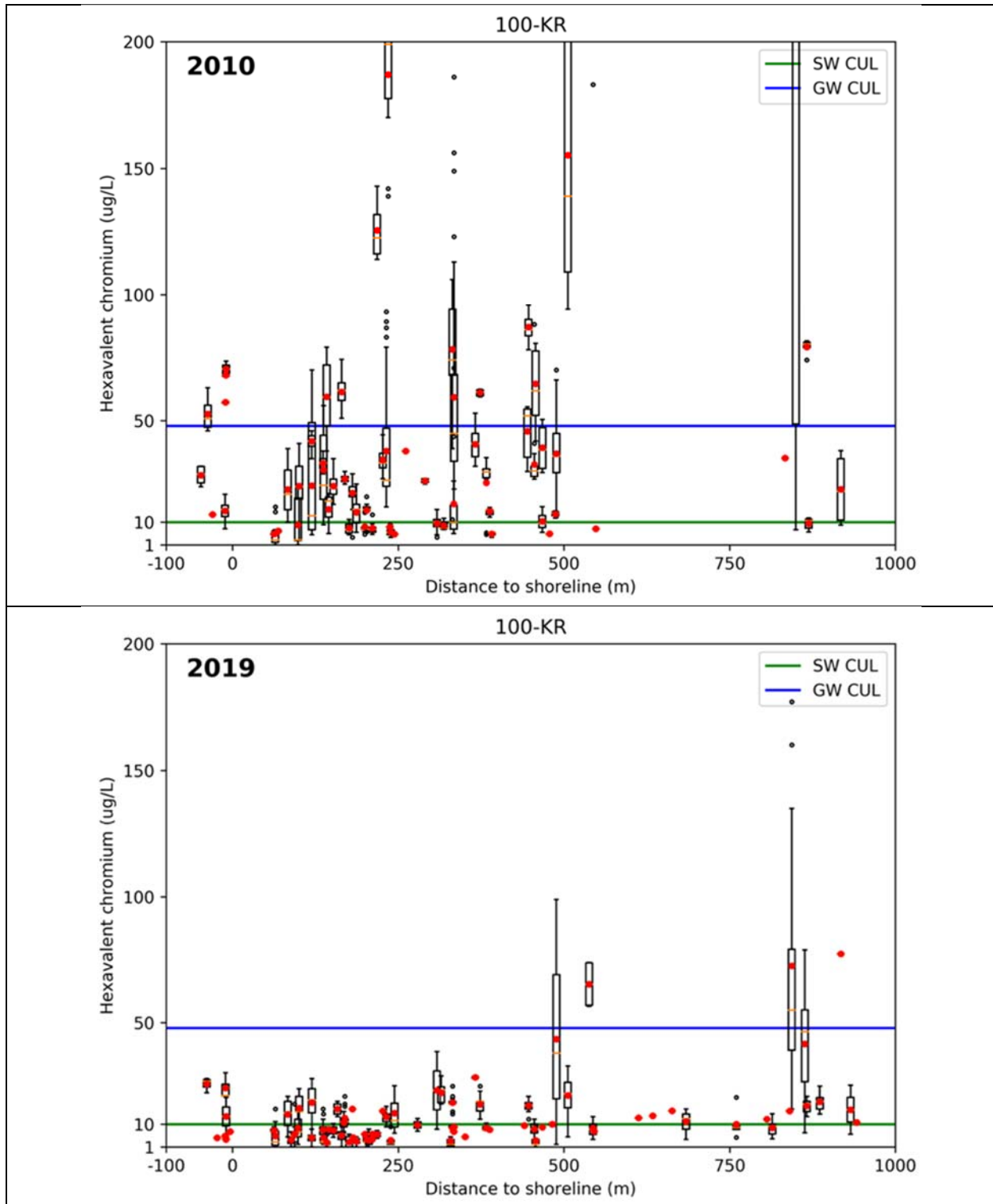


Figure 3.7. Cr(VI) Concentration Data from 2010 (top) and 2019 (bottom) Versus Distance from the Columbia River Shoreline for the 100-KR OU. Red points are mean values; boxes define the 25th and 75th percentiles. The horizontal blue and green lines represent the GW and SW CUL.

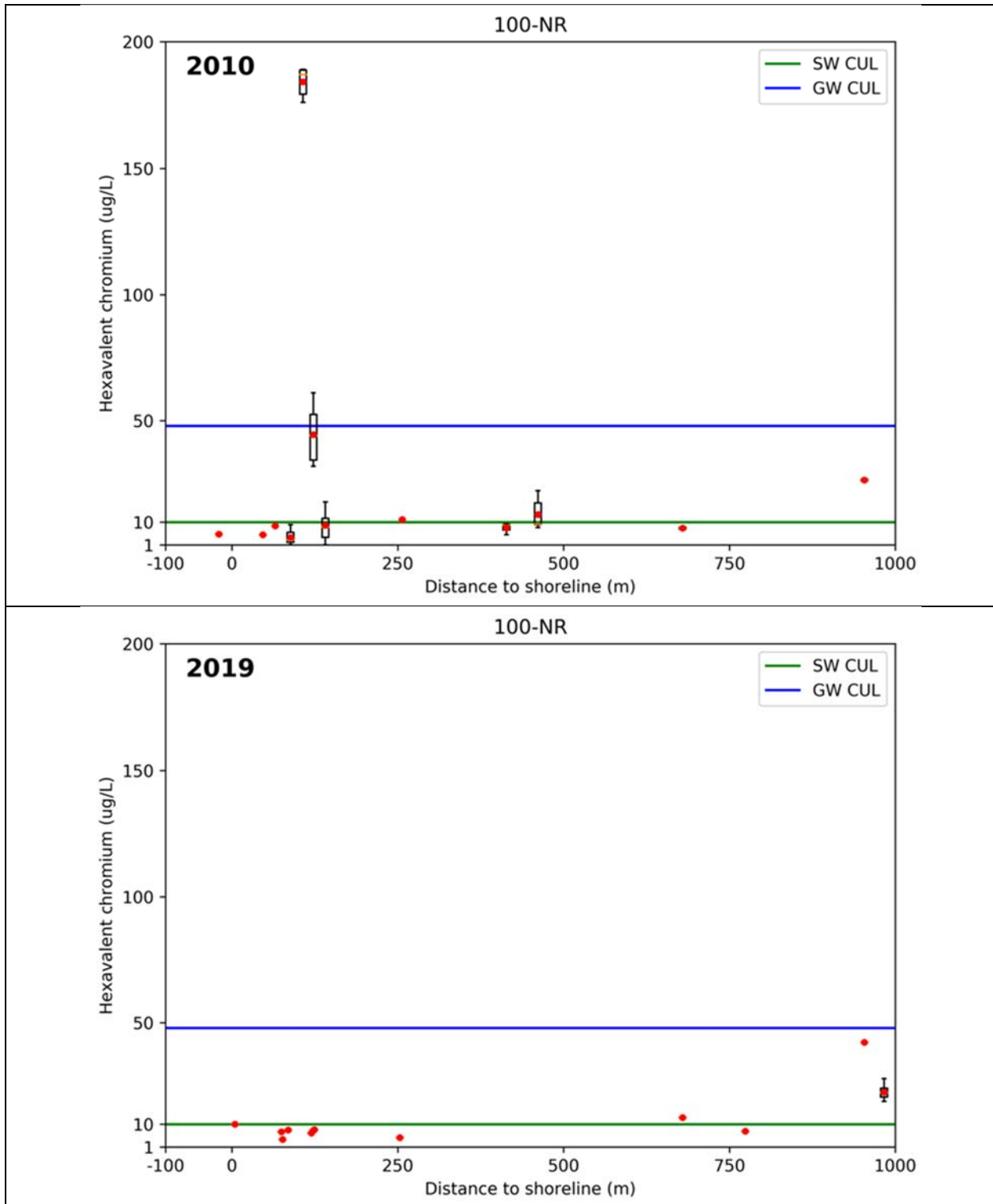


Figure 3.8. Cr(VI) Concentration Data from 2010 (top) and 2019 (bottom) Versus Distance from the Columbia River Shoreline for the 100-NR OU. Red points are mean values; boxes define the 25th and 75th percentiles. The horizontal blue and green lines represent the GW and SW CUL.

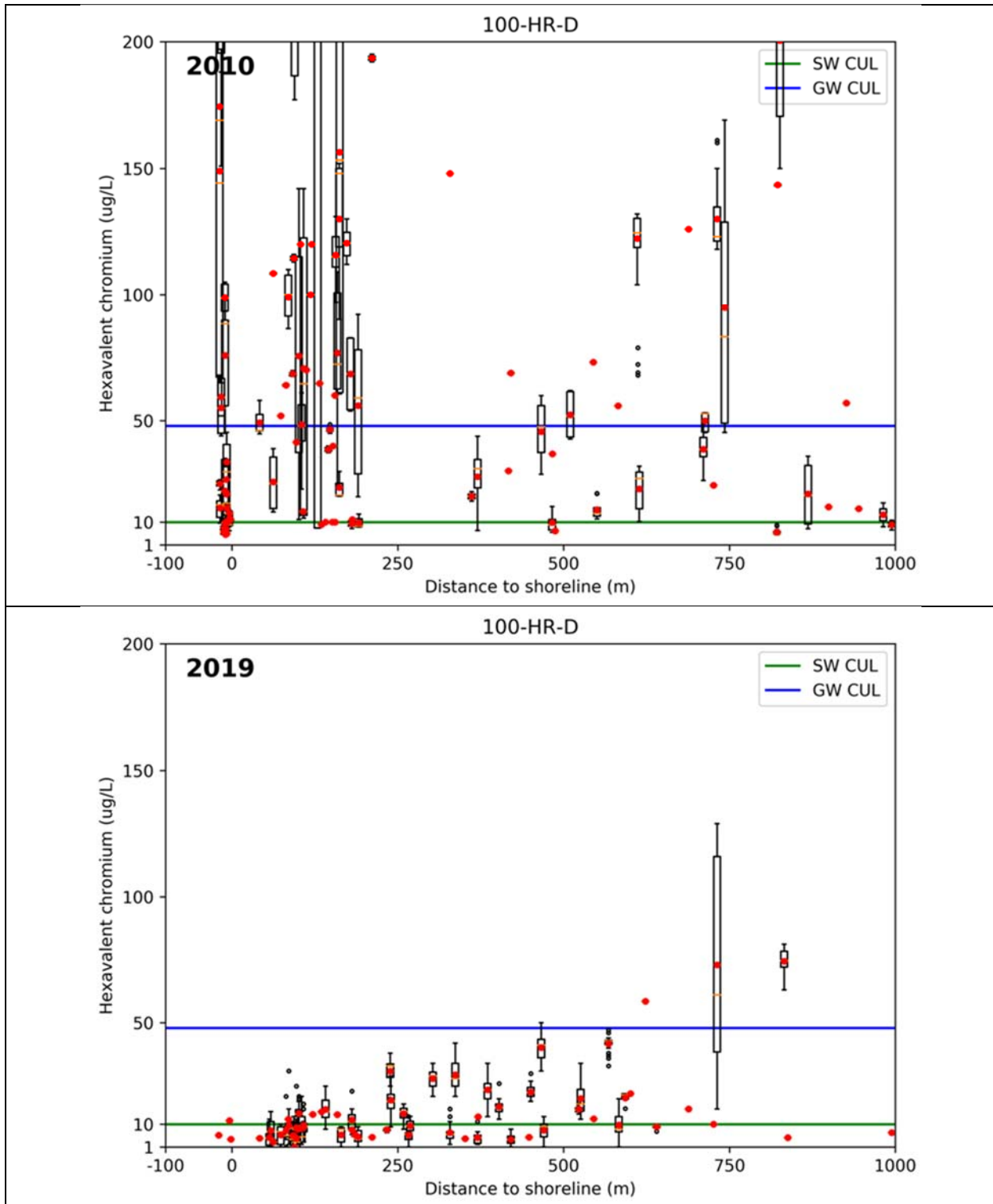


Figure 3.9. Cr(VI) Concentration Data from 2010 (top) and 2019 (bottom) Versus Distance from the Columbia River Shoreline for the 100-NR OU. Red points are mean values; boxes define the 25th and 75th percentiles. The horizontal blue and green lines represent the GW and SW CUL.

Figure 3.10 shows the Cr(VI) aqueous concentration data from the 100-HR-H OU. In 2010, Cr(VI) concentrations for many of the GW monitoring wells at this site exceeded the GW CUL. The majority of the aquifer tubes sampled in 2010 also exceeded the SW CUL. In 2019, only about six GW monitoring wells had Cr(VI) concentrations above the GW CUL. Fewer aquifer tubes were sampled in 2019 relative to 2010, but they had concentrations below the SW CUL. There are no clear relationships evident between inland concentrations and shoreline concentrations for the 100-HR-H OU. This is likely due, in part, to changes in the P&T system over time that have been made to adaptively manage plume migration behavior.

Figure 3.11 shows the Cr(VI) aqueous concentration data from the 100-FR OU. In 2010, nearly all aqueous Cr(VI) measurements were below the GW CUL, but no aquifer tubes were sampled at this site. In 2019, all measured GW concentrations were below the GW CUL, and the one aquifer tube sampled had a concentration below the SW CUL. Cr(VI) concentrations in the 100-FR OU are generally low, but there are no clear relationships between inland concentrations and shoreline concentrations.

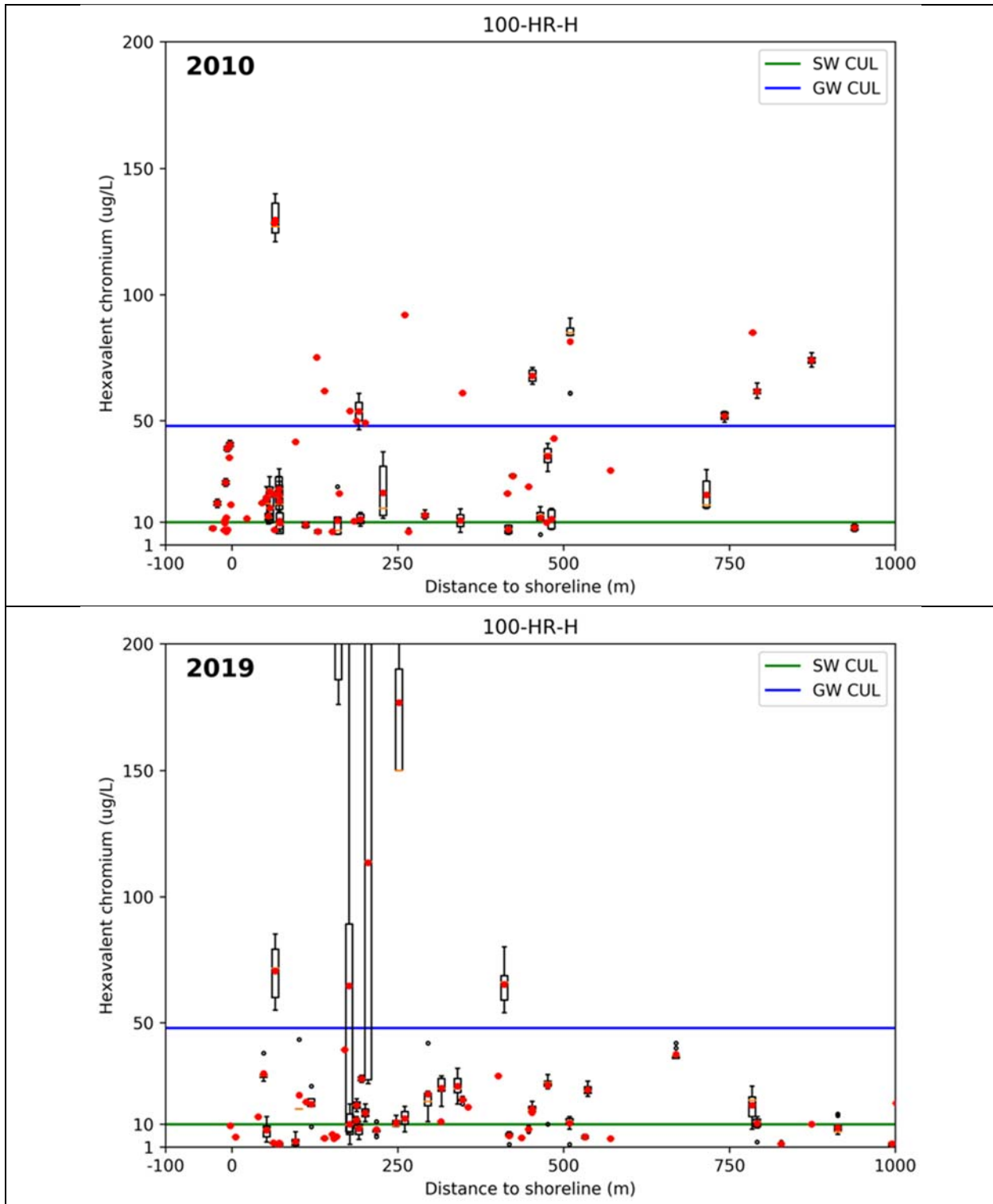


Figure 3.10. Cr(VI) Concentration Data from 2010 (top) and 2019 (bottom) Versus Distance from the Columbia River Shoreline for the 100-HR-H OU. Red points are mean values; boxes define the 25th and 75th percentiles. The horizontal blue and green lines represent the GW and SW CUL.

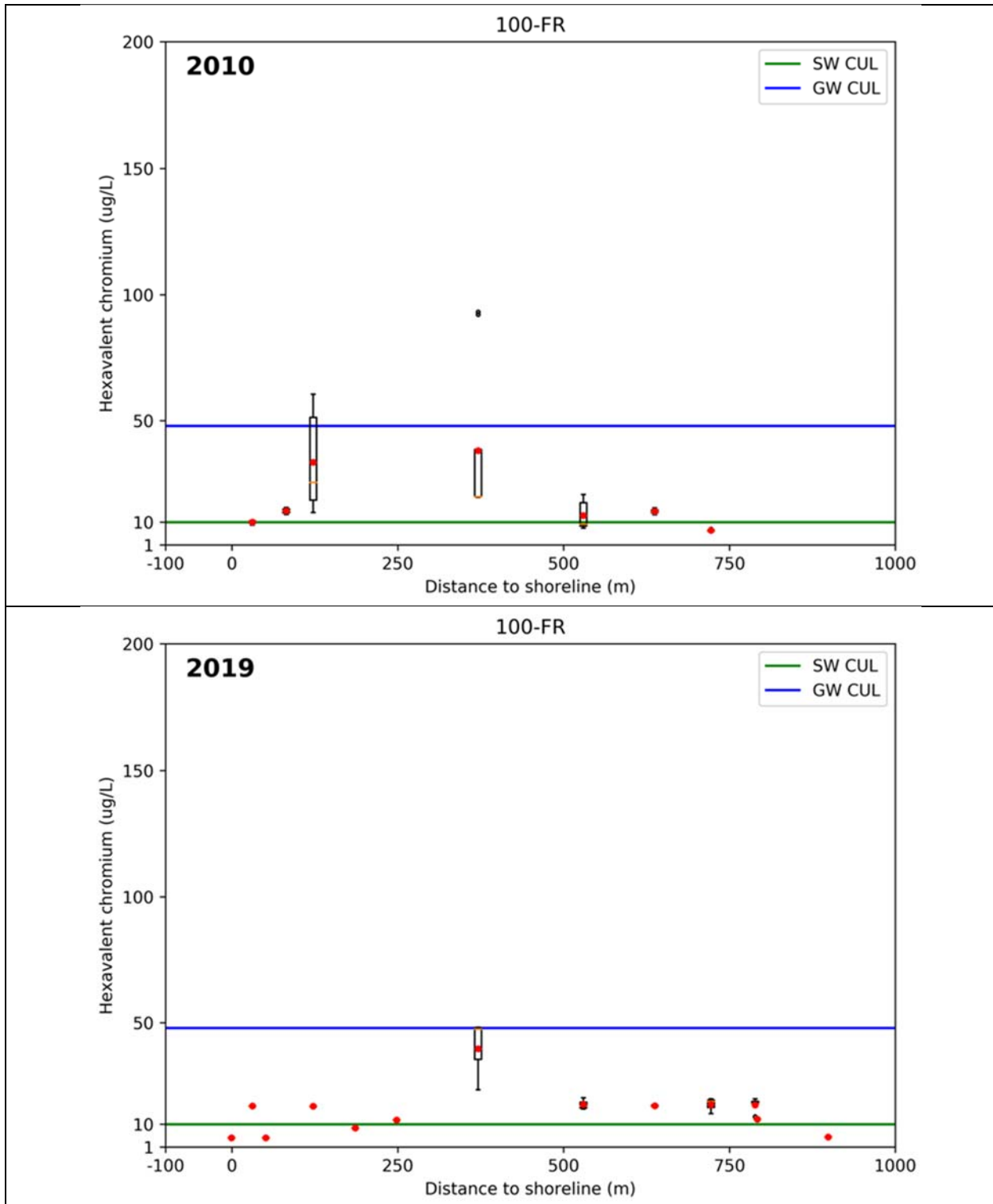


Figure 3.11. Cr(VI) Concentration Data from 2010 (top) and 2019 (bottom) Versus Distance from the Columbia River Shoreline for the 100-FR OU. Red points are mean values; boxes define the 25th and 75th percentiles. The horizontal blue and green lines represent the GW and SW CUL.

3.2.2 Data from Interpreted Plume Maps

DOE publishes annual GW monitoring reports for the Hanford Site that include interpreted Cr(VI) plume maps for the 100 Areas at both LRS and HRS. These maps, which are generated using kriging with control points, use available GW monitoring well and aquifer tube data (such as shown in the previous section). Data for selected times or time periods that are determined to be representative of LRS and HRS conditions are used to produce the plume maps. The same map-generation process is used every year to produce consistent plume maps for the annual reports. This consistency allows for better comparisons and detection of any significant changes that might occur from one year to the next.

Geographic information system polygon files representing the outlines of the Cr(VI) plumes from the annual GW monitoring reports for different concentration contours (10, 20, and 48 $\mu\text{g/L}$) were rasterized at 10 m resolution and used for additional calculations to further examine possible relationships between plume concentrations and distance to shoreline. For these calculations, the plume centroid coordinates were first computed. The closest points on the shoreline to each plume centroid were then determined. The lines defined by these two points represent the distances between the plume centroids and the closest shoreline points for each plume. The points of intersection of these lines with the 10, 20, and 48 $\mu\text{g/L}$ Cr(VI) concentration contours were used to determine the distances to the shoreline for each concentration level.

Although there are six GW OUs within the 100 Areas, there are more than six distinct, large Cr(VI) GW plumes. The raster data were separated into groups representing eight different Cr(VI) plumes, or portions of plumes, as shown in Figure 3.12. This figure shows the maximum extent of these plumes over the period of interest (2010-2019). The Cr(VI) concentration data representing each plume were used to calculate the locations of the centers of mass of the plumes in the x-y plane at both LRS and HRS, and the distances to the shoreline for each concentration level represented in the plume data. Note that although plumes 6 and 7 are associated with the 100-D Area and 100-H Area, respectively, they have merged and separated over time, making it difficult to distinguish separate, distinct plumes in these areas. Therefore, the eastern boundary of the 100-D Area shown in Figure 3.12 was used as a dividing line for the purpose of computing centers of mass and associated distances to the shoreline for plumes 6 and 7.

Figure 3.13 shows the Cr(VI) concentrations versus distance to shoreline plot for the plume associated with the 100-B/C Area. No clear relationships are apparent for the inland and shoreline (or near shore) concentrations for this plume, owing in part to its proximity to the shoreline. Figure 3.14 and Figure 3.15 show similar plots for the two GW Cr(VI) plumes associated with the 100-K Area. The distance of each concentration contour from the shoreline is shown to gradually increase over time. Identifying possible relationships between Cr(VI) concentrations for inland plumes versus shoreline concentrations is further complicated by dynamic P&T operations, resulting in changing plume trajectories, and by other remedial actions such as a source zone removal and soil flushing.

Figure 3.16 and Figure 3.17 show Cr(VI) concentration versus distance to shoreline plot for the plumes associated with the 100-N Area. Results for the southwestern plume associated with the 100-N Area, shown in Figure 3.16, indicate that the plume is moving away from the river, such that by year 2015 the 10 $\mu\text{g/L}$ contour was more than 200 m away from the shoreline at both high and low river stages.

Figure 3.18 and Figure 3.19 show concentrations versus distance to shoreline computed from GW Cr(VI) plumes associated with the 100-D and 100-H Areas, respectively. Both of these figures indicate that the distance between the plumes and the shoreline is increasing over time at these sites. P&T operations at these sites are such that the plumes are being drawn away from the river by extraction wells, and/or pushed away from the river by injection wells that are being used for hydraulic containment. The position of these two sites along the river corridor, and the predominant GW flow direction, from west-southwest

to east-northeast across the “horn,” are resulting in the net migration of Cr(VI) away from the 100-D Area toward the 100-H Area. Although relationships between inland and shoreline or nearshore concentrations could potentially be inferred from these results, these data and temporal trends are highly dependent on the ongoing P&T operations in these areas.

Figure 3.20 shows concentrations versus distance to shoreline computed from GW Cr(VI) plumes associated with the 100-F Area. As noted previously, recent GW Cr(VI) plume concentrations in the 100-F Area are below the 10 $\mu\text{g/L}$ SW CUL during HRS. Figure 3.20 shows that at LRS, the 10 $\mu\text{g/L}$ concentration contour was moving away from the shoreline over the 2010-2014 time period but has been moving closer to the shoreline in more recent years. There are no P&T operations in the 100-F Area, so these changes may be a result of sources of Cr(VI) from the vadose zone or RUM aquifer.

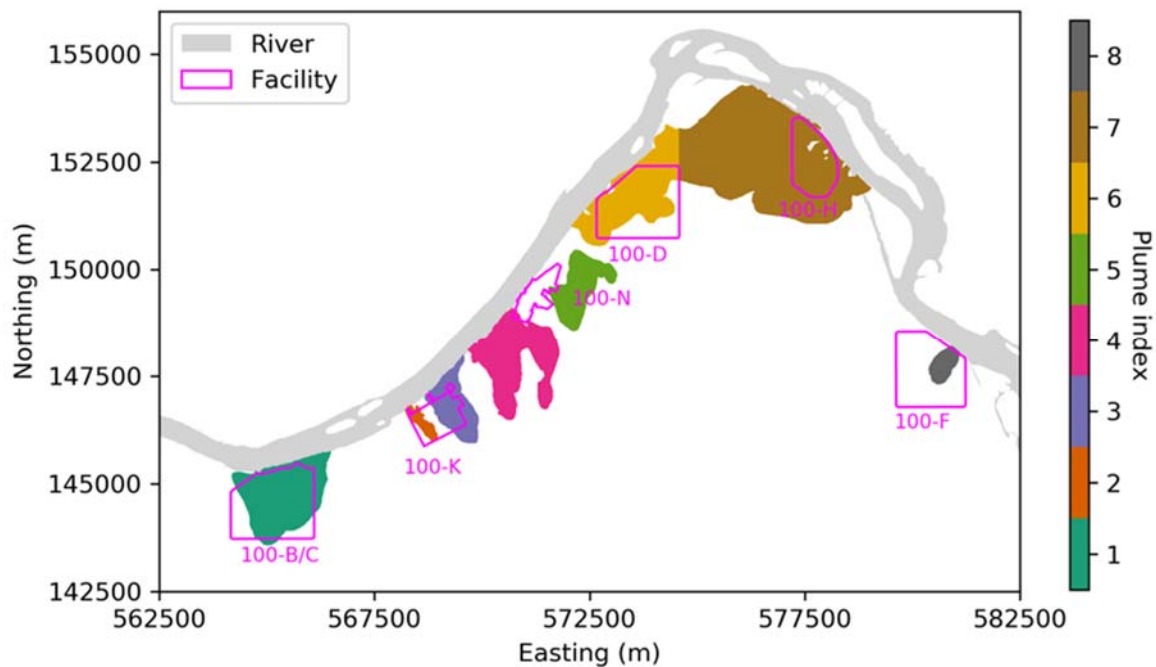


Figure 3.12. Maximum Spatial Extent of Distinct Large Cr(VI) Plumes in the 100 Areas

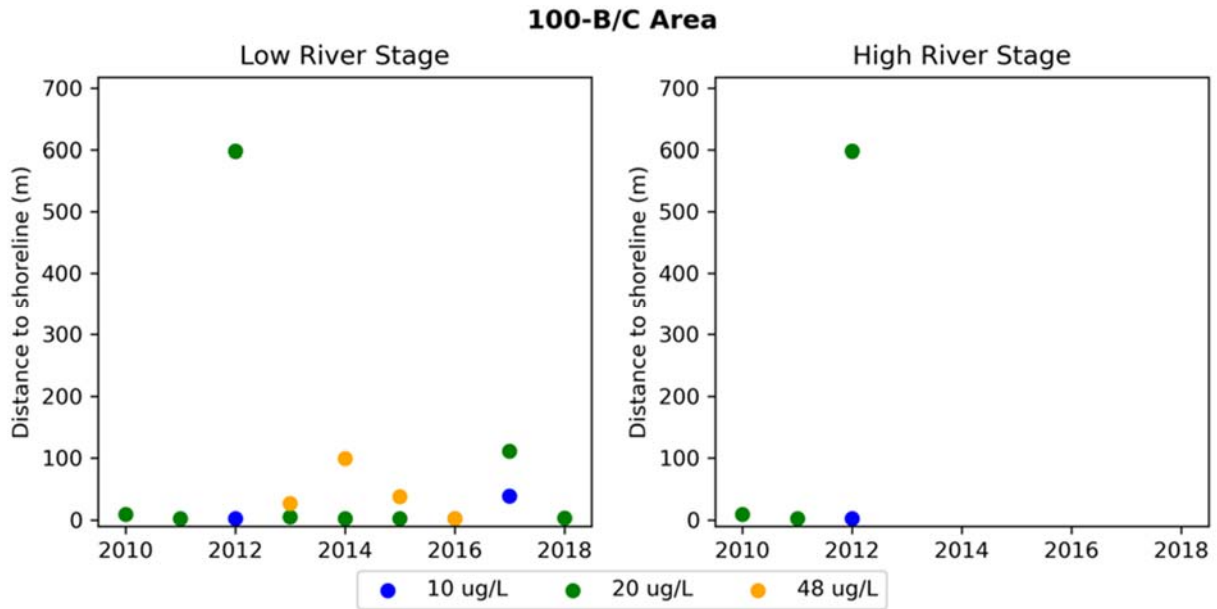


Figure 3.13. Concentration Versus Distance to Shoreline Computed from GW Cr(VI) Plume Maps Associated with the 100-B/C Area (shown as Plume 1 in Figure 3.12)

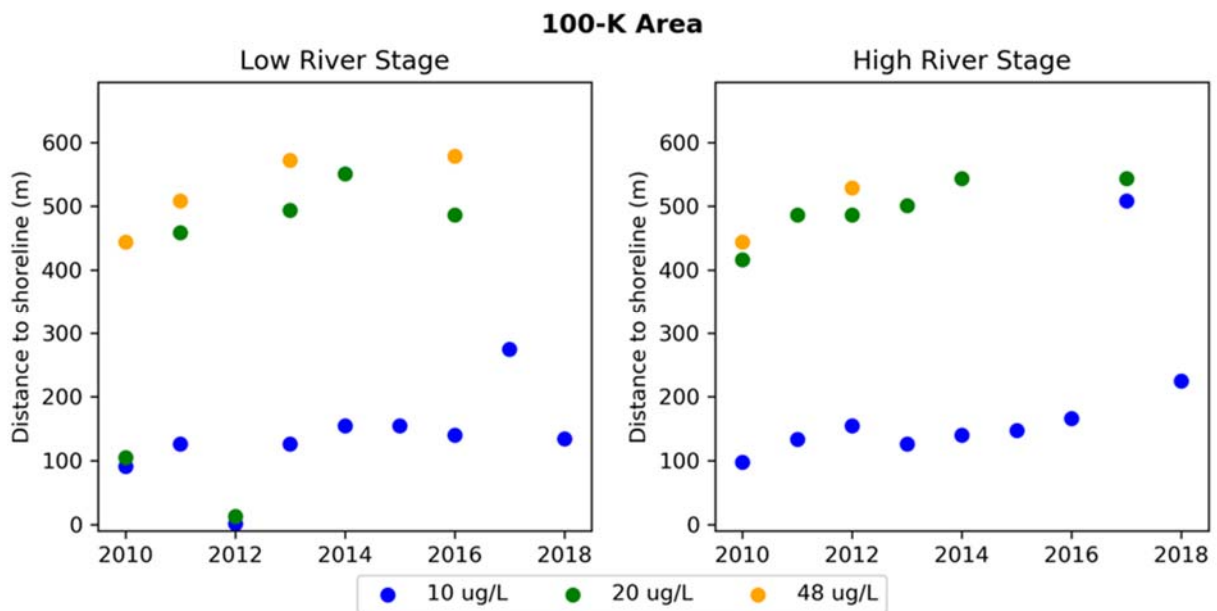


Figure 3.14. Concentration Versus Distance to Shoreline Computed from GW Cr(VI) Plume Maps for the Southwestern Plume Associated with the 100-K Area (shown as Plume 2 in Figure 3.12)

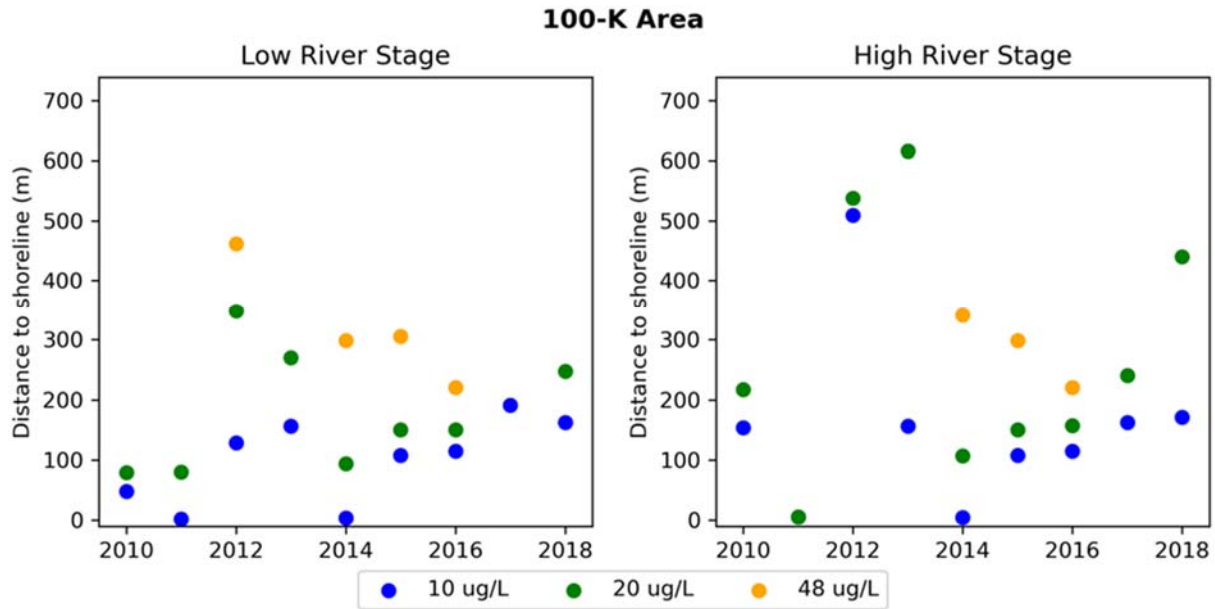


Figure 3.15. Concentration Versus Distance to Shoreline Computed from GW Cr(VI) Plume Maps for the Northeastern Plume Associated with the 100-K Area (shown as Plume 3 in Figure 3.12).

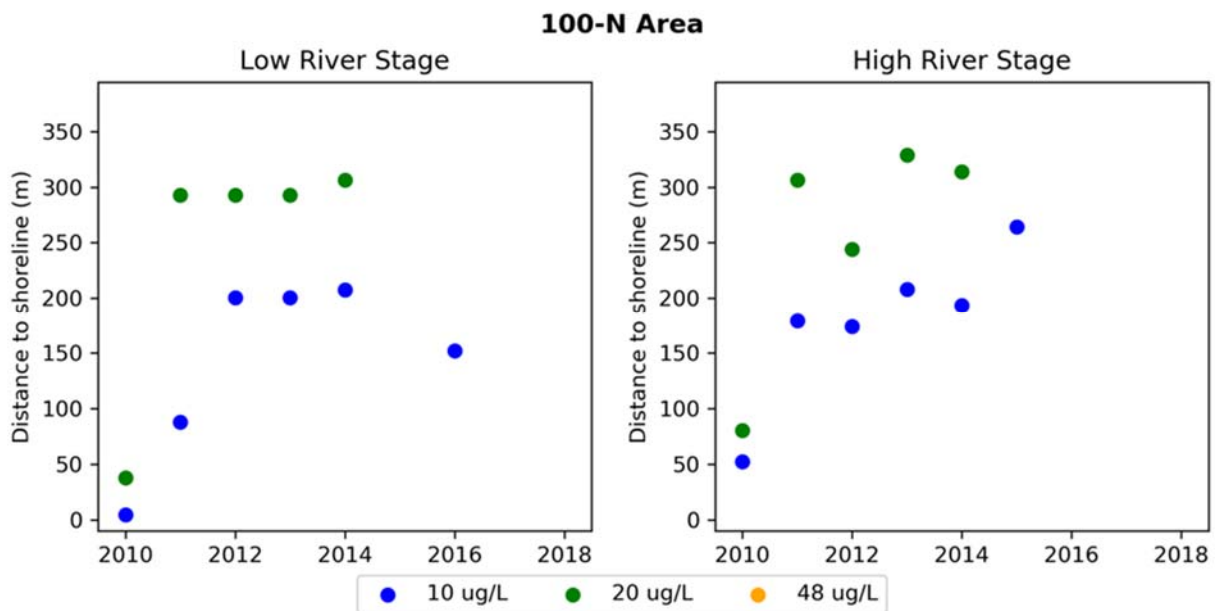


Figure 3.16. Concentration Versus Distance to Shoreline Computed from GW Cr(VI) Plume Maps for the Southwestern Plume Associated with the 100-N Area (shown as Plume 4 in Figure 3.12).

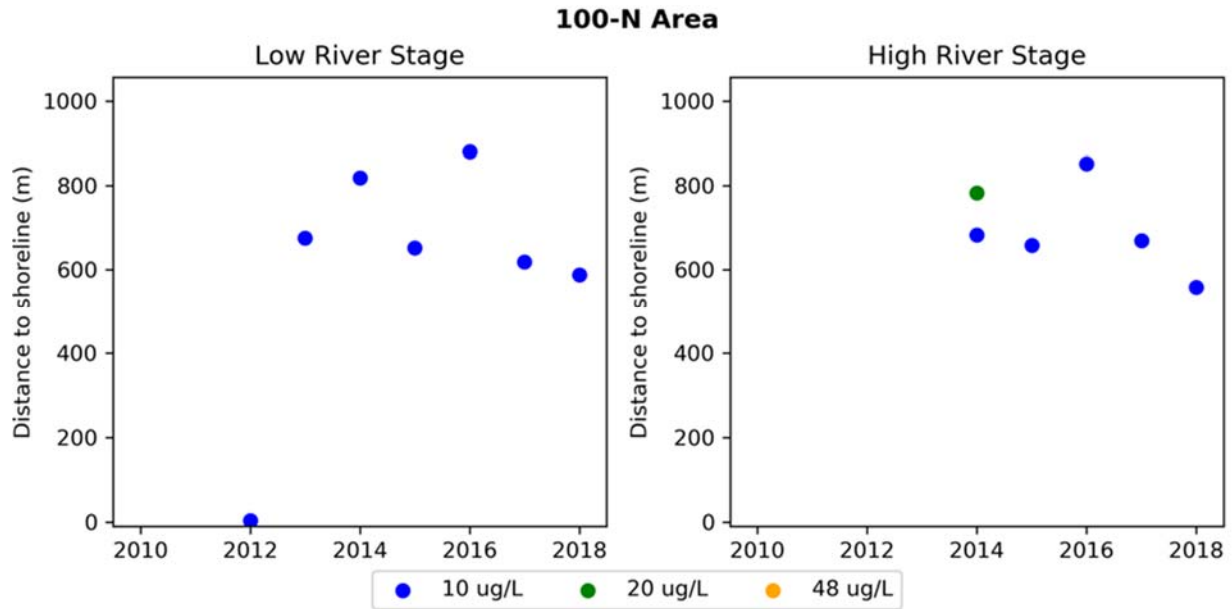


Figure 3.17. Concentration Versus Distance to Shoreline Computed from GW Cr(VI) Plume Maps for the Northeastern Plume Associated with the 100-N Area (shown as Plume 5 in Figure 3.12).

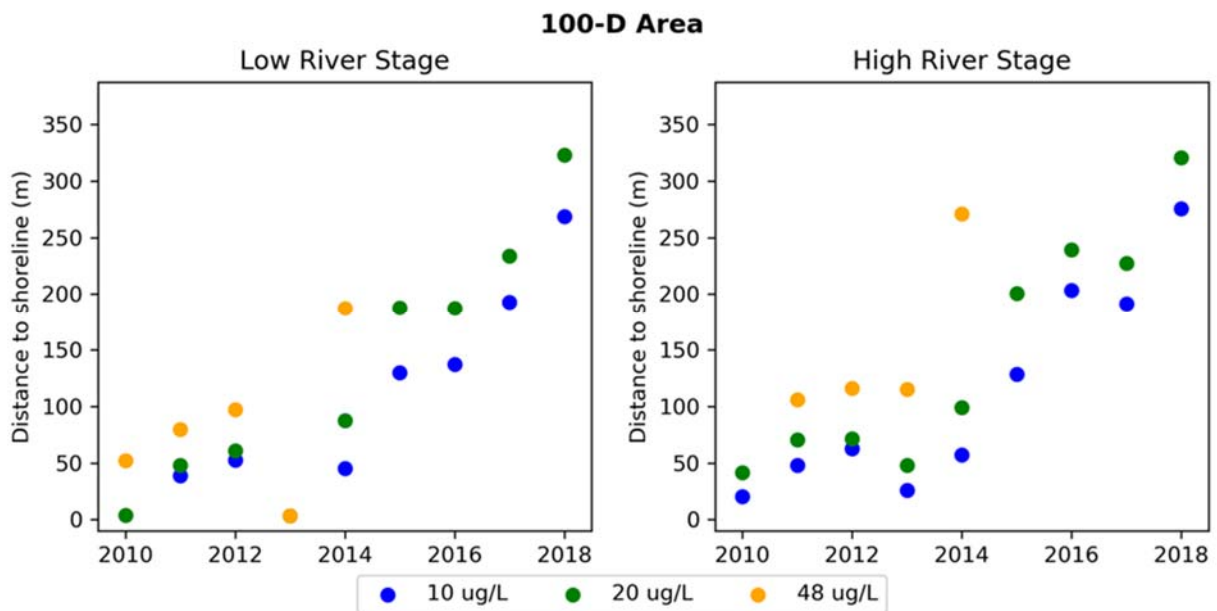


Figure 3.18. Concentration Versus Distance to Shoreline Computed from GW Cr(VI) Plume Maps Associated with the 100-D Area (shown as Plume 6 in Figure 3.12).

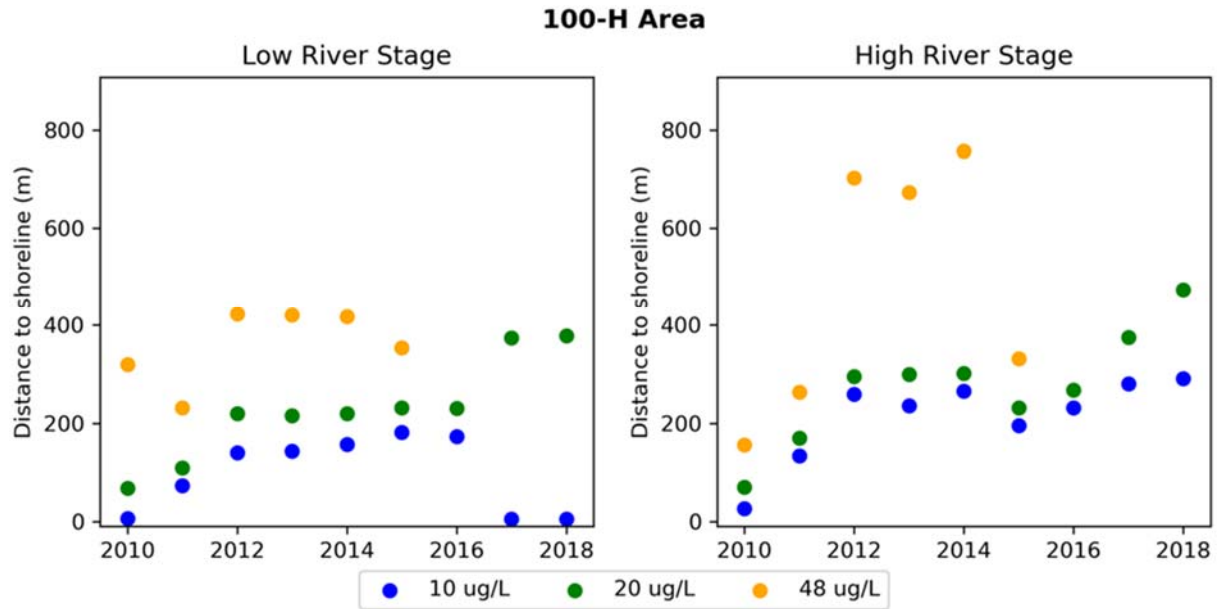


Figure 3.19. Concentration Versus Distance to Shoreline Computed from GW Cr(VI) Plume Maps Associated with the 100-H Area (shown as Plume 7 in Figure 3.12)

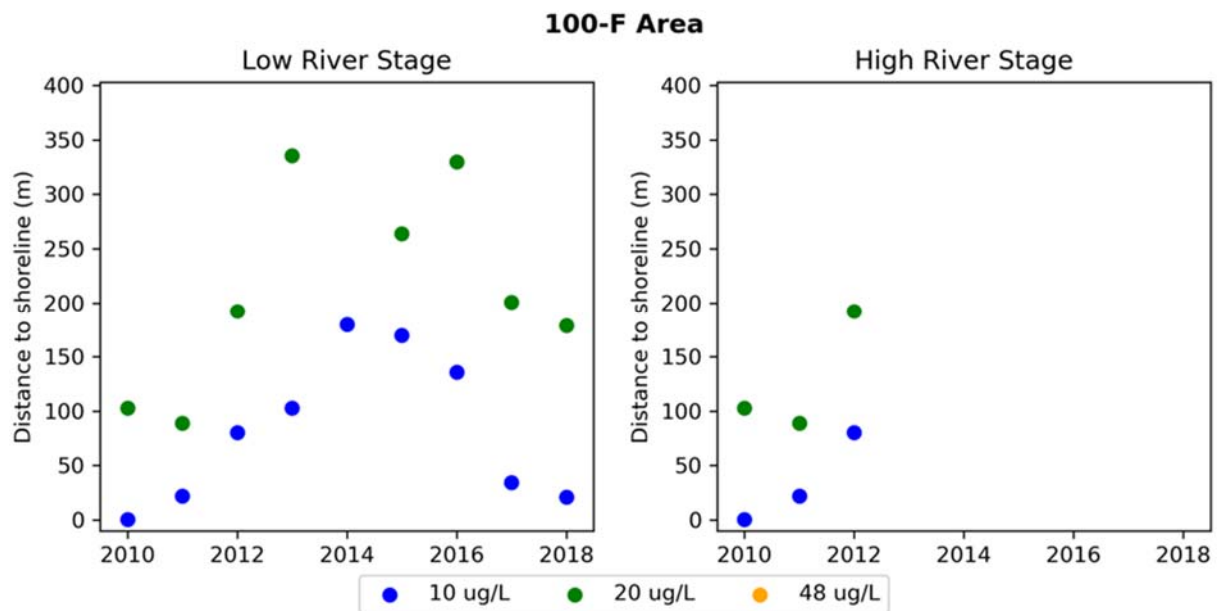


Figure 3.20. Concentration Versus Distance to Shoreline Computed from GW Cr(VI) Plume Maps Associated with the 100-F Area (shown as plume 8 in Figure 3.12)

In summary, no single relationship could be identified between inland GW and shoreline Cr(VI) concentrations for the Hanford 100 Areas. For the 100-BC area, aquifer tube and hyporheic zone sampler data show persistently high Cr(VI) concentrations above the SW CUL. Concentrations in the 100-FR and 100-NR OUs are relatively low, with all inland Cr(VI) concentrations in 2019 being below the GW CUL and the very limited number of aquifer tube samples that were collected being below the SW CUL. There are currently no P&T activities in the 100-FR or 100-NR OU, so no rebound in Cr(VI) concentrations is expected at these sites. Dramatic reductions in Cr(VI) concentrations have occurred at the 100-KR and

100-HR-D OUs, and to a lesser extent at 100-HR-H, as a result of P&T operations. However, a recent rebound study at 100-KR indicated that when P&T was discontinued, GW Cr(VI) concentrations rebounded (CH2M 2018b), suggesting that continuing sources of Cr(VI) exist, possibly within in the vadose zone or PRZ. In 2019, aquifer tube data for the 100-KR and 100-HR-D OUs were mostly below the SW CUL and GW Cr(VI) concentrations increased with distance from the river. However, interpretation of possible relationships between inland and shoreline Cr(VI) concentrations for the 100-HR-H OU is complicated by dynamic P&T operations.

3.3 Plume Trajectories

The previous analysis utilized calculated plume centroids, which were also used to evaluate plume trajectories (Figure 3.21 through Figure 3.26). The trajectories of the plumes are determined by the predominant flow directions in each area, which are influenced by P&T operations at sites where P&T has been implemented. Plume trajectory analysis provides another way to assess the effects of the P&T remedy on plume migration behavior, and to forecast future movement of plumes under similar conditions.

For 100-B/C, which does not have a P&T system, Figure 3.21 indicates that the Cr(VI) plume migrated to the south during the 2009-2012 time period, during both LRS and HRS, but since then has been migrating to the northeast, toward the shoreline during LRS. After 2012, the plume trajectory at HRS in 100-B/C could not be computed because GW Cr(VI) concentrations were all below 10 µg/L.

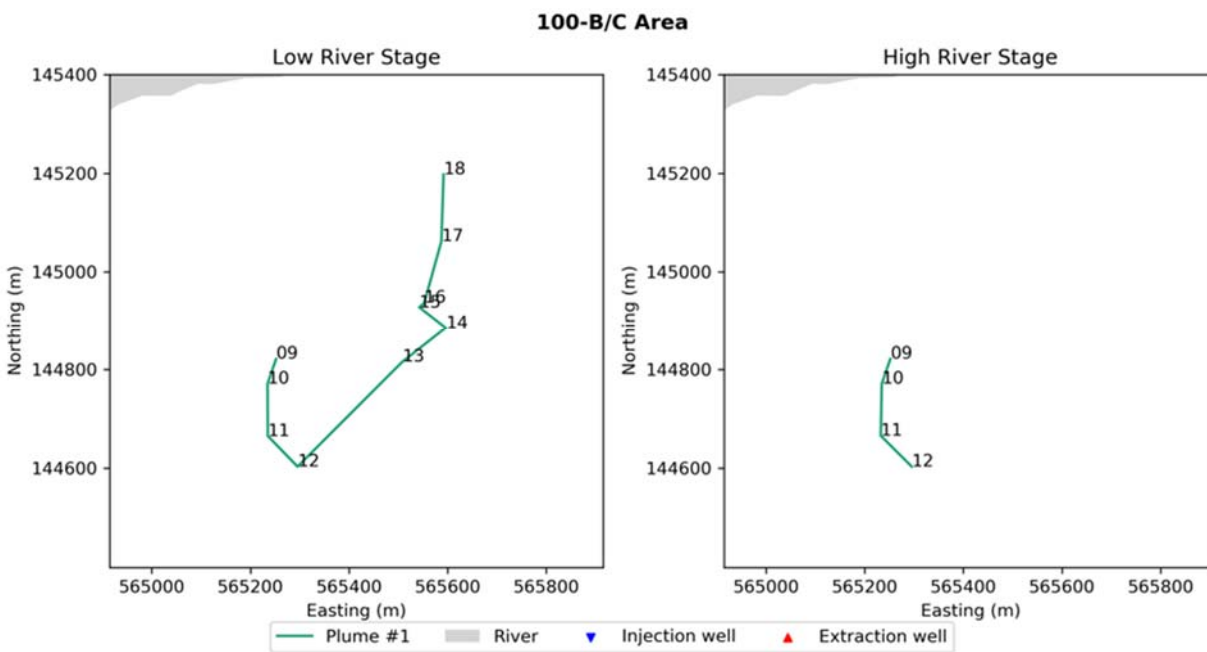


Figure 3.21. Calculated Trajectory of Plume 1 (see Figure 3.11 for Location), Associated with the 100-B/C Area Based on Data from Interpreted CR(VI) Plume Maps for LRS and HRS. Numbers represent the years.

For the 100-K Area, Figure 3.22 indicates that the southern plume (plume 2 in Figure 3.12) has oscillated back and forth, more-or-less perpendicular to the shoreline, during both LRS and HRS. The northern plume (plume 3 in Figure 3.12) has progressively moved to the south, away from the river, in response to GW extraction from the P&T system.

For the 100-N Area, Figure 3.23 indicates that the southern plume’s center of mass (plume 4 in Figure 3.12) has shifted away from the river through time, while the northern plume (plume 5 in Figure 3.12) appears to be relatively stationary but is oscillating back and forth parallel to the river. There was a P&T system in 100-N, but it was put on cold standby in 2006 and was decommissioned in 2016.

Figure 3.24 shows the Cr(VI) plume associated with the 100-D Area is moving very slowly to the northeast, and with slow migration toward the river. This trajectory is consistent with the locations of injection and monitoring wells that are shown in Figure 3.24.

The Cr(VI) plume associated with 100-H Area is shown in Figure 3.25. The changes in locations of the plume centroids over time indicate that the plume migrated to the southeast during the 2009-2013 timeframe, and then to the northwest during the 2014-2019 timeframe. Not all of the P&T wells associated with the 100-H Area are shown in Figure 3.25 because the center of plume mass is located relatively far away from many of the P&T wells (outside the area shown in the plot).

Figure 3.26 indicates that the center of mass of the Cr(VI) plume associated with 100-F Area is moving away from the shoreline. There are no P&T wells in 100-F, so the slow apparent drift of the center of mass of the Cr(VI) plume away from the river may be due to a continuing source in the vadose zone or aquifer.

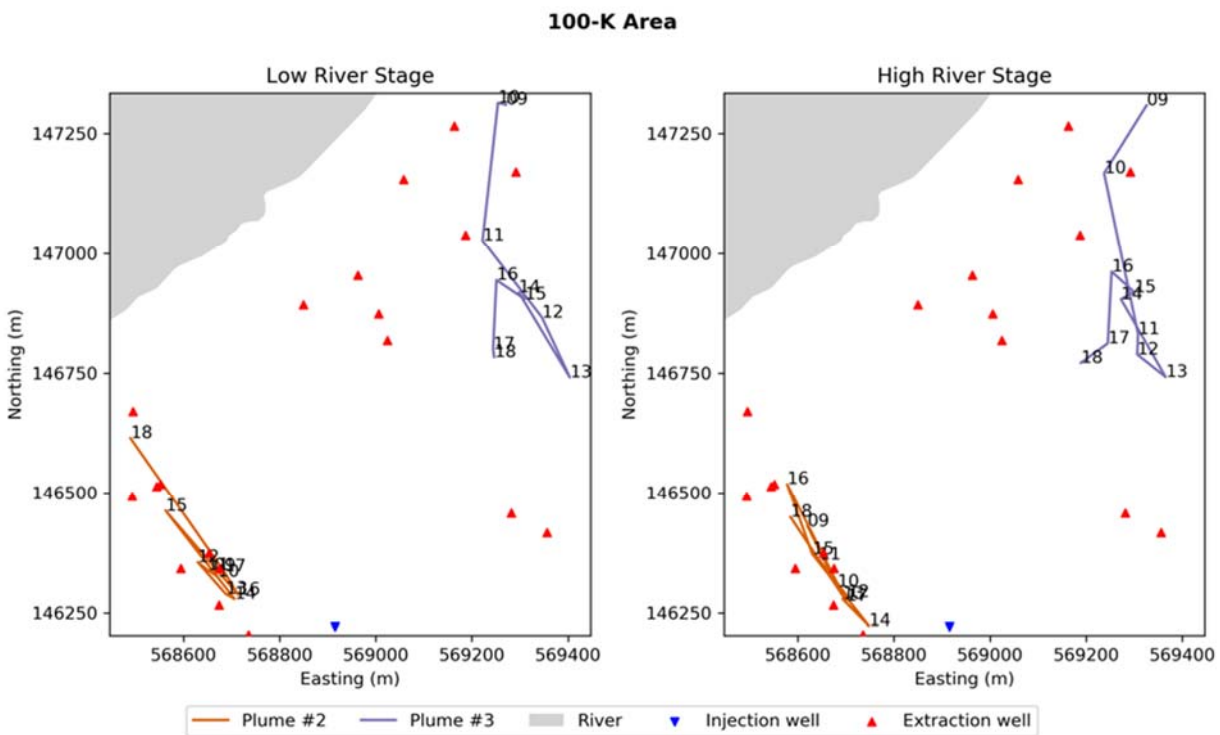


Figure 3.22. Calculated Trajectories of Plumes 2 and 3 Associated with the 100-K Area (see Figure 3.12 for location), Based on Data from Interpreted CR(VI) Plume Maps for LRS and HRS. Numbers represent the years.

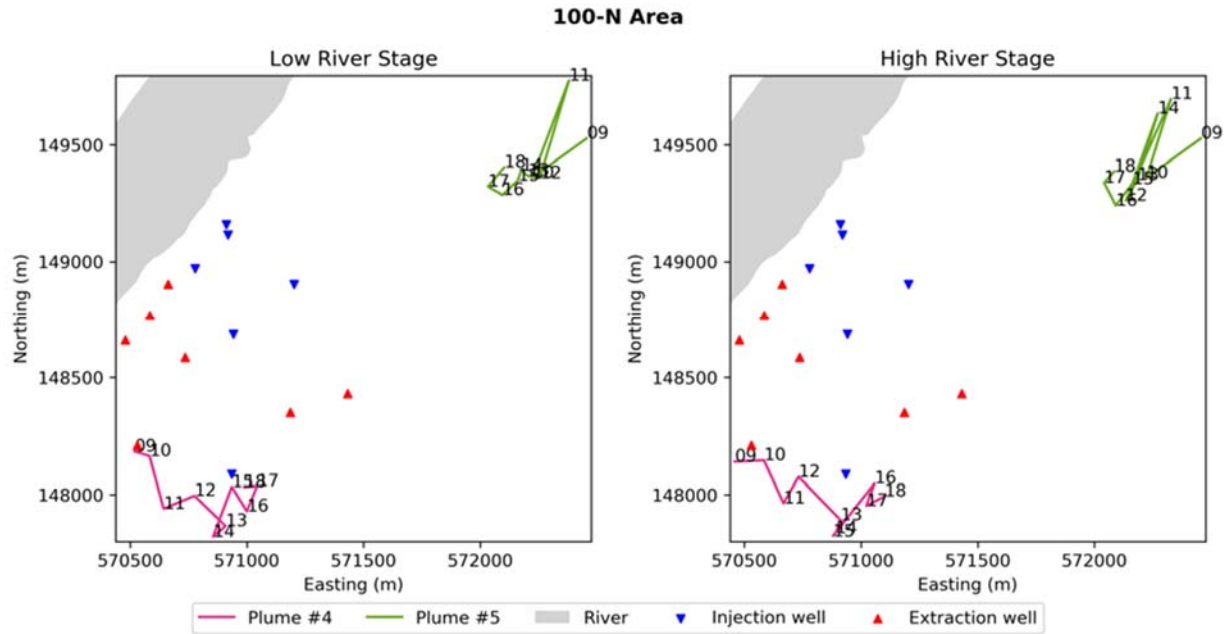


Figure 3.23. Calculated Trajectories of Plumes 4 and 5 Associated with 100-N Area (see Figure 3.12 for location), Based on Data from Interpreted Cr(VI) Plume Maps for LRS and HRS. Numbers represent the years.

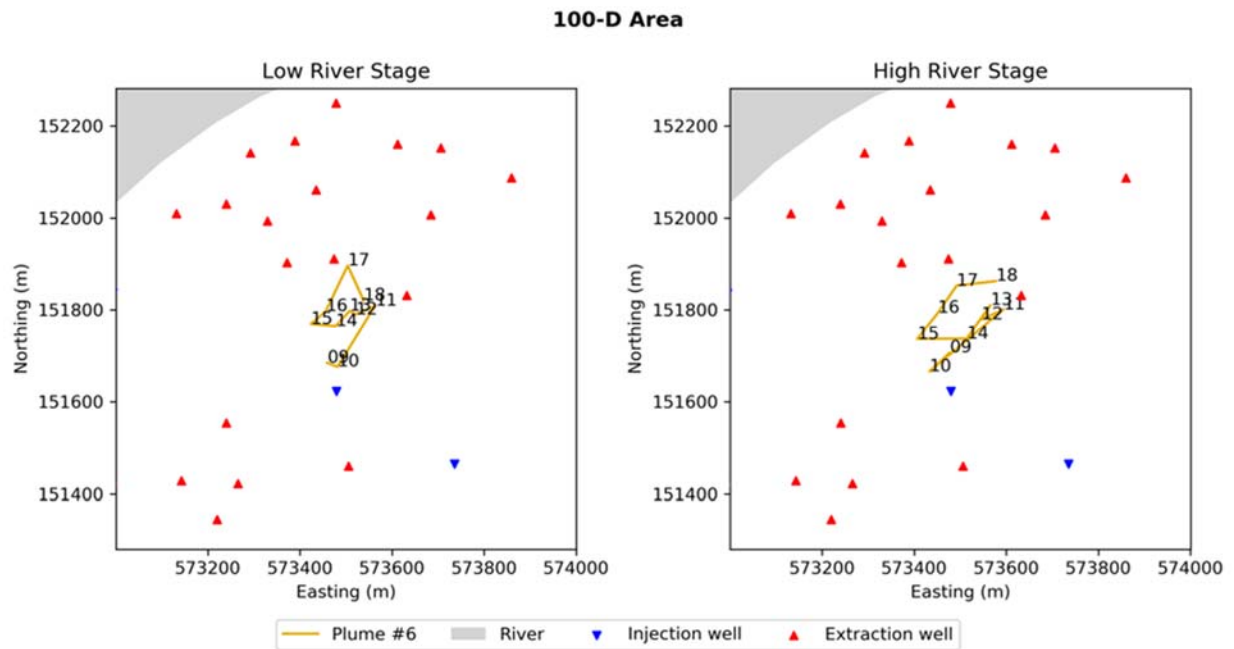


Figure 3.24. Calculated Trajectories of Plume 6 Associated with 100-D Area (see Figure 3.12 for Location), Based on Data from Interpreted Cr(VI) Plume Maps for LRS and HRS. Numbers represent the years.

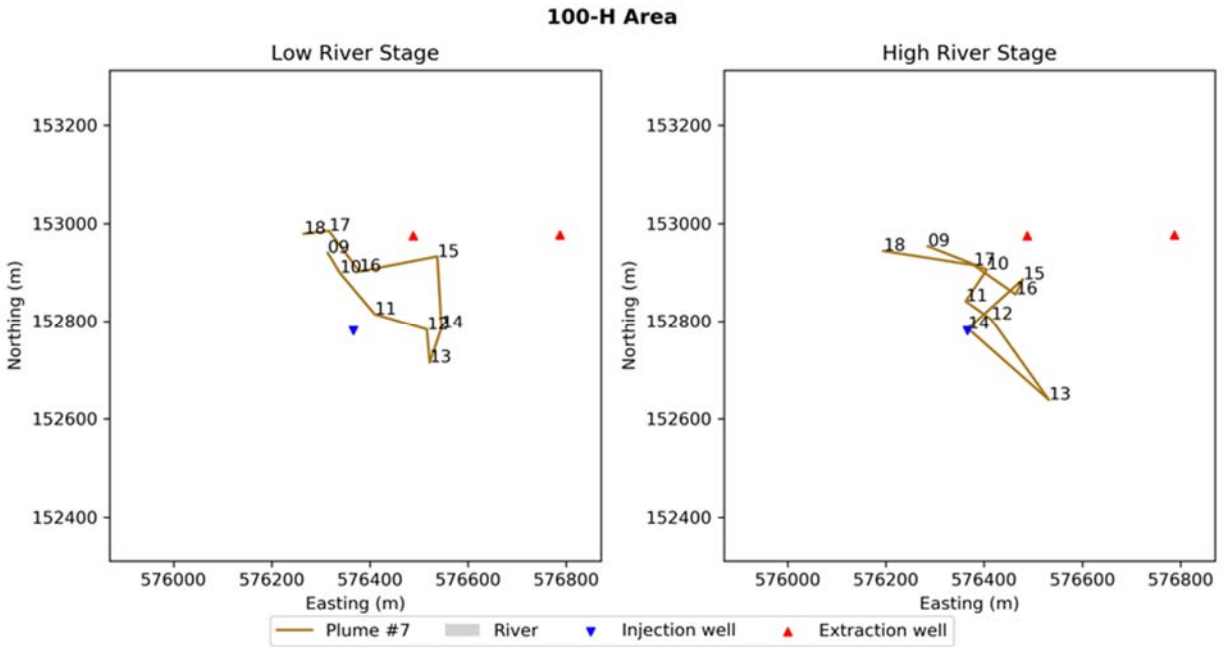


Figure 3.25. Calculated Trajectories of Plume 7 Associated with 100-H Area (see Figure 3.12 for location), Based on Data from Interpreted Cr(VI) Plume Maps for LRS and HRS. Numbers represent the years.

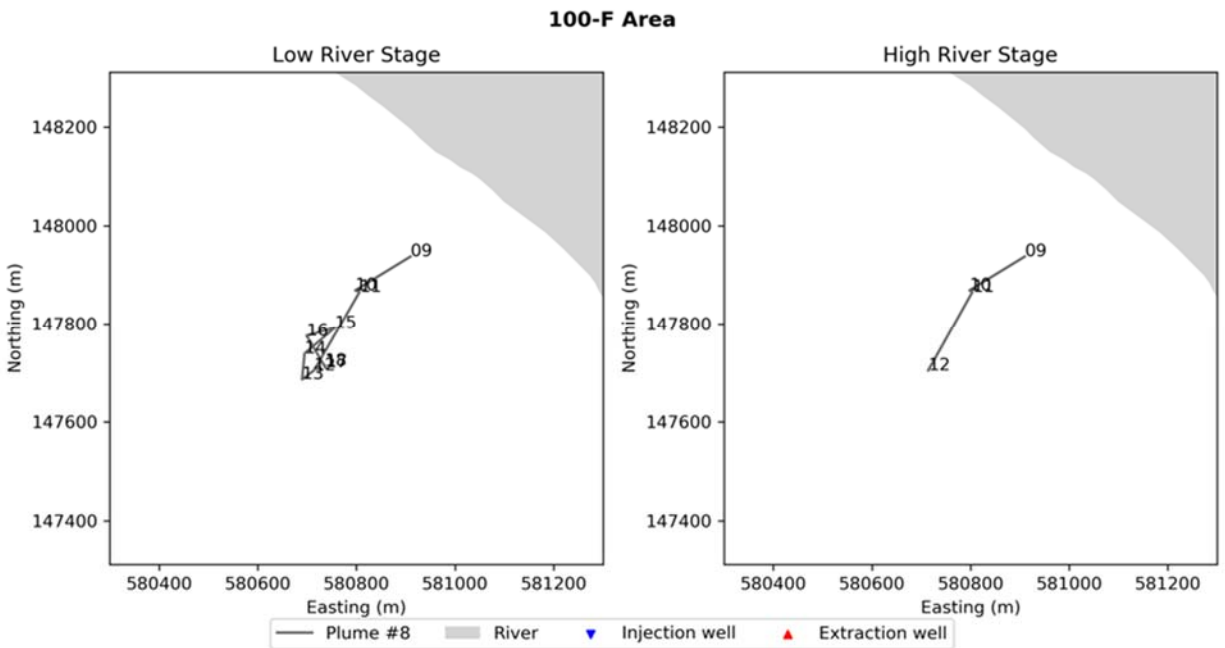


Figure 3.26. Calculated Trajectories of Plume 8 Associated with 100-F Area (see Figure 3.12 for location), Based on Data from Interpreted Cr(VI) Plume Maps for LRS and HRS. Numbers represent the years.

3.4 Cluster Analysis

Cluster analysis was performed using the 2010-2019 Cr(VI) aqueous concentration data from all wells and aquifer tubes in the 100 Areas. This type of analysis is useful for identifying groups of wells or aquifer tubes that behave similarly in terms of concentrations versus time. This information can also potentially be used in conjunction with the results of other analyses (i.e., plume maps, and trend and trajectory analysis) to identify wells or aquifer tubes that can most inform the analysis of inland and shoreline concentrations.

A classic, agglomerative hierarchical clustering method was applied in this analysis (<https://docs.scipy.org/doc/scipy/reference/generated/scipy.cluster.hierarchy.fcluster.html>; last accessed Sept 17, 2020), which initially treats each set of observations (i.e., a time series of data for a single location) as a separate cluster. Then, the following two steps are repeatedly executed: 1) identify two clusters that are the most similar to each other among all of the existing clusters, and 2) merge the two most similar clusters. This iterative process continues until all the clusters are merged together. The direct output of the agglomerative hierarchical clustering is a dendrogram, which shows the hierarchical relationships between the clusters. A key operation is to measure the dissimilarity of two clusters, which depends on 1) a distance metric, and 2) a linkage criterion that specifies dissimilarity of clusters as a function of the distance metric. Dynamic time warping (Keogh and Ratanamahatana 2005; Berndt and Clifford 1994) was used to calculate the distance metric, and Ward's method (Ward 1963) was used to define the linkage criterion. Further details on these methods are provided in Appendix A.

For 100-BC, Figure 3.27 and Figure 3.28 show the dendrogram and map of color-coded well and aquifer tube locations, respectively, illustrating the clustering results for the Cr(VI) aqueous concentration data. For these and other similar figures, sample location labels appended with "GW" in the dendrogram plots represent GW monitoring wells, and the pink and blue labeled text indicates wells that are screened in the Hanford formation and Ringold Formation, respectively.

Figure 3.29 through Figure 3.35 show the time series of Cr(VI) concentration data for the wells and aquifer tubes in each cluster. The *fcluster* algorithm produces a user-specified number of clusters (six for the results reported here), but in some cases also produces another cluster for data sets that exhibit much larger variance or have more extreme values than the data in other clusters. This extreme value cluster is designated "cluster0" in the time series plots. Inspection of Figure 3.29 through Figure 3.35 shows that the algorithms are very effective in grouping time-series data from wells and aquifer tubes that exhibit similar magnitude, variability, and trends in Cr(VI) concentrations, and distinguishing between groups with less similar behavior.

In some cases, well clusters correspond with areas of elevated concentrations in the main bodies of the Cr(VI) plumes. For example, the wells grouped into clusters 2 (blue symbols) and 3 (green symbols) for the 100-B/C data shown in Figure 3.28 are in areas of higher Cr(VI) concentrations near the center of the plume (SGW-58308, Rev. 0). The alignment of these wells also corresponds roughly with the trajectory of the 100-B/C plume. Figure 3.36 shows the time series of Cr(VI) concentration data for 100-BC corresponding to both clusters 2 and 3 on the same plot. The outlined areas on the plot identify what appear to be breakthrough curves of Cr(VI) at different wells along a flow path. Figure 3.37 through Figure 3.39 show the locations of the wells in these two clusters, together with the interpreted GW Cr(VI) plumes for 2010, 2014, and 2018, at LRS. The progression of the plume along a flow path roughly aligned with wells in clusters 2 and 3 is evident.

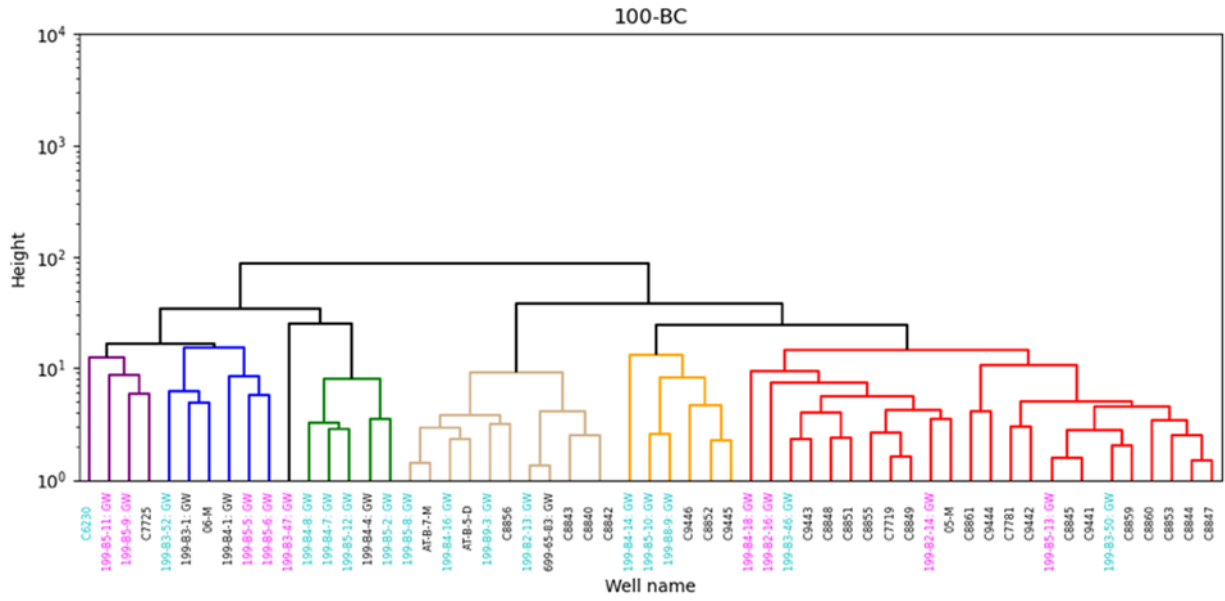


Figure 3.27. Dendrogram of Clustering Results for Cr(VI) Concentration Data from 100-B/C

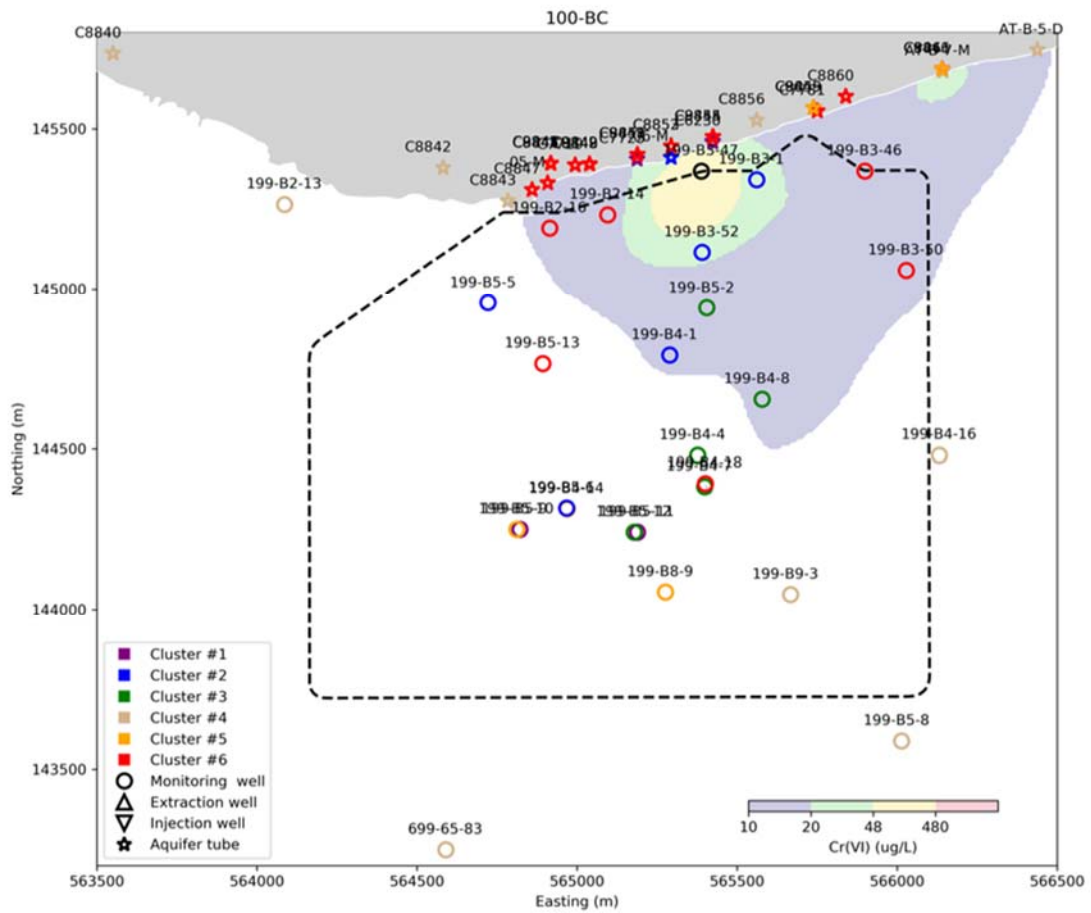


Figure 3.28. Map Showing Well and Aquifer Tube Clustering Results for 100-BC with Overlay of 2018 Cr(VI) Plume Map at LRS

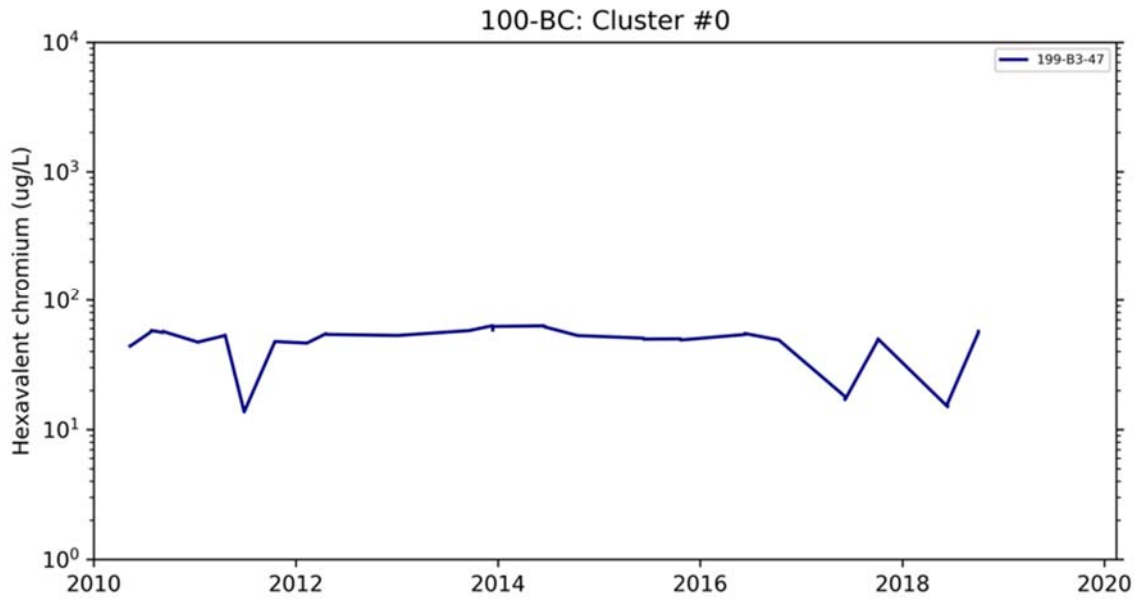


Figure 3.29. Time Series of Cr(VI) Concentration Data from Wells in Cluster 0 for 100-BC

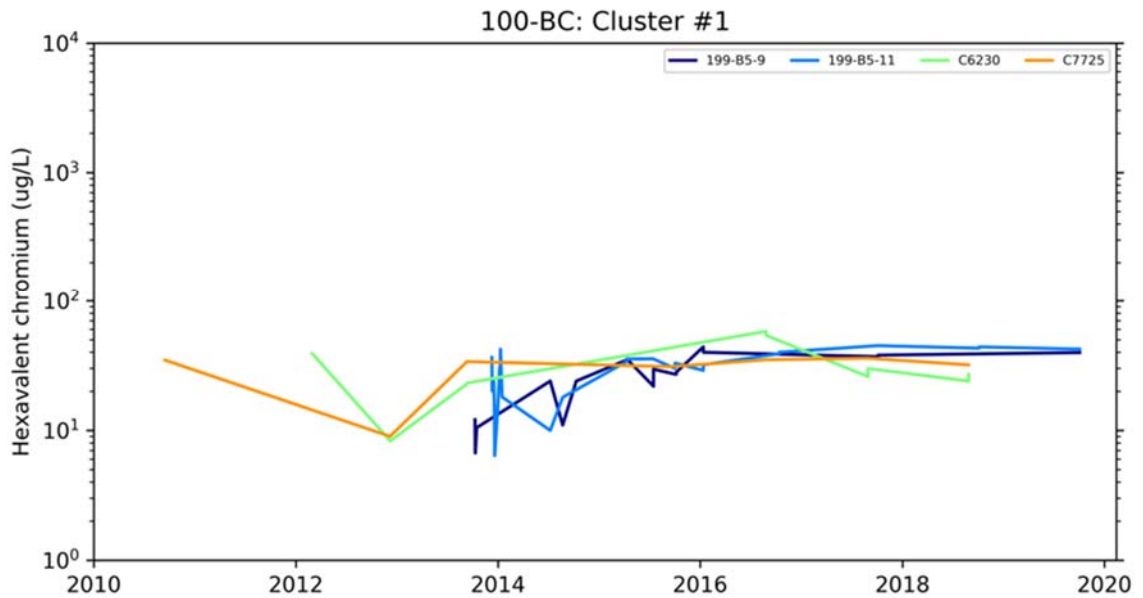


Figure 3.30. Time Series of Cr(VI) Concentration Data from Wells and Aquifer Tubes in Cluster 1 for 100-BC

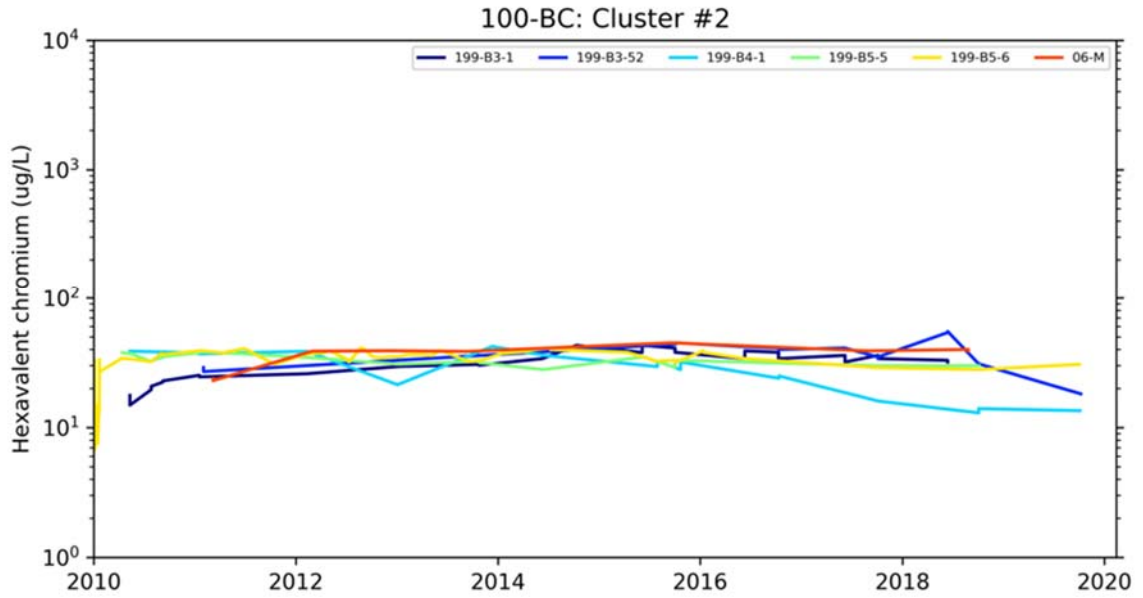


Figure 3.31. Time Series of Cr(VI) Concentration Data from Wells and Aquifer Tubes in Cluster 2 for 100-B/C

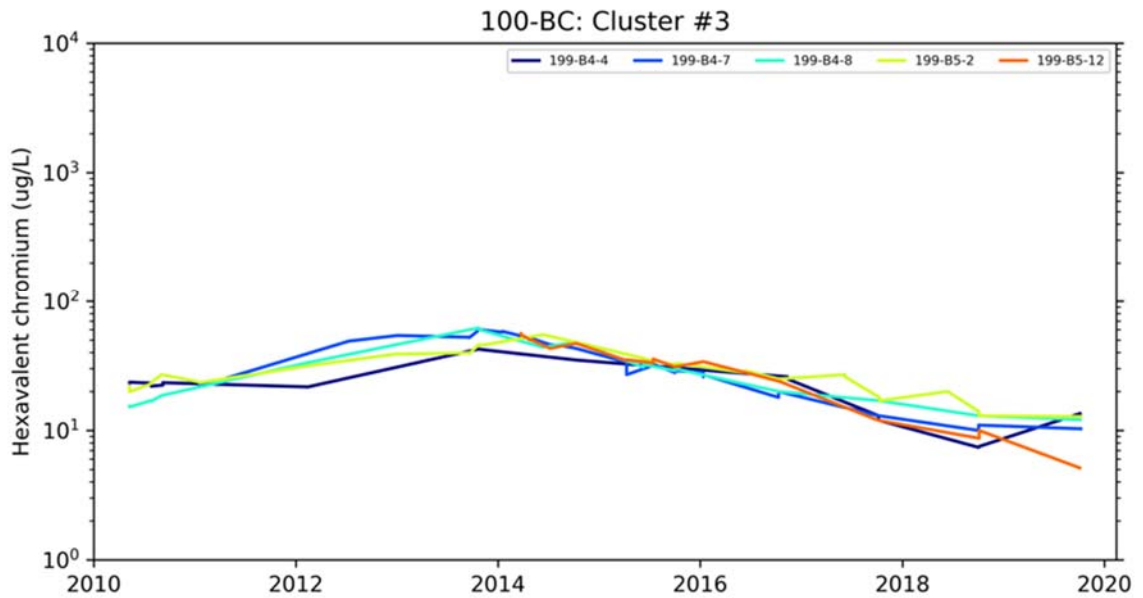


Figure 3.32. Time Series of Cr(VI) Concentration Data from Wells and Aquifer Tubes in Cluster 3 for 100-B/C

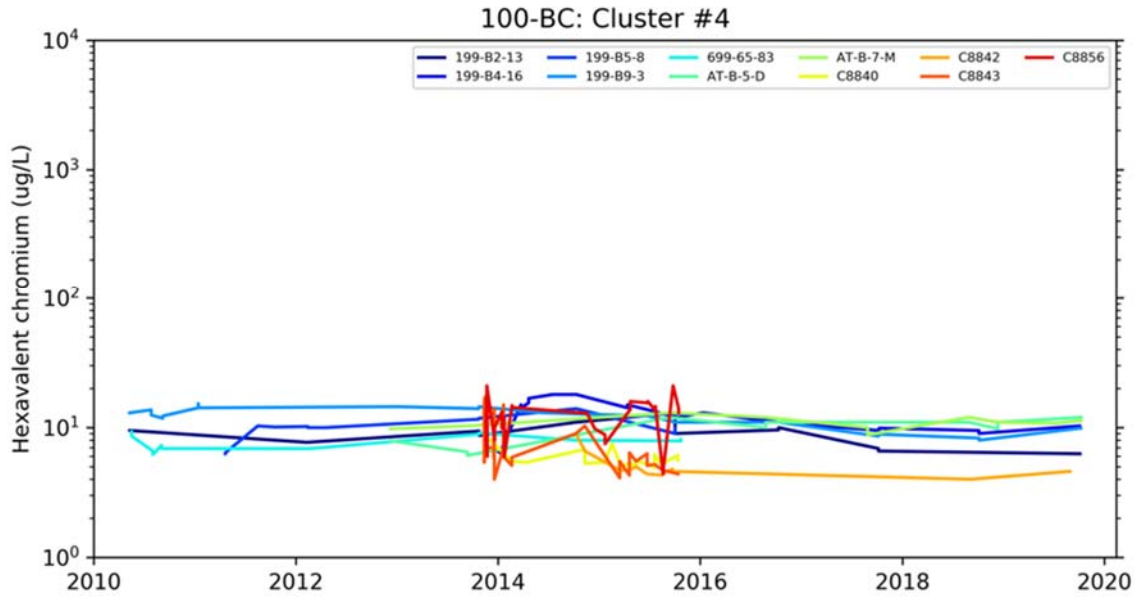


Figure 3.33. Time Series of Cr(VI) Concentration Data from Wells and Aquifer Tubes in Cluster 4 for 100-B/C

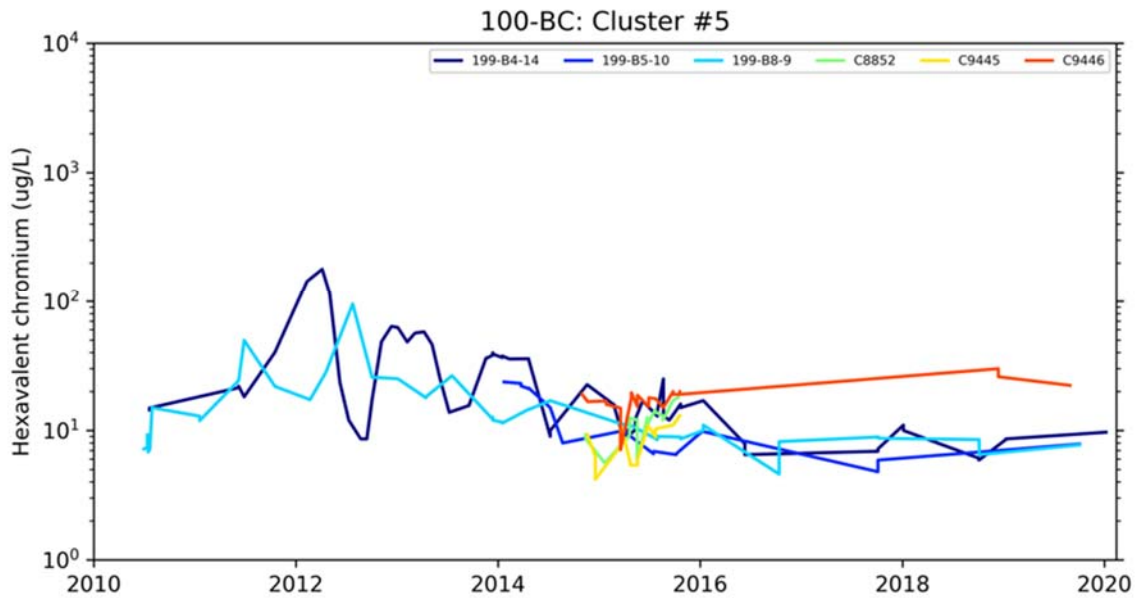


Figure 3.34. Time Series of Cr(VI) Concentration Data from Wells and Aquifer Tubes in Cluster 5 for 100-B/C

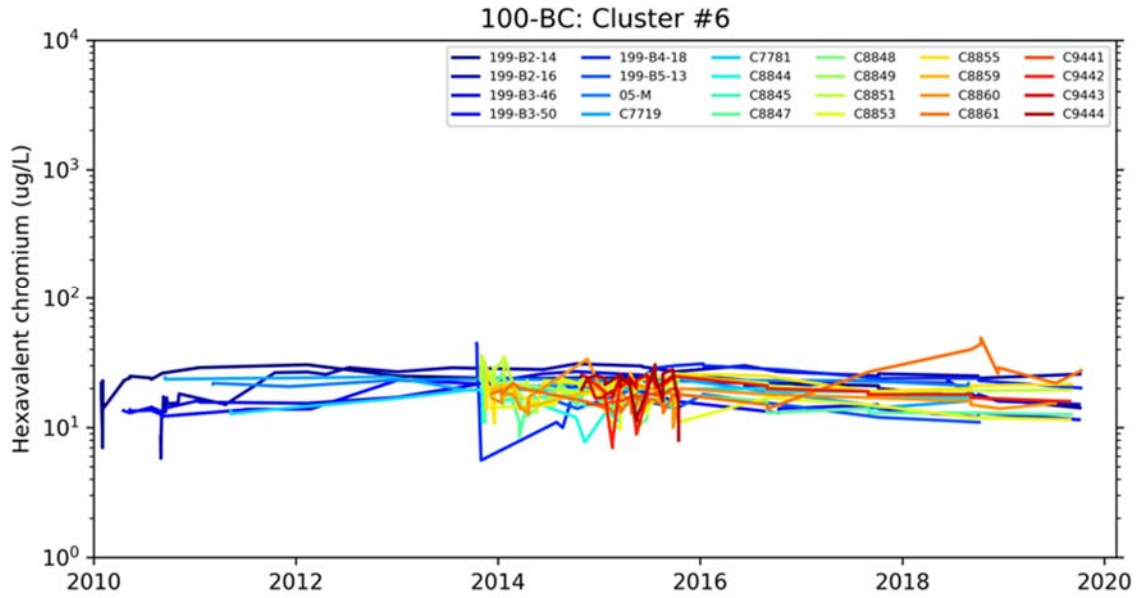


Figure 3.35. Time Series of Cr(VI) Concentration Data from Wells and Aquifer Tubes in Cluster 6 for 100-B/C

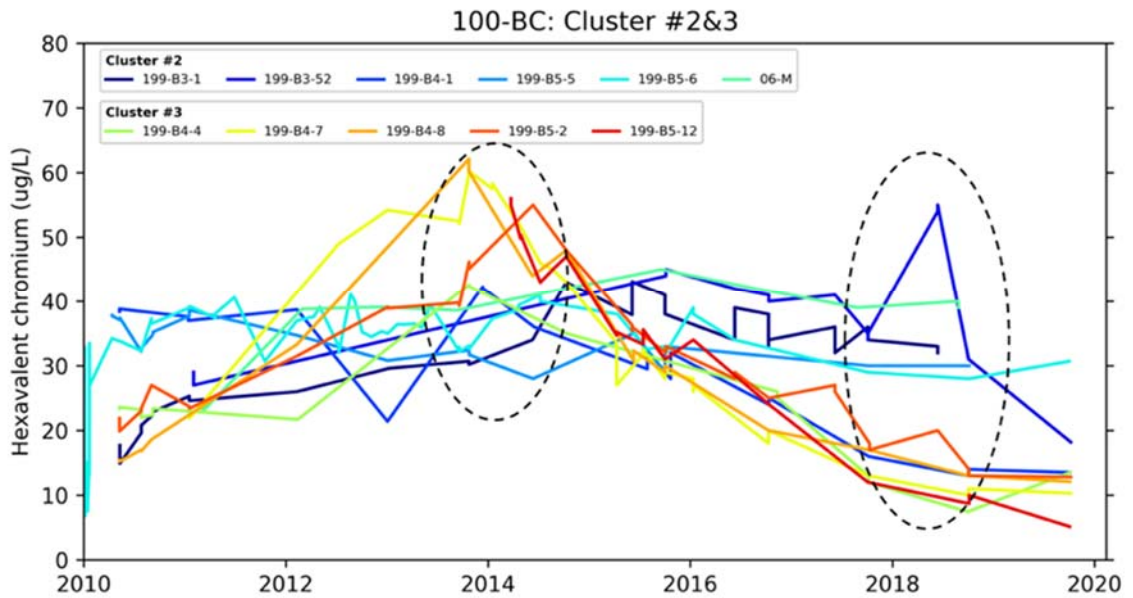


Figure 3.36. Time Series Cr(VI) Concentration Data from Wells and Aquifer Tubes in Clusters 2 and 3 for 100-B/C. Circled areas indicate peaks of apparent breakthrough curves in different wells along a flow path toward the river.

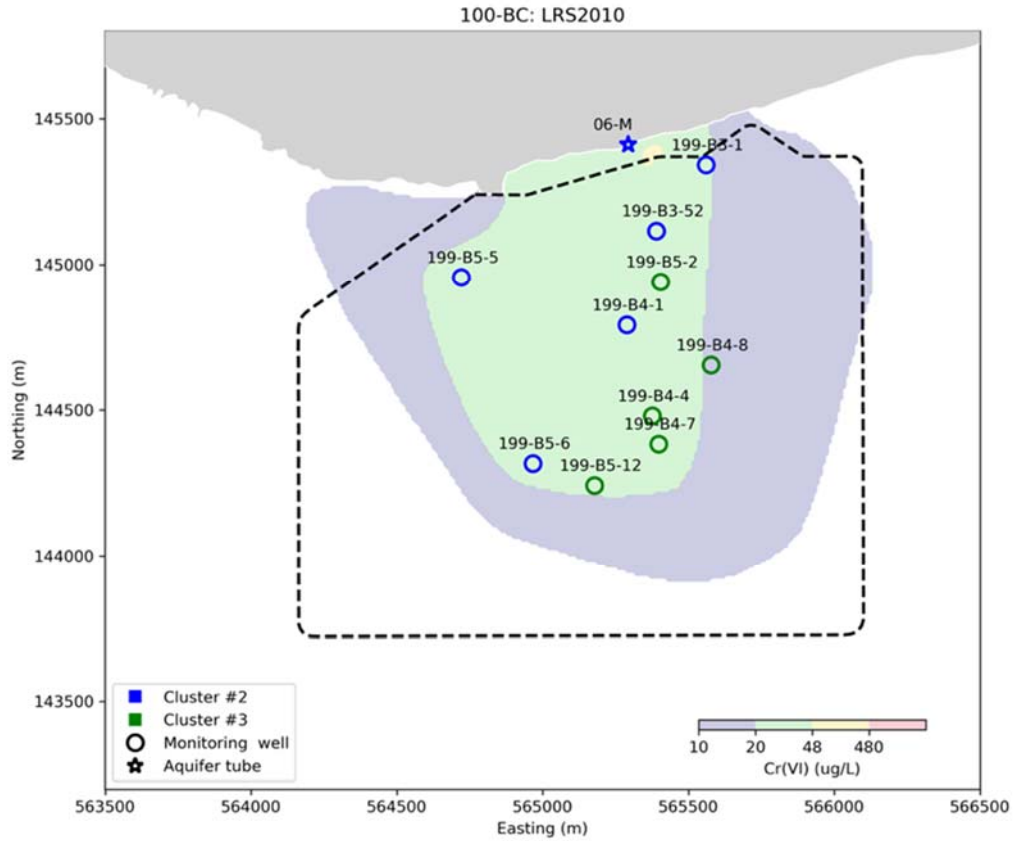


Figure 3.37. Map Showing Well and Aquifer Tubes Locations for Clusters 2 and 3 in the 100-BC Area with Overlay of 2010 Cr(VI) Plume Map at LRS

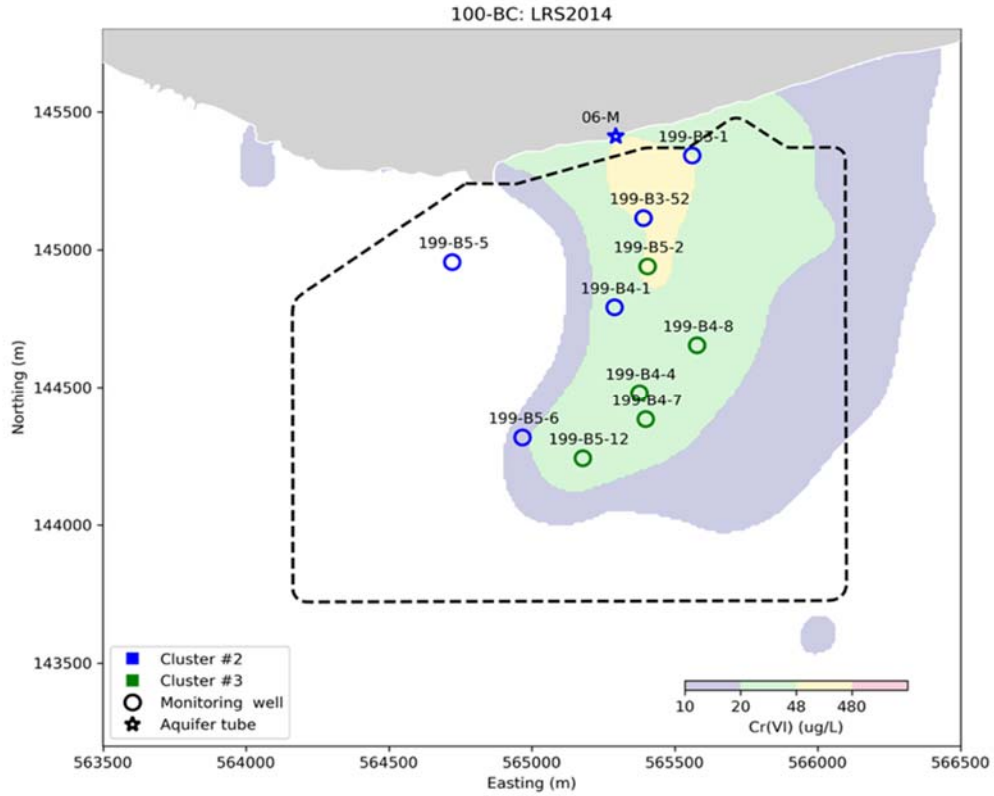


Figure 3.38. Map Showing Well and Aquifer Tubes Locations for Clusters 2 and 3 in the 100-BC Area with Overlay of 2014 Cr(VI) Plume Map at LRS

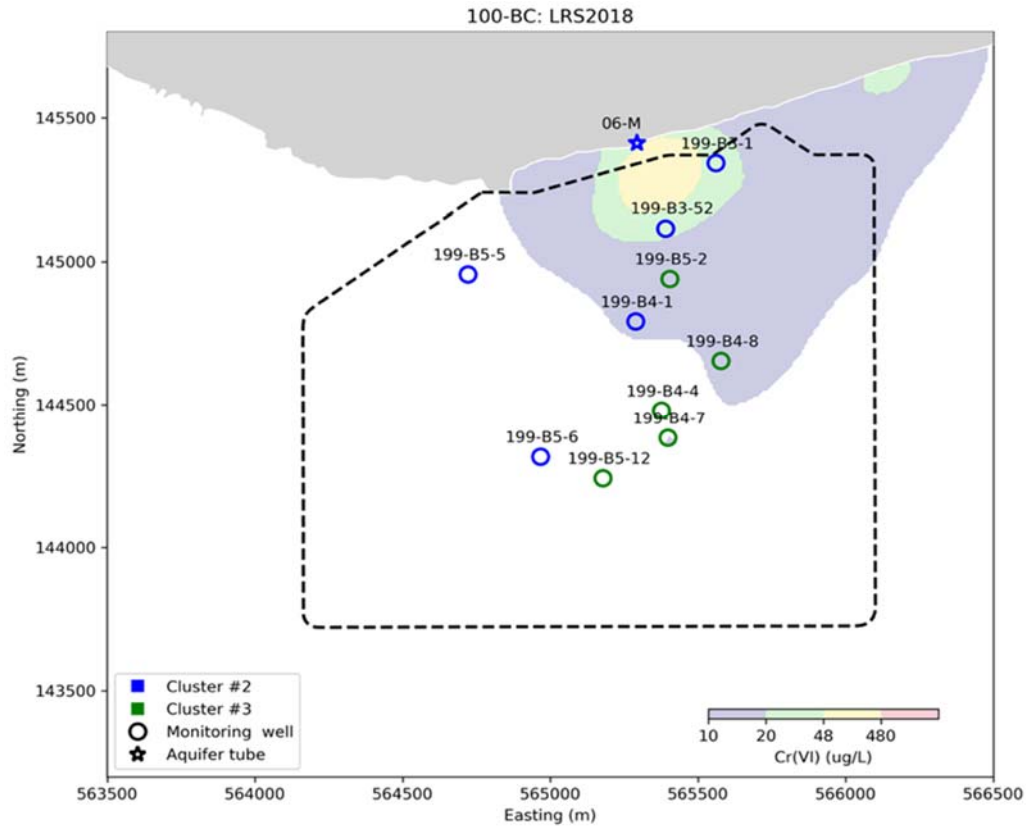


Figure 3.39. Map Showing Well and Aquifer Tubes Locations for Clusters 2 and 3 in the 100-BC Area with Overlay of 2018 Cr(VI) Plume Map at LRS

For 100-KR, the dendrogram and map of color-coded well and aquifer tube locations are shown in Figure 3.40 and Figure 3.41, respectively, depicting the clustering results for the Cr(VI) aqueous concentration data. Figure 3.42 through Figure 3.48 show the time series of Cr(VI) concentration data for 100-K corresponding to clusters 0 through 6. The clustering results and associated time-series data (e.g., Figure 3.42) can potentially be used to identify hot spots associated with continuing sources of Cr(VI) contamination from the vadose zone or aquifer. As shown in Figure 3.43, the cluster results and time-series data can also be used to identify groups of wells that have persistent concentrations below the GW and/or SW CULs.

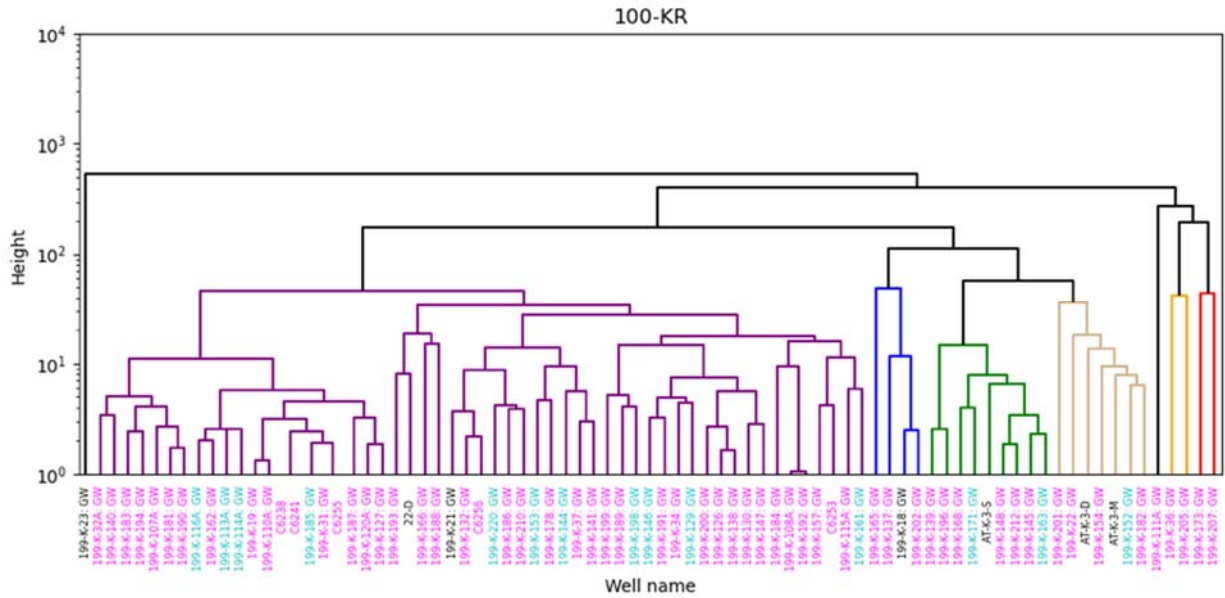


Figure 3.40. Dendrogram of Clustering Results for Cr(VI) Concentration Data from 100-KR

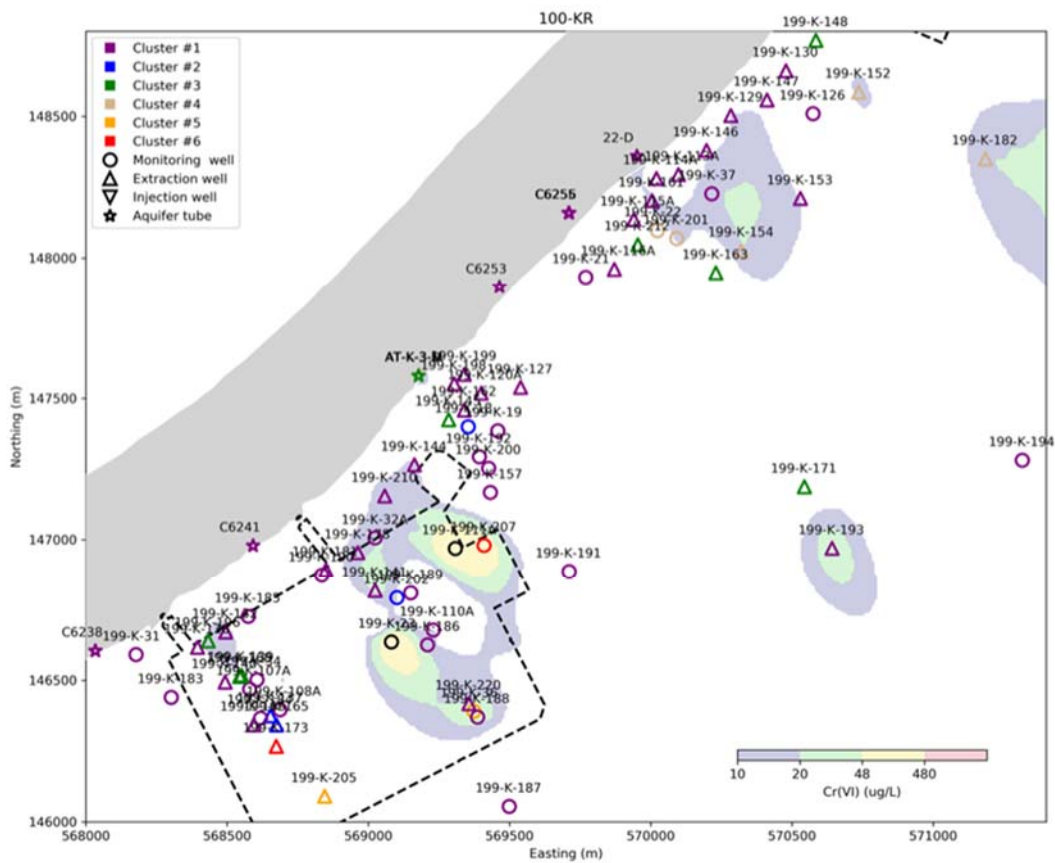


Figure 3.41. Map Showing Well and Aquifer Tube Clustering Results for 100-KR with Overlay of 2018 Cr(VI) Plume Map at LRS

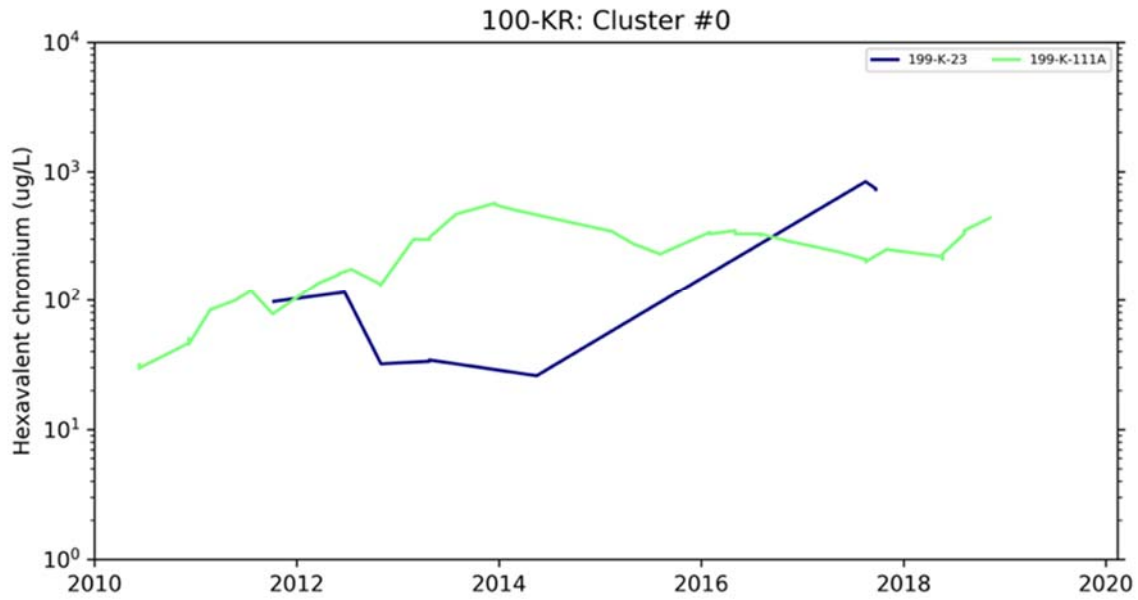


Figure 3.42. Time Series of Cr(VI) Concentration Data from Wells in Cluster 0 for 100-KR

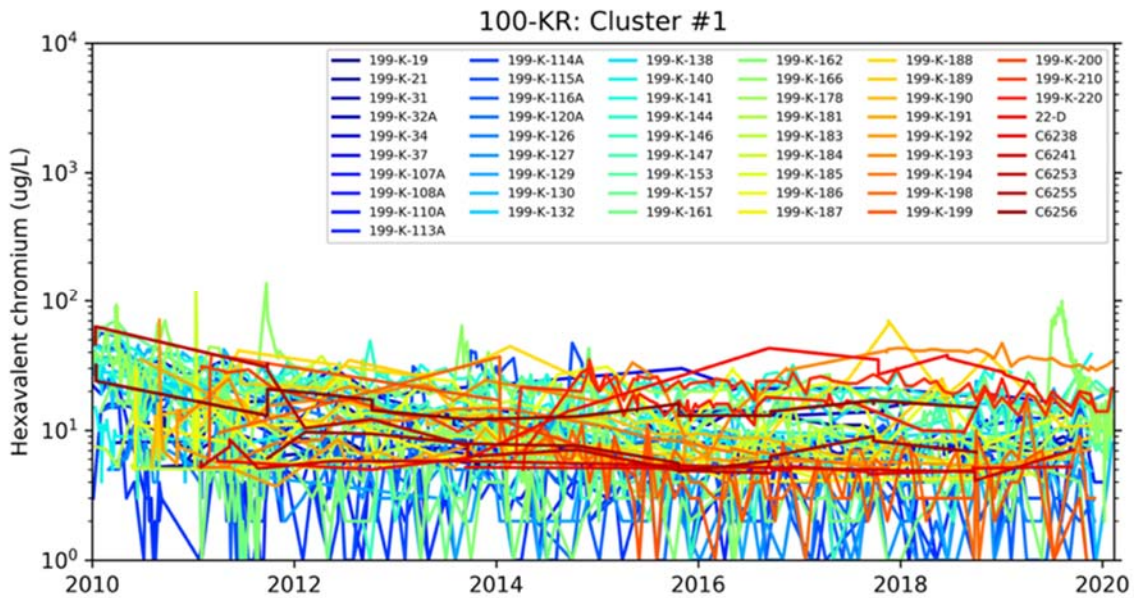


Figure 3.43. Time Series of Cr(VI) Concentration Data from Wells in Cluster 1 for 100-KR

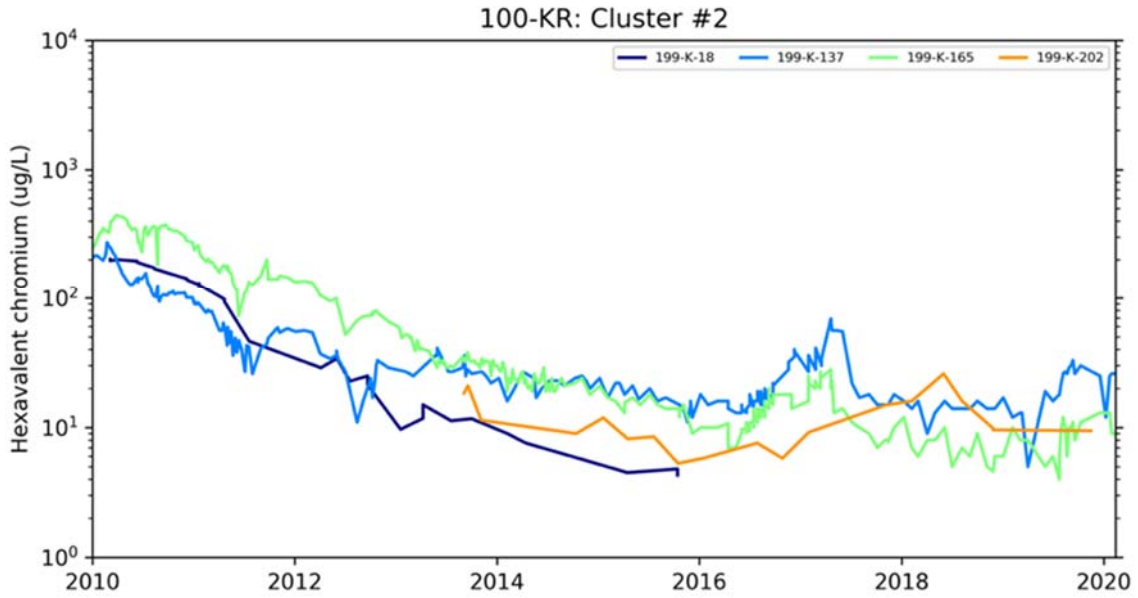


Figure 3.44. Time Series of Cr(VI) Concentration Data from Wells in Cluster 2 for 100-KR

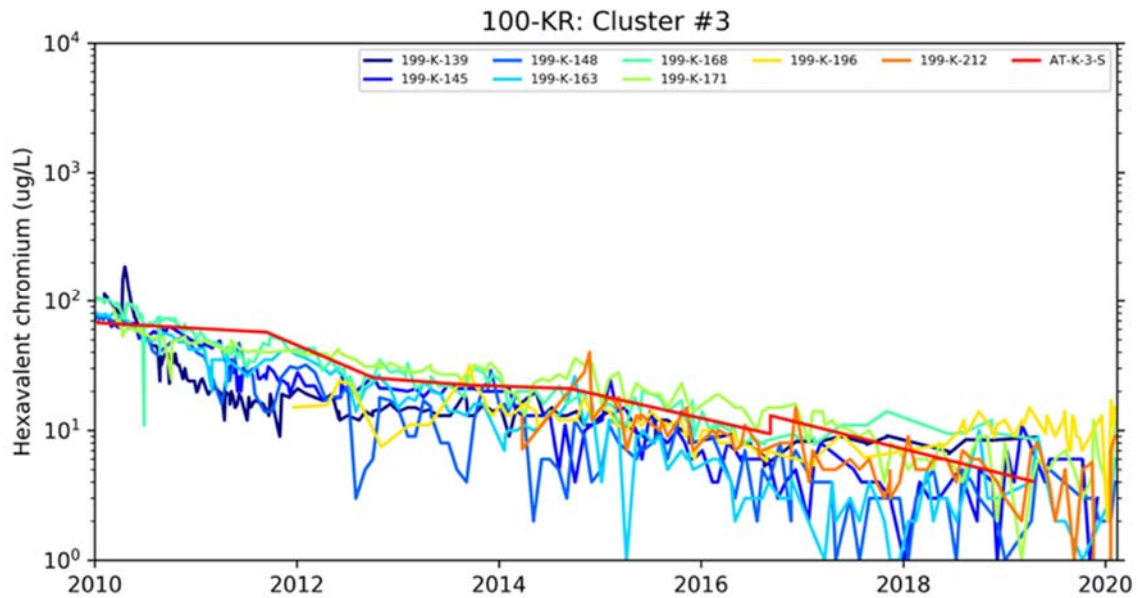


Figure 3.45. Time Series of Cr(VI) Concentration Data from Wells in Cluster 3 for 100-KR

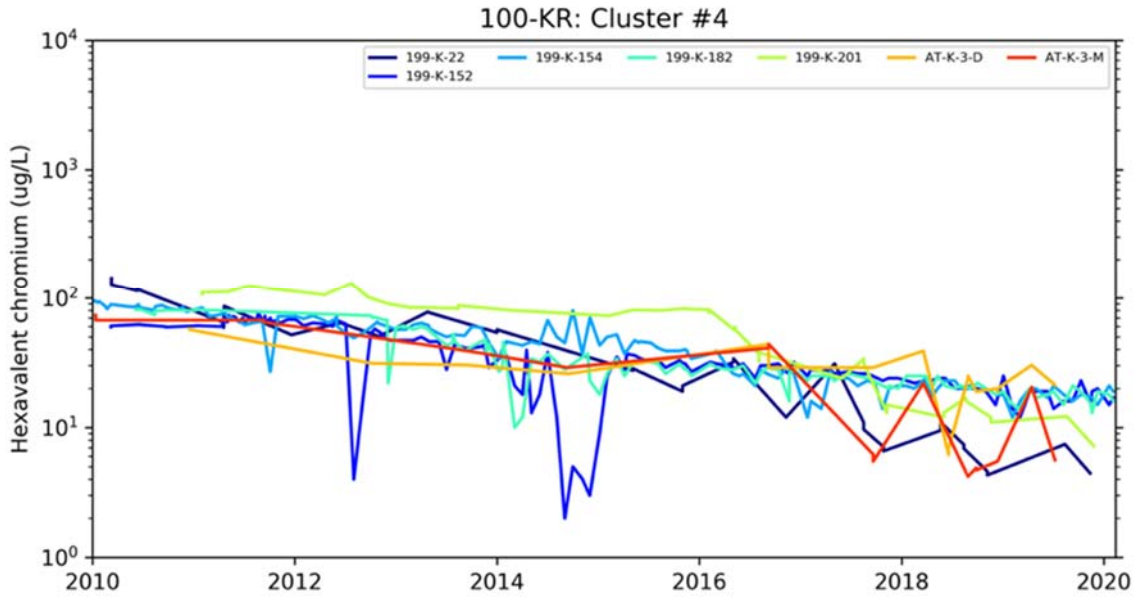


Figure 3.46. Time Series of Cr(VI) Concentration Data from Wells in Cluster 4 for 100-KR

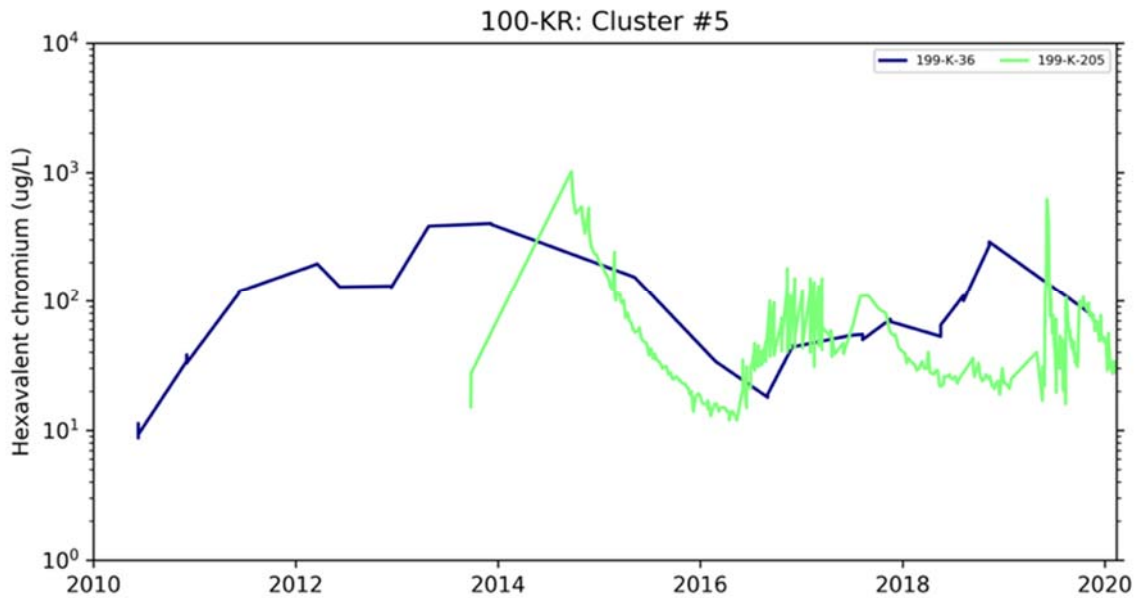


Figure 3.47. Time Series of Cr(VI) Concentration Data from Wells in Cluster 5 for 100-KR

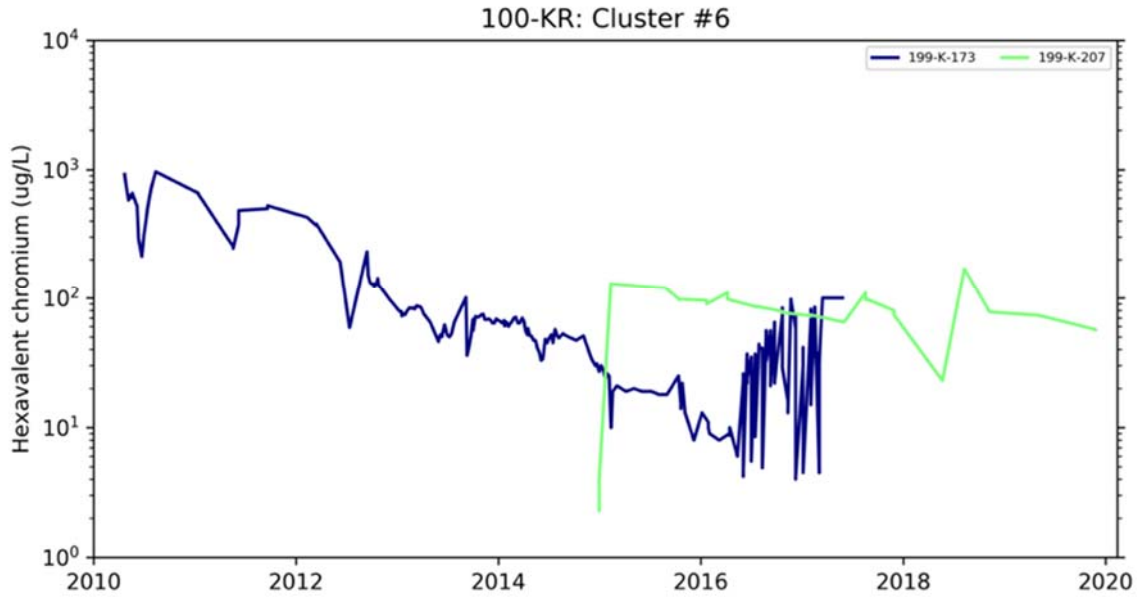


Figure 3.48. Time Series of Cr(VI) Concentration Data from Wells in Cluster 6 for 100-KR

Figure 3.49 and Figure 3.50 present the dendrogram and map of color-coded well and aquifer tube locations, respectively, for 100-HR-D to show the clustering results for the Cr(VI) aqueous concentration data. Figure 3.51 through Figure 3.57 show the Cr(VI) concentration data for 100-HR-D corresponding to clusters 0 through 6.

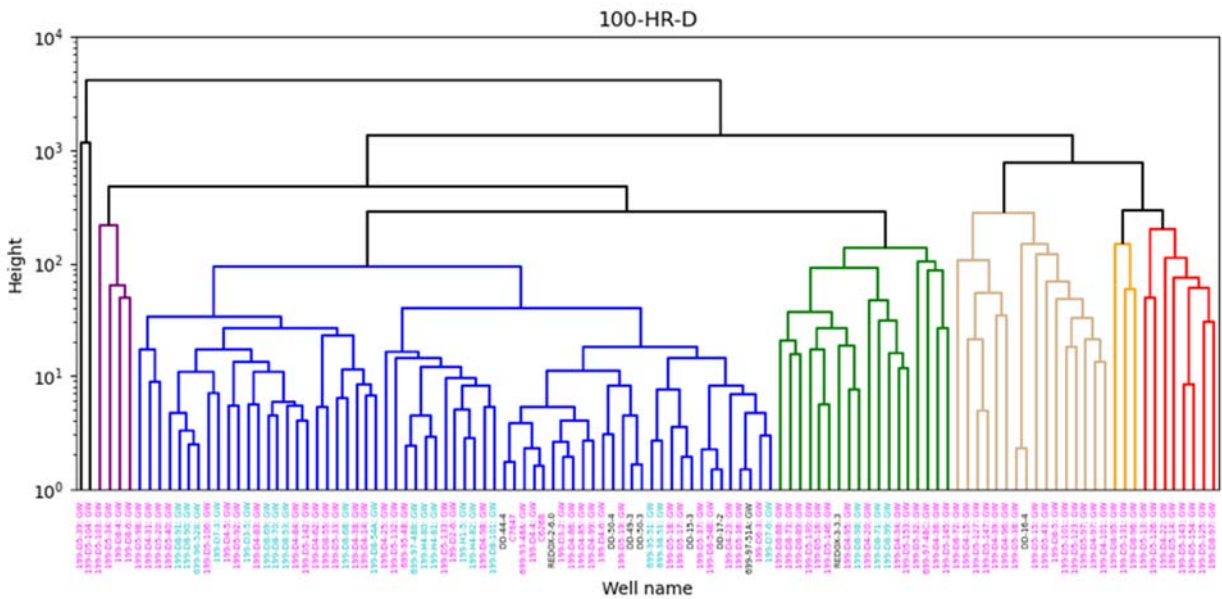


Figure 3.49. Dendrogram of Clustering Results for Cr(VI) Concentration Data from 100-HR-D

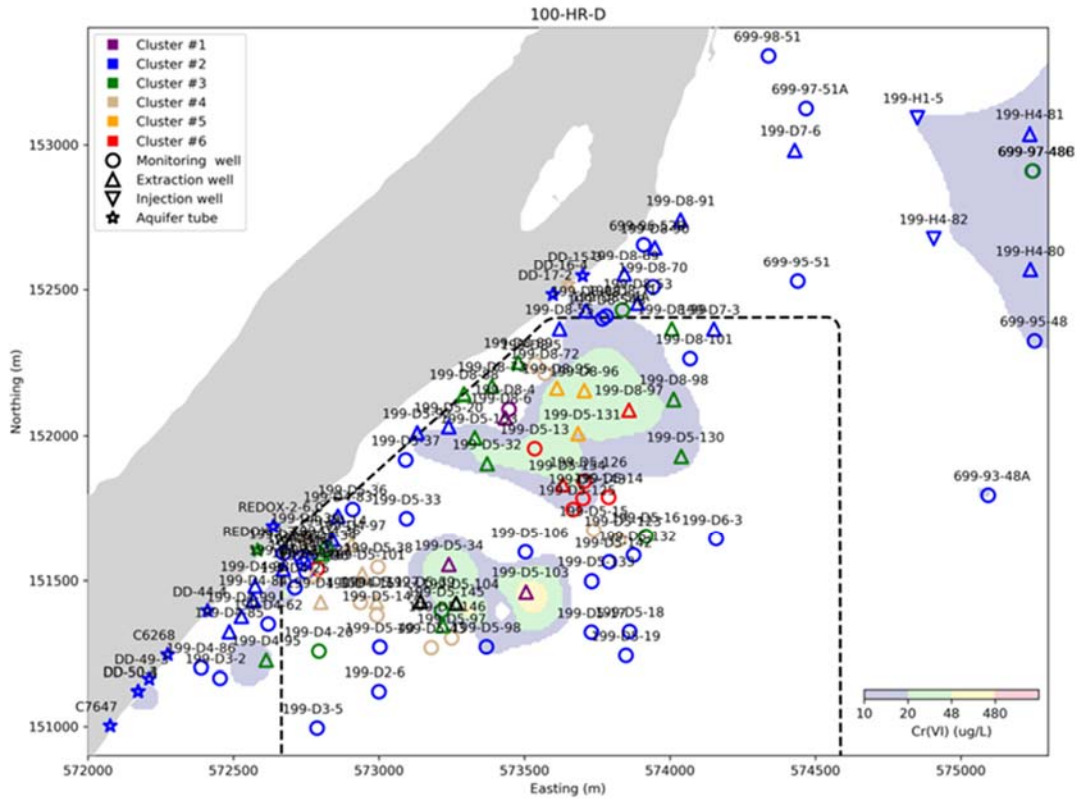


Figure 3.50. Map Showing Well and Aquifer Tube Clustering Results for 100-HR-D with Overlay of 2018 Cr(VI) Plume Map at LRS

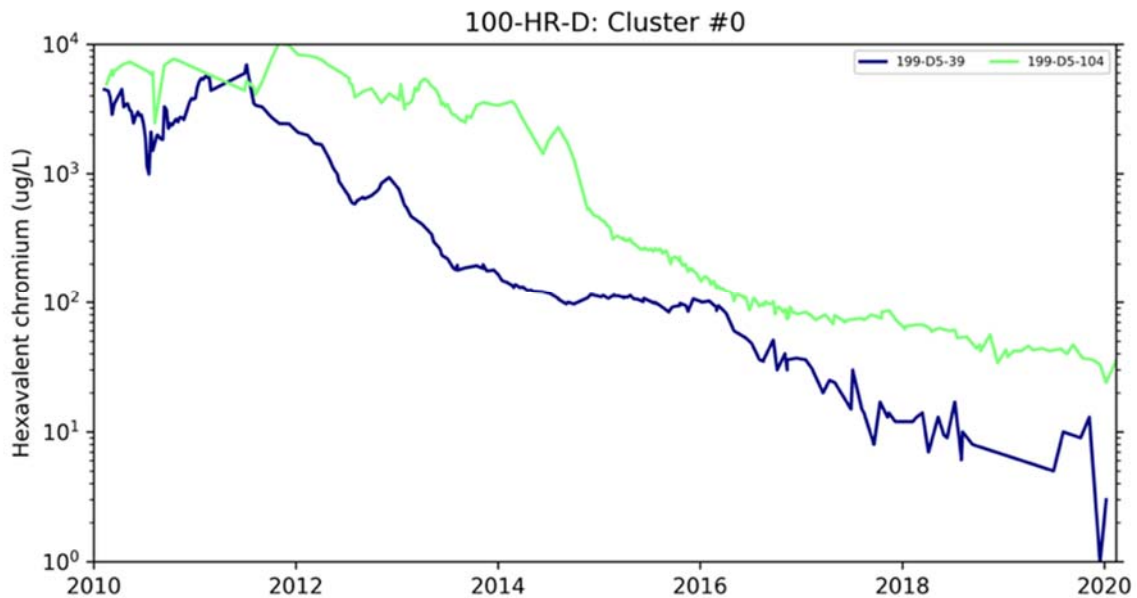


Figure 3.51. Time Series of Cr(VI) Concentration Data from Wells in Cluster 0 for 100-HR-D

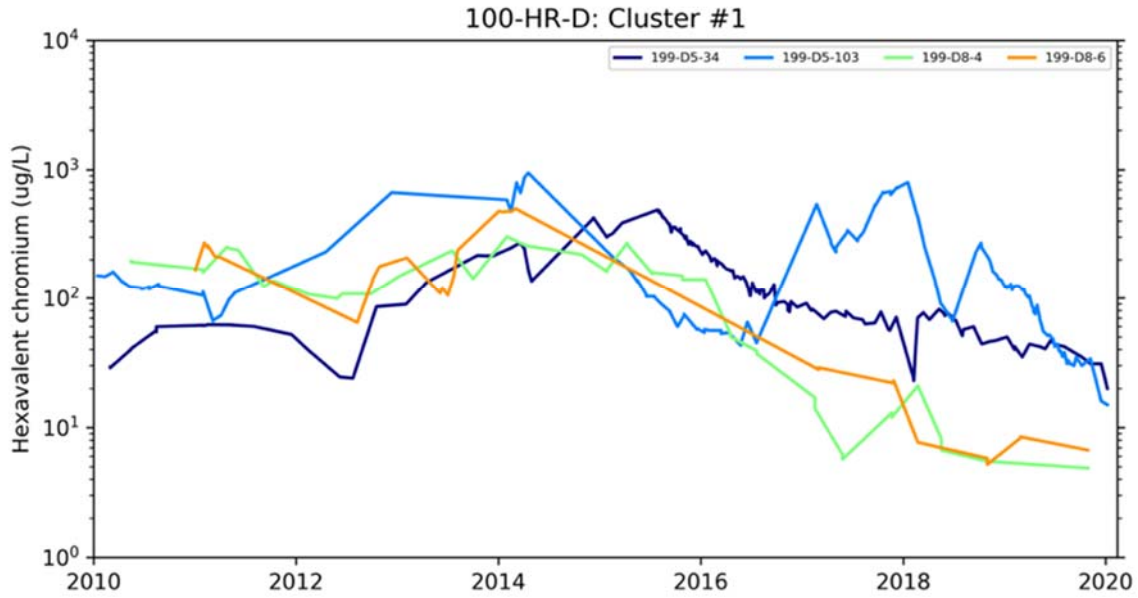


Figure 3.52. Time Series of Cr(VI) Concentration Data from Wells in Cluster 1 for 100-HR-D

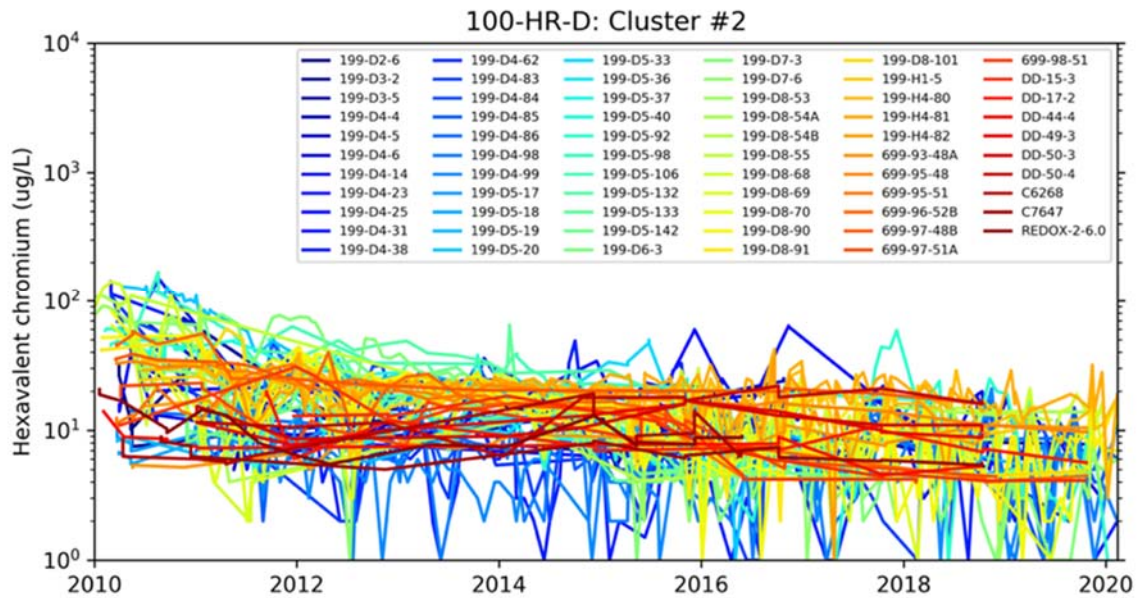


Figure 3.53. Time Series of Cr(VI) Concentration Data from Wells in Cluster 2 for 100-HR-D

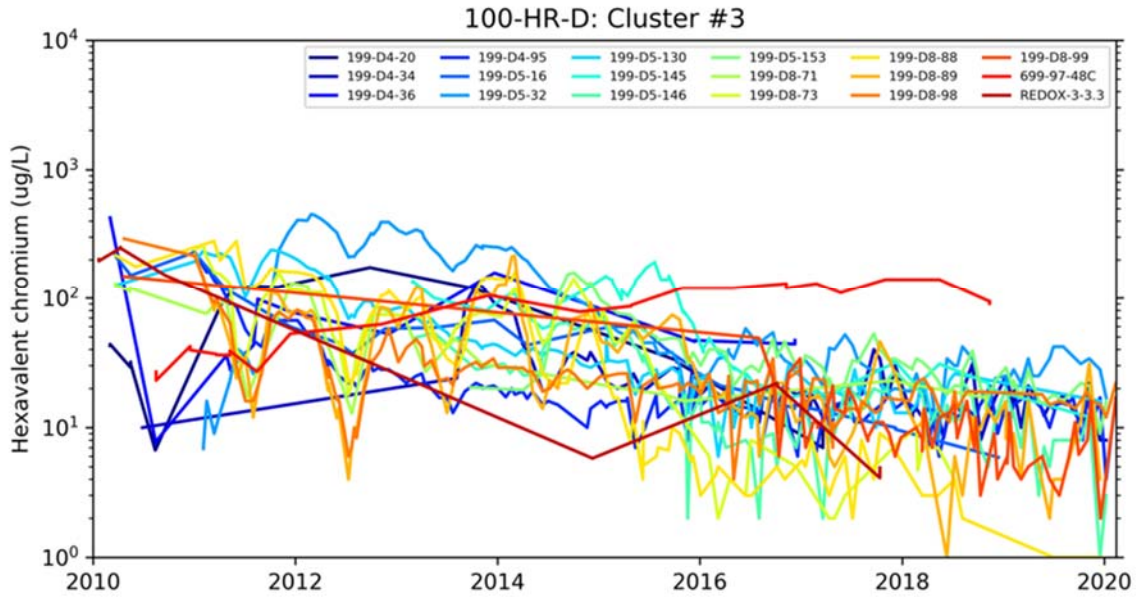


Figure 3.54. Time Series of Cr(VI) Concentration Data from Wells in Cluster 3 for 100-HR-D

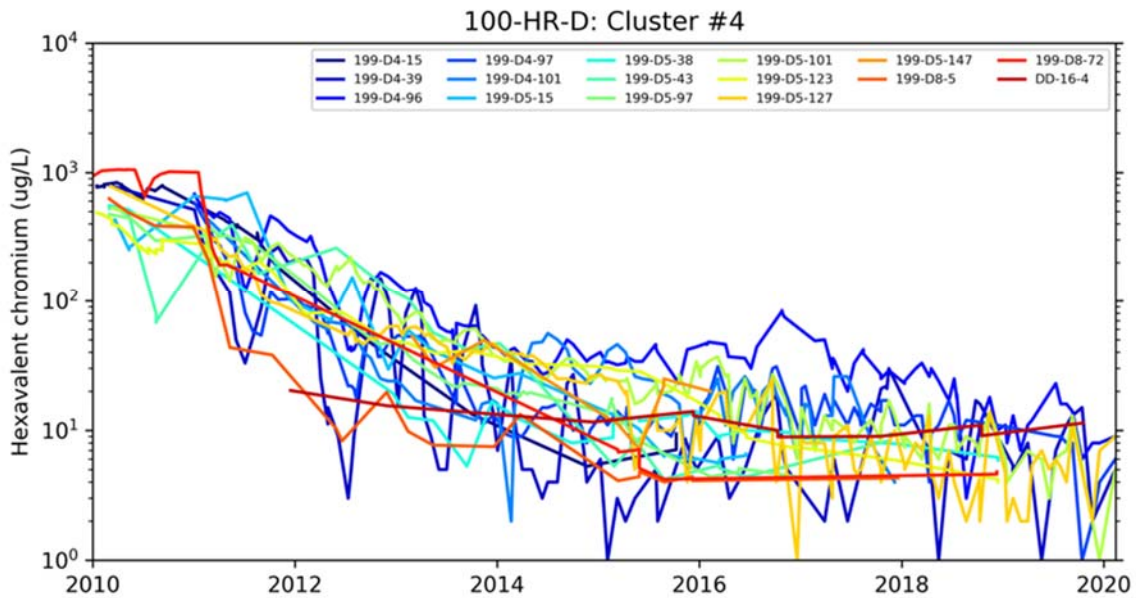


Figure 3.55. Time Series of Cr(VI) Concentration Data from Wells in Cluster 4 for 100-HR-D

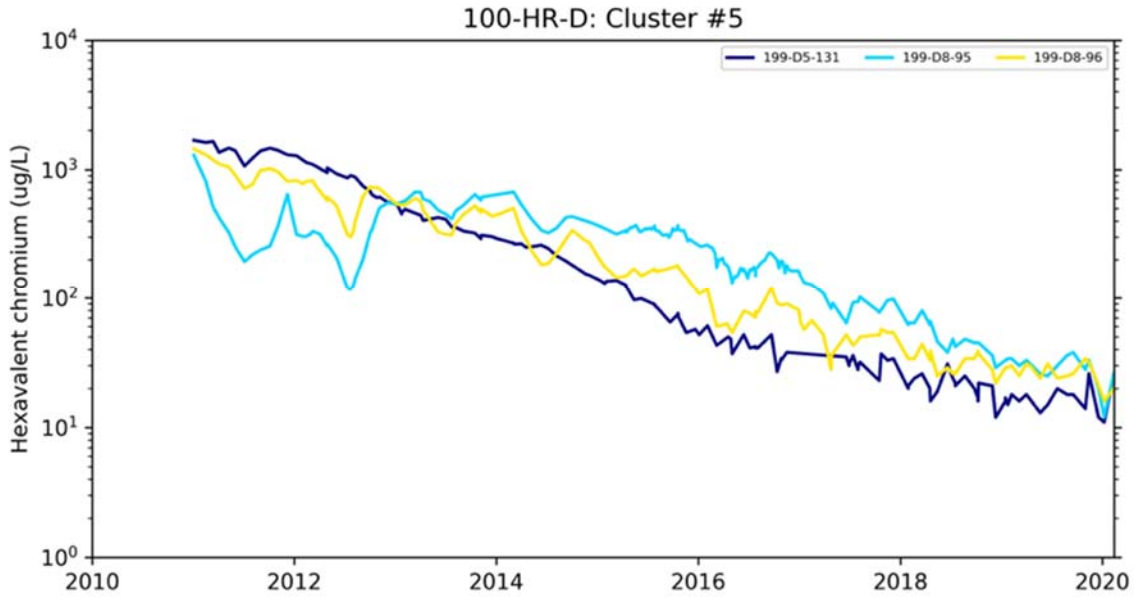


Figure 3.56. Time Series of Cr(VI) Concentration Data from Wells in Cluster 5 for 100-HR-D

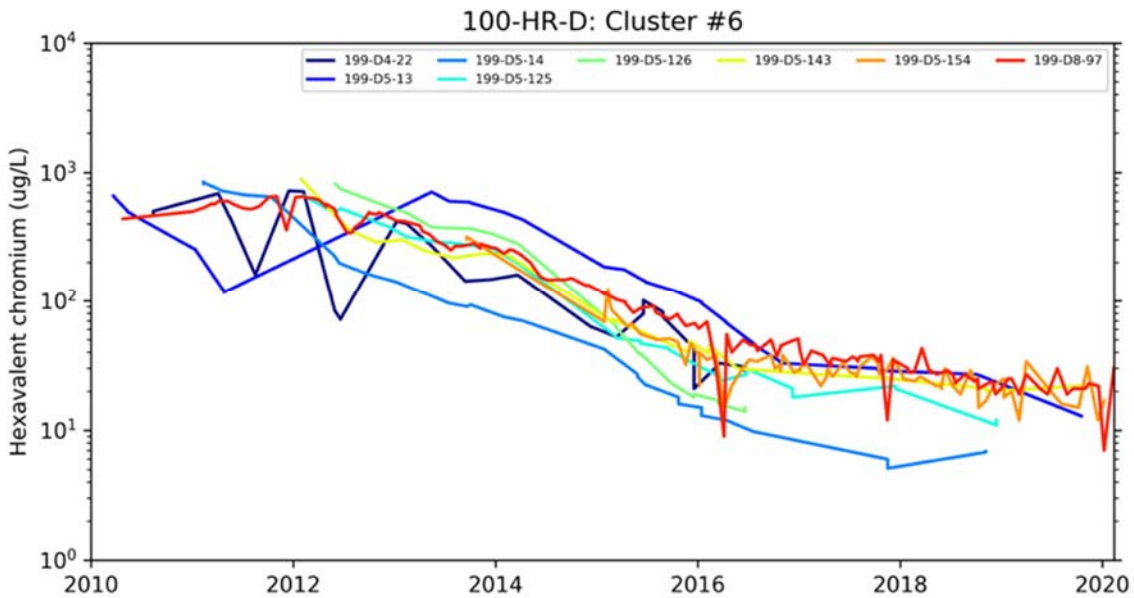


Figure 3.57. Time Series of Cr(VI) Concentration Data from Wells in Cluster 6 for 100-HR-D

Figure 3.58 and Figure 3.59 present the dendrogram and map of color-coded well and aquifer tube locations, respectively, for 100-HR-H, showing the clustering results for the Cr(VI) aqueous concentration data. Figure 3.60 through Figure 3.65 show the time series of Cr(VI) concentration data for well and aquifer tubes in clusters 1 through 6, respectively. P&T wells that being operated similarly and that have similar GW conditions, such as the group of extraction wells in cluster 2 (green triangles) aligned parallel to the shoreline (including well 199-H-32), should cluster together due to similar behaviors. The results of this analysis confirm this expectation.

Note that the time-series data for many clusters show highly oscillatory behavior with concentrations fluctuating around the 10 µg/L concentration level. Some of these fluctuations are likely due to dilution effects during HRS, but this behavior is more exaggerated for sites with P&T operations. Each site appears to behave somewhat differently, and conditions have evolved over time as the P&T systems have been adaptively managed to optimize performance.

If there were consistent relationships between Cr(VI) concentrations and distances to the shoreline, these relationships would likely be apparent in the clustering results, in the form of well and aquifer tube clusters aligned parallel to the shoreline (similar to the results shown for cluster 3 of the 100-HR-H data). The lack of well and aquifer tube clusters aligned parallel to the shoreline is further indication that there are no strong or consistent relationships between Cr(VI) concentrations and distance to shoreline. The clustering results are consistent in this regard with the other analyses described in this report.

Beyond corroborating some of the other analyses, the clustering results may be used in conjunction with plume maps and other information to identify wells that may be more-or-less useful in defining plumes, and to help inform decisions regarding changes that are made to the P&T and monitoring well networks. For example, if recent plume maps and a trajectory analysis indicate that a plume has moved beyond a set of monitoring wells or aquifer tubes, and is moving away from them, clustering results could be used to select wells that may be providing unnecessary or redundant information.

Figure 3.60 through Figure 3.65 show the time series of Cr(VI) concentration data for 100-HR-H corresponding to clusters 1 through 6. Once again, the clustering results illustrate the similarity in behavior of Cr(VI) concentration data from wells within a cluster, and the differences in behavior for wells in different clusters. The similarities and differences in behavior can be attributed to factors including proximity to the shoreline; hydrologic conditions, including forcing by P&T systems; and continuing sources in the vadose zone, PRZ, and possibly the RUM aquifer.

Insufficient data were available to perform the cluster analysis for the 100-NR and 100-FR OUs.

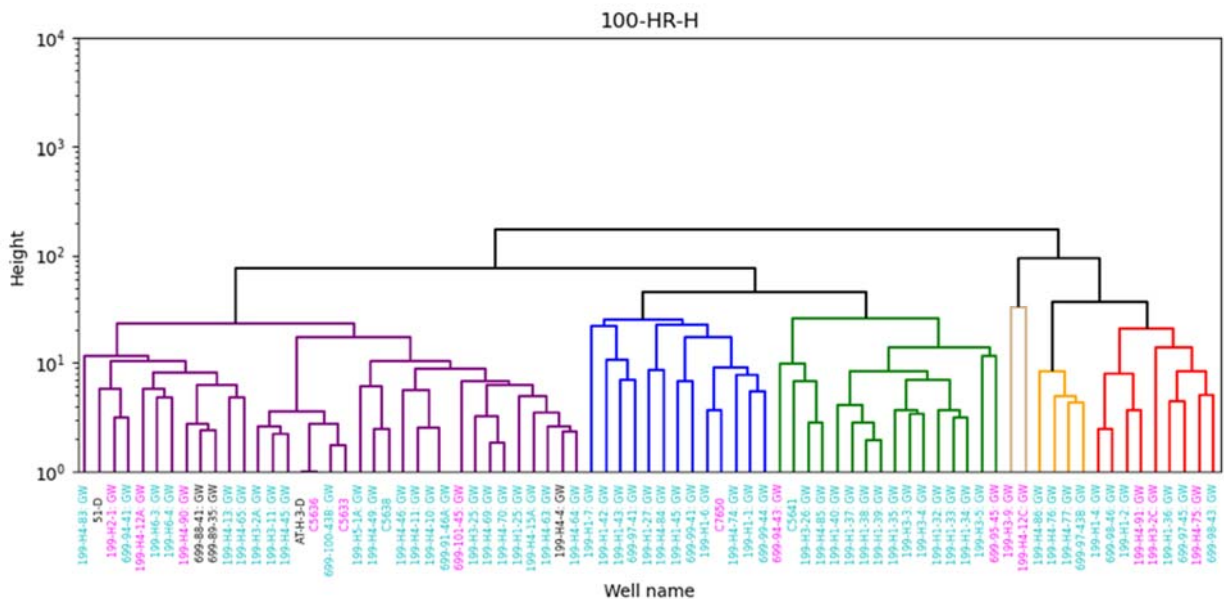


Figure 3.58. Dendrogram of Clustering Results for Cr(VI) Concentration Data from 100-HR-H

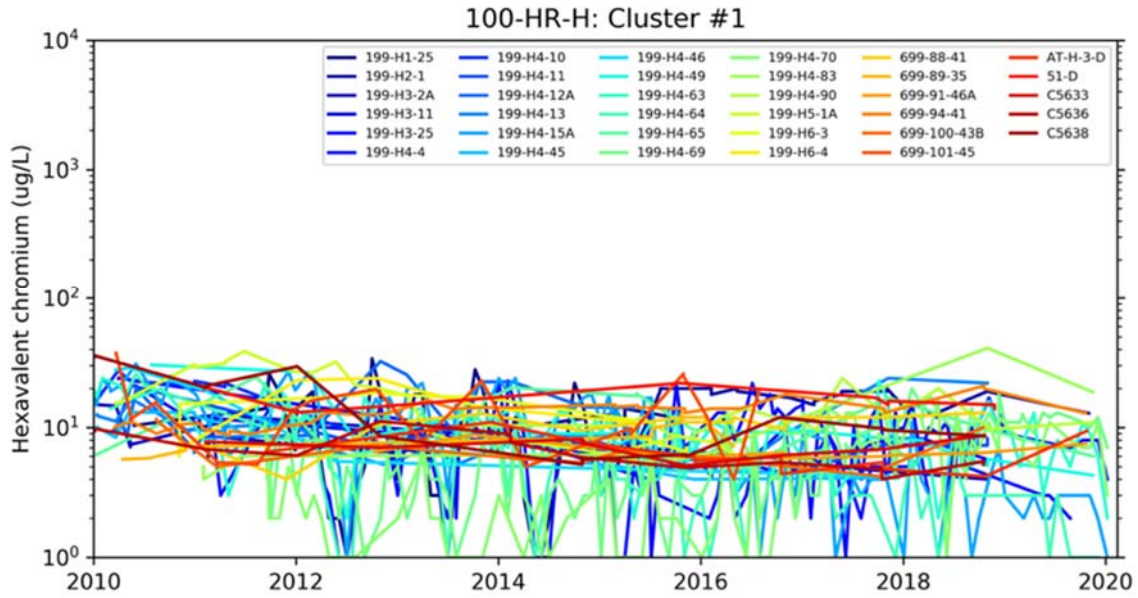


Figure 3.60. Time Series of Cr(VI) Concentration Data from Wells in Cluster 1 for 100-HR-H

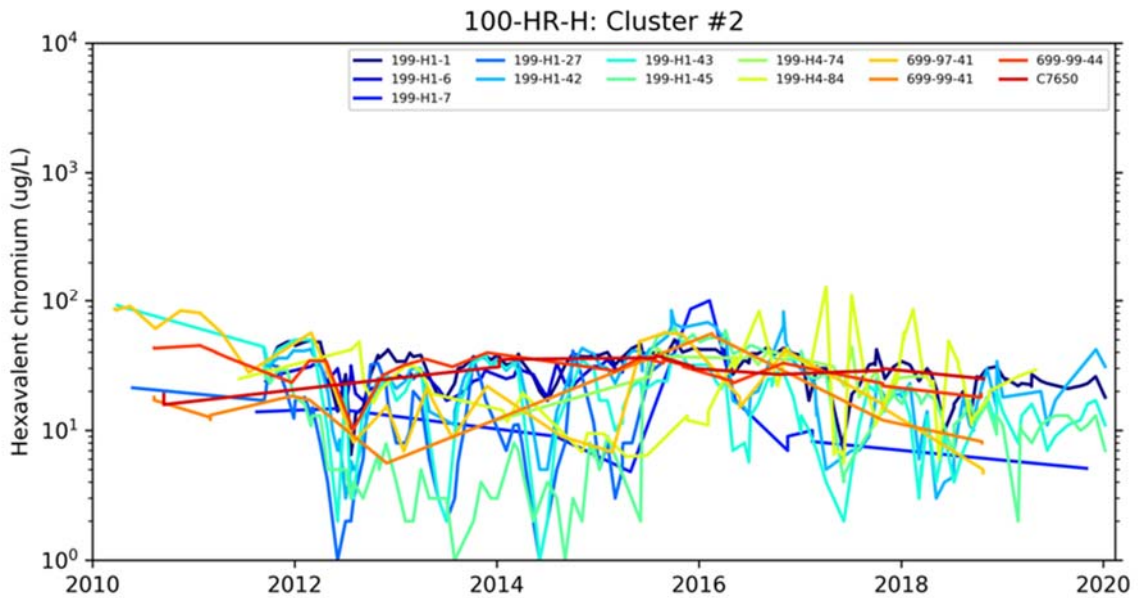


Figure 3.61. Time Series of Cr(VI) Concentration Data from Wells in Cluster 2 for 100-HR-H

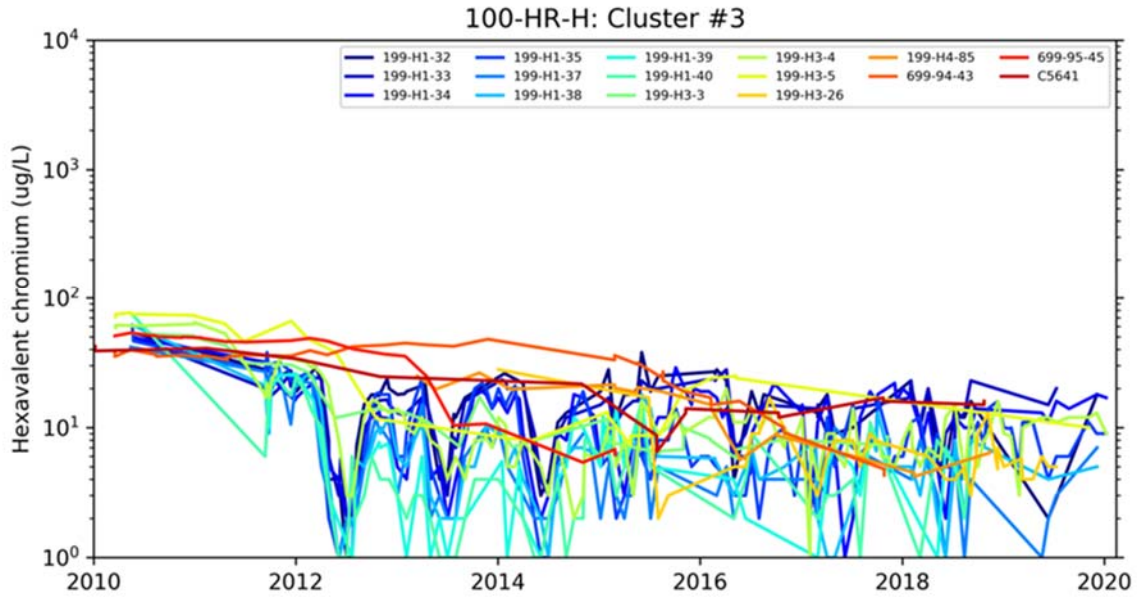


Figure 3.62. Time Series of Cr(VI) Concentration Data from Wells in Cluster 3 for 100-HR-H

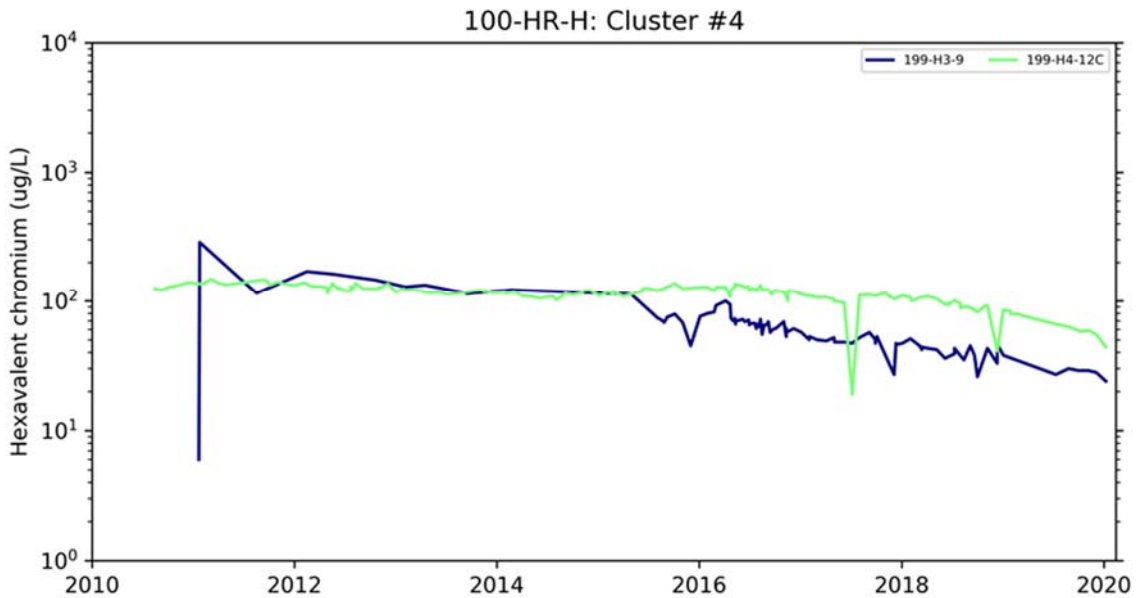


Figure 3.63. Time Series of Cr(VI) Concentration Data from Wells in Cluster 4 for 100-HR-H

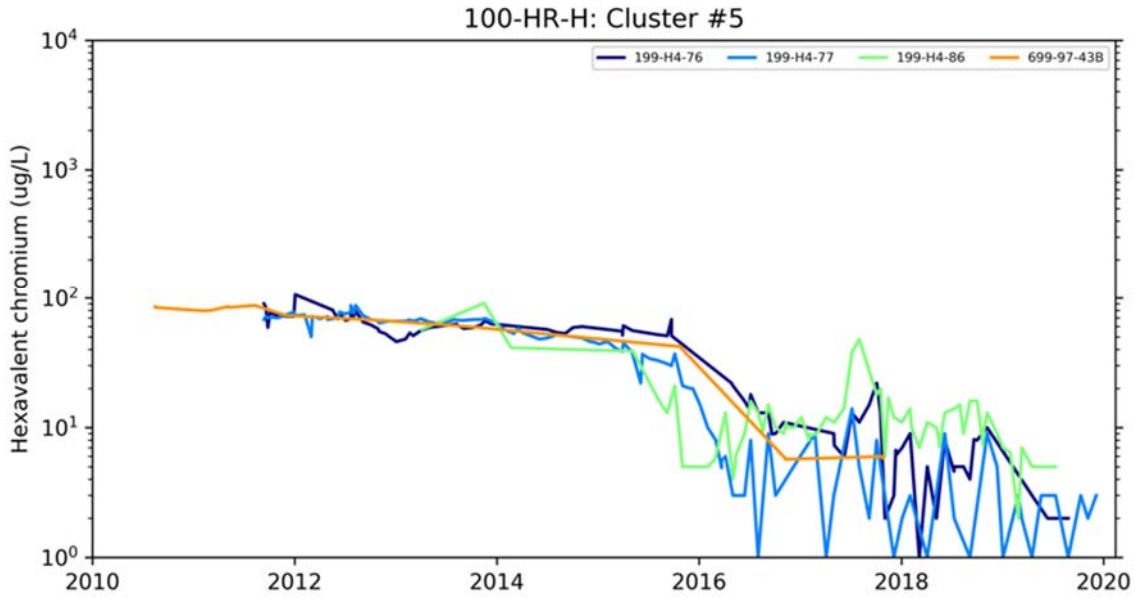


Figure 3.64. Time Series of Cr(VI) Concentration Data from Wells in Cluster 5 for 100-HR-H

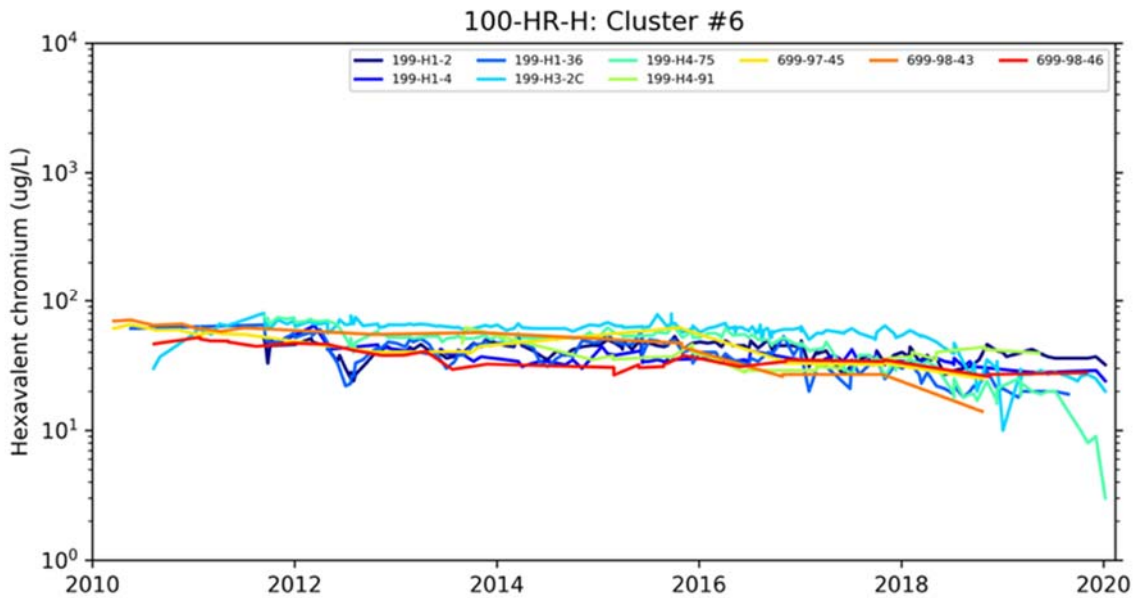


Figure 3.65. Time Series of Cr(VI) Concentration Data from Wells in Cluster 6 for 100-HR-H

3.5 Trends

Trends in Cr(VI) concentrations measured in GW monitoring wells and aquifer tubes have been previously identified (CH2M 2019), but were also examined here to complement the other analyses in this report. The notion that there might be consistent relationships between Cr(VI) concentrations and distance to the shoreline hinges on the assumption that concentrations within the areas containing the Cr(VI) plumes are relatively stable or are changing systematically with time. Trend analysis provides another method for accessing these behaviors.

The non-parametric Mann-Kendall (M-K) test was used. One requirement of the M-K test is that the data not exhibit seasonality. Therefore, the data were separated into two groups, representing time periods when the river stage is generally lower (Aug-Dec), which is referred to below as LRS, or generally higher (Jan-July), which is referred to as HRS. To be valid, the M-K test requires at least 10 data points. If a GW monitoring well or aquifer tube had fewer than 11 measurements, it was excluded from the analysis.

Figure 3.66 and Figure 3.67 show maps depicting the locations of GW monitoring wells and aquifer tubes that exhibit decreasing trends, increasing trends, or no trend in Cr(VI) concentrations according to the M-K test, for LRS and HRS, respectively. The majority of the wells show decreasing trends or no trends for both the LRS and HRS periods. Decreasing trends can be indicative of reductions in Cr(VI) concentrations resulting from P&T operations, or from plume migration. Increasing Cr(VI) concentration trends in wells or aquifer tubes at LRS could be attributable to the migration of higher concentration portions of contaminant plumes into different areas. Increasing trends at HRS could be attributable to remaining sources of Cr(VI) contamination in the vadose zone or PRZ that are accessed by GW when water levels are high. No trend in concentrations at a well suggests that the plume is relatively stable, or perhaps absent, in the vicinity of the well. Additional details on the M-K test and tabulated results are given in Appendix A.

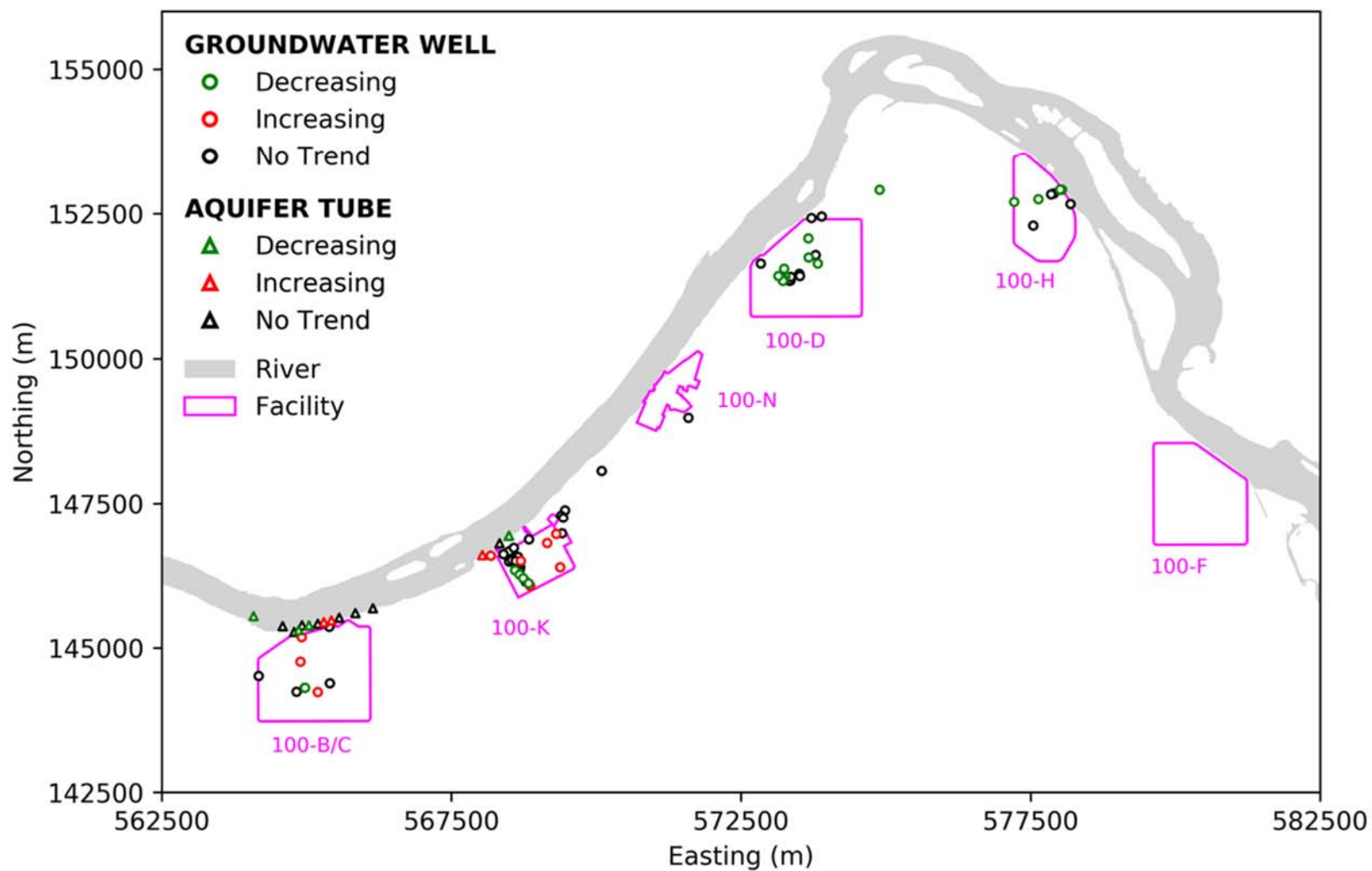


Figure 3.66. Mann-Kendall Trend Analysis Results for Cr(VI) in the 100 Areas at LRS

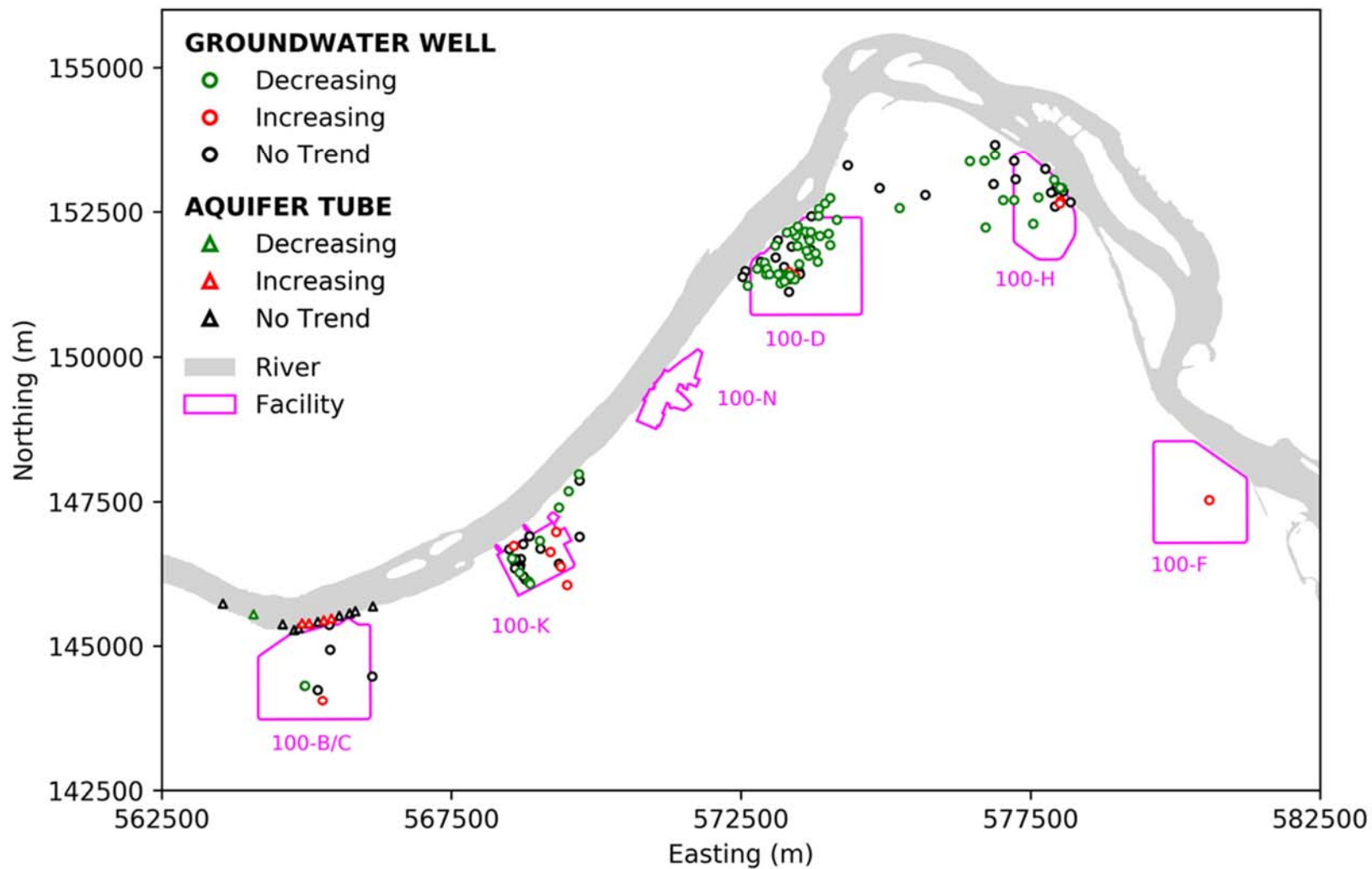


Figure 3.67. Mann-Kendall Trend Analysis Results for Cr(VI) in the 100 Areas at HRS

3.6 Cumulative Probabilities

Cumulative probability plots (Figure 3.68 through Figure 3.73) were generated by year for the 2010 to 2019 time period using the aqueous Cr(VI) concentration data from GW monitoring wells and aquifer tubes in all 100 Area GW OUs to evaluate the fraction of monitoring locations with concentrations above or below different CULs. The cumulative probability plots can be interpreted as follows. For any given Cr(VI) concentration (e.g., 10 µg/L), the corresponding cumulative probability value indicates the fraction of the total number of wells and aquifer tubes that are monitored in the OU that have concentrations lower than that value. These calculations do not directly address concentration versus distance to shoreline relationships, but the changes in concentrations over time are one of the reasons why distinct relationships are not apparent. These calculations provide another way to quantify the collective changes in concentrations that were measured by the well and aquifer tube monitoring networks at each of the 100 Area OUs over the 10-year analysis period.

In general, the fraction of monitored wells and aquifer tubes with concentrations below various CULs has increased over time. Changes have been greater for sites with active P&T systems (e.g., 100-HR-D) relative to those with MNA (e.g., 100-FR), as expected.

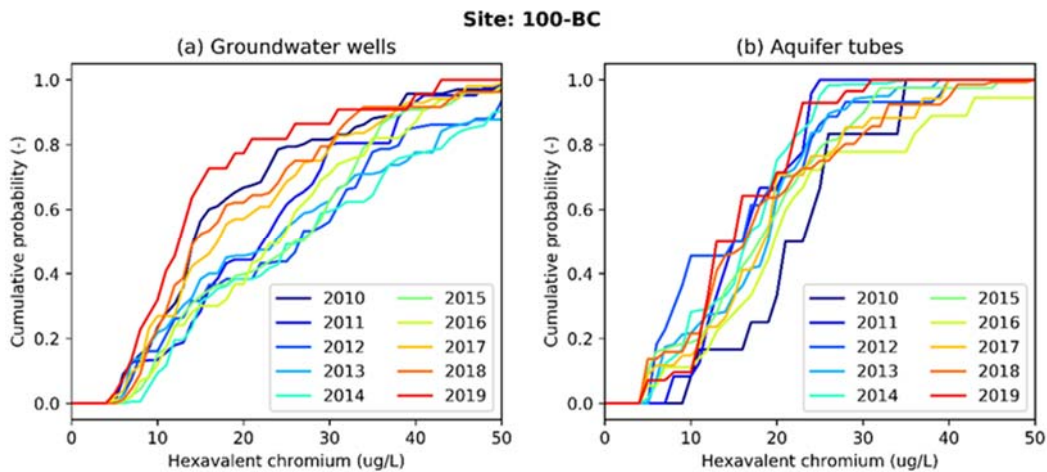


Figure 3.68. Cumulative Probability Distributions for Cr(VI) Sample Data from GW Monitoring Wells (a) and Aquifer Tubes (b) in the 100-BC OU

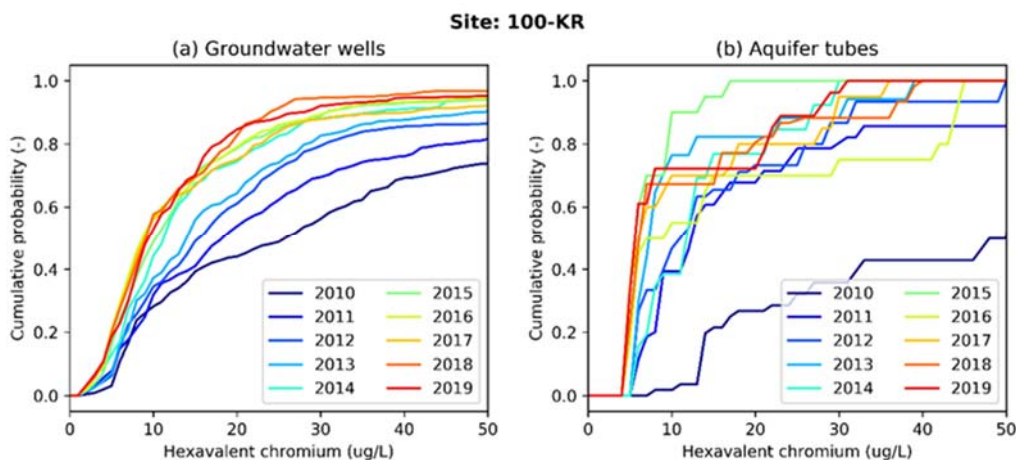


Figure 3.69. Cumulative Probability Distributions for Cr(VI) Sample Data from GW Monitoring

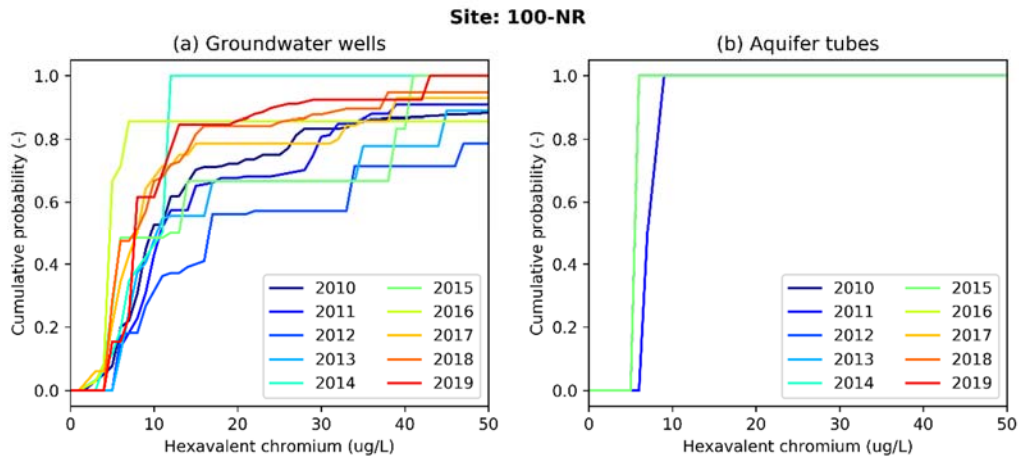


Figure 3.70. Cumulative Probability Distributions of Cr(VI) Sample Data from (a) GW Monitoring Wells and (b) Aquifer Tubes in the 100-NR OU

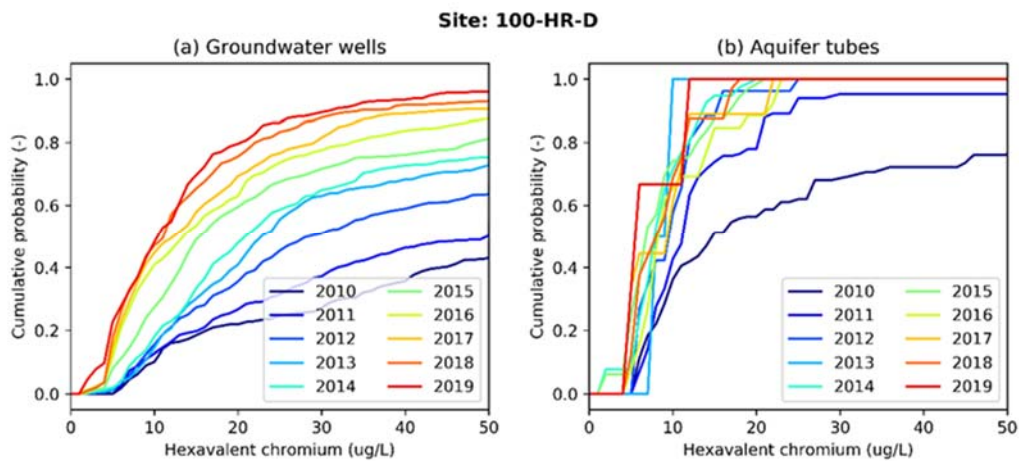


Figure 3.71. Cumulative Probability Distributions of Cr(VI) Sample Data from (a) GW Monitoring Wells and (b) Aquifer Tubes in the 100-HR-D OU

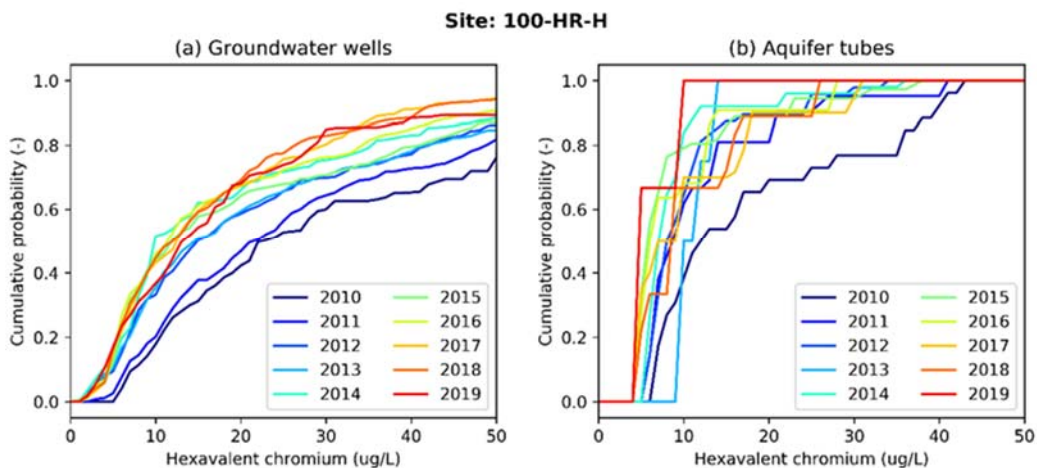


Figure 3.72. Cumulative Probability Distributions of Cr(VI) Sample Data for (a) GW Monitoring Wells and (b) Aquifer Tubes in the 100-HR-H OU

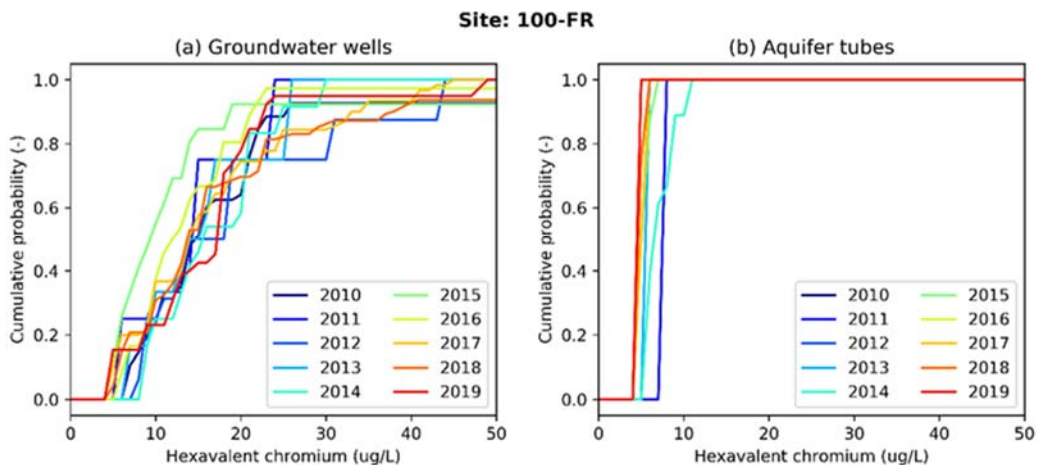


Figure 3.73. Cumulative Probability Distributions of Cr(VI) Sample Data from (a) GW Monitoring Wells and (b) Aquifer Tubes in the 100-FR OU

Table 3.1 and Table 3.2 summarize these results for GW monitoring wells and aquifer tubes, respectively, for each of the 100 Area GW OUs. Monitoring data for 2019 show that the majority of the monitoring wells and all of the aquifer tubes in all of the 100 Area GW OUs had concentrations below the 48 µg/L GW CUL. Progressively smaller percentages of monitoring wells and aquifer tubes had concentrations below 20 and 10 µg/L.

The numbers and locations of wells and aquifer tubes that have been monitored in the 100 Area have changed over time. However, plots of the well and aquifer tube sampling locations for each year (not shown) suggest that similar numbers and spatial distributions of sampling points are used every year. It is likely that the locations with the highest concentrations are sampled most frequently in an effort to better characterize the plumes and optimize remediation. Through time, the lower-concentration locations have been dropped from sampling. Thus, there is a conservative bias toward higher concentrations through time, and the observed decreases in concentrations are real and not an artifact of sampling locations with lower concentrations.

Table 3.1. Percentage of Monitoring Wells with Cr(VI) Concentrations Below Target CULs in 2010 and 2019

GW OU	10 µg/L		20 µg/L		48 µg/L	
	2010	2019	2010	2019	2010	2019
100-BC	23	32	67	77	97	100
100-KR	28	53	44	85	73	95
100-NR	53	62	72	86	88	100
100-HR-D	10	48	22	80	42	96
100-HR-H	18	37	42	68	72	89
100-FR	24	23	64	78	93	97

Table 3.2. Percentage of Aquifer Tubes with Cr(VI) Concentrations Below Target CULs in 2010 and 2019

GW OU	10 µg/L	20 µg/L	48 µg/L

	2010	2019	2010	2019	2010	2019
100-BC	8	10	33	71	100	100
100-KR	2	72	27	72	50	100
100-NR	100	-	100	-	100	-
100-HR-D	36	67	56	100	76	100
100-HR-H	38	100	69	100	100	100
100-FR	-	100	-	100	-	100

4.0 Summary and Recommendations

To quantify possible attenuation of Cr(VI) concentrations between inland GW monitoring wells and aquifer tubes measuring shoreline concentrations, a systematic series of data analyses were performed. Results are summarized as follows:

- This study focused initially on the 100-BC OU because it had higher frequency data collection from aquifer tubes and hyporheic zone samplers, and it does not have a P&T system that influences groundwater Cr(VI) plume behavior. Examination of correlations between Cr(VI) concentrations and specific conductance data from the 100-BC OU during a period when higher frequency sampling was performed suggests that aquifer tube and hyporheic zone sampler locations are well connected to aquifer sediments and the inland Cr(VI) GW plume. These findings may or may not be more broadly applicable to other 100 Area OUs, depending on site-specific characteristics, and whether or not the P&T remedy has been implemented in a given OU.
- Plots of Cr(VI) concentrations versus distance to shoreline show that there is no consistent relationship for all 100 Area GW OUs. For the 100-BC OU, which is currently undergoing MNA, the highest Cr(VI) concentrations are observed immediately adjacent to the shoreline and concentrations diminish with distance inland away from the shoreline. For the 100-HR-D OU, aggressive nearshore P&T operations, combined with the predominant GW flow direction away from the river, have resulted in the lowest concentrations immediately adjacent to the shoreline and higher concentrations inland. Each OU exhibits different characteristics, which change in response to remediation activities.
- Trajectory analysis, using plume centroid locations computed from interpreted plume maps, shows that the net migration of some of Cr(VI) plumes has been strongly influenced by P&T operations while other plumes have exhibited more oscillatory behavior consistent with river stage fluctuations.
- Cluster analysis using time series of Cr(VI) concentration data reveals groups of wells and aquifer tubes that behave similarly owing to, for example, consistency in P&T operational parameters for groups of wells, or other variables. However, the clustering results do not show any systematic relationships between the locations of well clusters and distance to shoreline for all areas.
- Trend analysis identified wells that are exhibiting decreasing or increasing trends in Cr(VI) concentration, or no trends. Results of these analyses can potentially be used to identify areas of continuing vadose zone and PRZ sources, and in combination with the other analyses to inform monitoring and remediation decisions.
- Cumulative probabilities for Cr(VI) concentrations measured in GW monitoring wells and aquifer tubes for all 100 Area GW OUs were computed. Results for 2019 indicate that the GW CUL of 48 µg/L for Cr(VI) was met for the majority of GW monitoring wells and aquifer tubes in the 100 Areas. The more stringent SW CUL of 10 µg/L for Cr(VI) has not yet been attained for most wells and aquifer tubes.

The analyses performed for this study did not identify consistent relationships between inland GW Cr(VI) concentrations and shoreline concentrations within the 100 Areas. Several ongoing remediation activities (e.g., P&T at the 100-D, 100-H, and 100-K Areas, soil flushing at 100-K) significantly impact flow direction and concentrations, which confounds the use of the available data to quantify consistent attenuation relationships between inland GW monitoring wells and the river. Seasonal and diurnal changes in river stage, and continuing sources of Cr(VI) contamination in the vadose zone and PRZ, further complicate the ability to identify individual contributions to concentration changes. Hence, monitoring to assess compliance with target CULs will need to be determined for each area individually, as is the current practice, since several factors influence Cr(VI) concentrations in the 100 Areas.

Increasing the number of aquifer tubes and hyporheic zone samplers and their sampling frequency would potentially enable more definitive conclusions to be reached. This action is recommended for the 100-HR-H Area in particular since aquifer tube sampling at this site is minimal and the predominant GW flow direction is such that the Cr(VI) plume is migrating toward the river. The current P&T remedy appears to be effective in this area, but better understanding of hyporheic zone exchange processes, and interactions between the unconfined aquifer and underlying RUM aquifer systems in this area, might be obtained with increased monitoring.

5.0 Quality Assurance

This work was performed in accordance with the Pacific Northwest National Laboratory Nuclear Quality Assurance Program (NQAP). The NQAP complies with the DOE Order 414.1D, *Quality Assurance*. The NQAP uses NQA-1-2012, *Quality Assurance Requirements for Nuclear Facility Application* as its consensus standard and NQA-1-2012 Subpart 4.2.1 as the basis for its graded approach to quality.

6.0 References

ASME NQA-1-2012. *Quality Assurance Requirements for Nuclear Facility Applications*. The American Society of Mechanical Engineers, New York, New York.

Berndt, DJ and J Clifford, 1994. *Using Dynamic Time Warping to Find Patterns in Time Series*, AAAI-94 Workshop on Knowledge Discovery in Databases, pp. 359-370.

BHI. 2000. *Cleanup Verification Package for the 100-D-12 Sodium Dichromate Pump Station*. CVP-2000-00016, Rev. 0, Bechtel Hanford, Inc., Richland, Washington.

CH2M. 2013. Systematic Method for Evaluating the Length of the Hanford Reach of the Columbia River Shoreline that is Protected from Further Discharges of Chromium for the 100 Area Operable Units. SGW-54209, Rev 0. CH2M Hill Plateau Remediation Company, Richland, Washington.

CH2M. 2014. *Evaluation of Potential Hydraulic Capture and Plume Recovery from the Ringold Upper Mud (RUM) in the 100-HR-3 Operable Unit (OU)*, ECF-100HR3-12-0025, Rev. 3, CH2M Hill Plateau Remediation Company, Richland, Washington.

CH2M. 2015a. *Persistent Source Investigation at 100-D Area*. SGW-58416, Rev. 1, CH2M Hill Plateau Remediation Company, Richland, Washington.

CH2M. 2015b. *100-BC-5 Remedial Investigation 2014 Status Report*. SGW-58308, Rev. 0. CH2M Hill Plateau Remediation Company, Richland, Washington.

CH2M. 2016. *Model Package Report: 100-BC Scale-Appropriate Fate and Transport Model Version 1.0*, SGW-59365, Rev. 0, CH2M, Richland, Washington. Available at <https://pdw.hanford.gov/document/0073923H>

CH2M. 2018a. *Water-Level Monitoring Plan for the Hanford Site Soil and Groundwater Remediation Project*. SGW-38815, Rev. 1, CH2M Hill Plateau Remediation Company. Richland, Washington. Available at <https://pdw.hanford.gov/document/0066065H>.

CH2M. 2018b. *KW Rebound Study Summary Report and Assessment*. SGW-62061, Rev. 0, CH2M Hill Plateau Remediation Company. Richland, Washington.

CH2M 2018c. *Model Package Report: 100-N Scale-Appropriate Fate and Transport Model Version 8.2*. CP-59563, Rev. 0, CH2MHILL Plateau Remediation Company. Richland, Washington.

CH2M. 2019. Description of Groundwater Calculations and Assessments for Calendar Year 2018 (CY2018) 100 Areas Pump and Treat Report. ECF-HANFORD-19-0011, Rev. 0, CH2M Hill Plateau Remediation Company, Richland, Washington.

Davis, JA and JO Leckie. 1980. Surface ionization and complexation at the oxide/water interface. 3. Adsorption of anions. *J. Colloid Interface Sci.* 74, 32-43.

DOE Order 414.1D. 2011. *Quality Assurance*. U.S. Department of Energy, Washington, D.C. Approved 4/25/2011.

DOE/RL-2017-67, Rev. 0. 2018. *Calendar Year 2017 Annual Summary Report for the 100-HR-3 and 100-KR-4 Pump and Treat Operations, and 100-NR-2 Groundwater Remediation*. CH2M Hill Plateau Remediation Company, Richland, Washington.

DOE-RL. 2011. *Hanford Site Groundwater Monitoring Report for 2010*. DOE/RL-2011-01, U.S. Department of Energy, Richland Operations Office, Richland, Washington.

DOE-RL. 2015. *Hanford Site Environmental Report for Calendar Year 2014*, DOE/RL-2014-52, Rev 0, U.S. Department of Energy, Richland Operations Office, Richland, Washington. Available at <https://msa.hanford.gov/files.cfm/DOE-RL-2014-52.pdf>.

DOE-RL. 2018. KW Soil Flushing/Infiltration Treatability Test Plan. DOE/RL-2017-30, Rev 0. U.S. Department of Energy, Richland Operations Office, Richland, Washington.

DOE-RL. 2019a. *Hanford Site Groundwater Monitoring Report for 2018*, DOE/RL-2018-66, U.S. Department of Energy, Richland Operations Office. Richland, Washington.

DOE-RL. 2019b. *Remedial Investigation/Feasibility Study for the 100-BC-1, 100-BC-2, and 100-BC-5 OUs*. DOE/RL-2010-96, Rev. 0, US Department of Energy, Richland Operations Office, Richland, Washington.

DOE-RL-2019-33, Rev. 0. *Hanford Annual Site Environmental Report for Calendar Year 2018*, US Department of Energy, Richland Operations Office. Richland, Washington. https://msa.hanford.gov/files.cfm/DOE-RL-2019-33_Rev0_public.pdf.

Domenico and Schwartz 1998. *Physical and Chemical Hydrogeology*. John Wiley and Sons, New York.

Dresel PE, NP Qafoku, JP McKinley, JS Fruchter, CC Ainsworth, C Liu, E Ilton, and JL Phillips. 2008. "Geochemical characterization of chromate contamination in the 100 Area vadose zone at the Hanford site." PNNL-17674, Pacific Northwest National Laboratory, Richland Washington.

ECF-HANFORD-19-0011, Rev. 0, 2019. *Description of Groundwater Calculations and Assessments for the Calendar Year 2018 (CY2018) 100 Areas Pump-and-Treat Report*. CH2M Hill Plateau Remediation Company, Richland, Washington.

EPA, Ecology, and DOE. 2018. Record of Decision Hanford 100 Area Superfund Site 100-DR-1, 100-DR-2, 100-HR-1, 100-HR-2, 100-HR-3 Operable Units, U.S. Environmental Protection Agency, Washington State Department of Ecology, and U.S. Department of Energy, Olympia, Washington. Online at <https://pdw.hanford.gov/arp/arpir/pdf.cfm?assession=0065047H>.

Foster, R. F. 1957. "Recommended limit on addition of dichromate to the Columbia River ". HW-49713, General Electric Company, Richland, Washington.

Fruchter JS, JE Amonette, CR Cole, YA Gorby, MD Humphrey, JD Istok, FA Spane, JE Szecsody, SS Teel, VR Vermeul, MD Williams, and SB Yabusaki. 1996. *In Situ Redox Manipulation Field Injection Test Report – Hanford 100-H Area*. PNNL-11372, Pacific Northwest National Laboratory, Richland, Washington.

Fruchter JS, CR Cole, MD Williams, VR Vermeul, JE Amonette, JE Szecsody, JD Istok, and MD Humphrey. 2000. "Creation of a subsurface permeable treatment zone for aqueous chromate contamination using in situ redox manipulation." *Groundwater Monitoring and Remediation* 66-77.

- Griffin, RA, AK Au, and RR Frost. 1977. "Effect of pH on Adsorption of Chromium from Landfill-Leachate by Clay Minerals." *Journal of Environmental Science Health*, 12:431-449.
- Hartman MJ. 2018. *Preparation of the March 2018 Hanford Site Water Table and Potentiometric Surface Maps*. ECF-HANFORD-18-0048 Rev. 0, CH2M Hill Plateau Remediation Company. Richland, Washington. Available at <https://pdw.hanford.gov/document/0064115H>
- Keogh E and CA Ratanamahatana. 2005. "Exact indexing of dynamic time warping." *Knowledge and Information Systems* 7:358-386. doi: 10.1007/s10115-004-0154-9
- Khaleel R and BA Williams. 2011. *Geohydrologic Data Package in Support of 100-BC-5 Modeling*. SGW-44022, Rev 1, CH2M, Richland, Washington.
- Last GV, GW Gee, EJ Freeman, WE Nichols, KJ Cantrell, BN Bjornstad, MJ Fayer, and DG Horton. 2006. *Vadose Zone Hydrogeology Data Package for Hanford Assessments*, PNNL-14702 Rev. 1, Pacific Northwest National Laboratory. Richland, Washington.
- Leckie, JO, MM Benjamin, K Hayes, G Kaufman, and S Altmann. 1980. *Adsorption/Coprecipitation of Trace Elements from Water with Iron Oxyhydroxide*. CS-1513, Electric Power Research Institute, Palo Alto, California.
- CH2M 2016. *Conceptual Framework and Numerical Implementation of 100 Areas Groundwater Flow and Transport Model*, SGW-46279, Revision 3, CH2M, Richland, Washington.
- NQAP-2012. *Nuclear Quality Assurance Program (NQAP) Manual*. Pacific Northwest National Laboratory, Richland, Washington.
- Peterson RE, Raidl RF, and Denslow CW. 1996. *Conceptual Site Models for Groundwater Contamination at 100-BC-5, 100-KR-4, 100-HR-3, and 100-FR-3 Operable Units*. BHI-00917 Rev. 0, Bechtel Hanford Inc., Richland, Washington.
- Peterson RE and MP Connelly. 2001. *Zone of Interaction between Hanford Site Groundwater and Adjacent Columbia River*. PNNL-13674, Pacific Northwest National Laboratory, Richland, Washington. Available at https://www.pnnl.gov/main/publications/external/technical_reports/pnnl-13674.pdf.
- Qafoku N., C.C. Ainsworth, J.E. Szecsody, O. Qafoku, and S.M. Heald. 2003. "Effect of Coupled Dissolution and Redox Reactions on Cr(VI)(aq) Attenuation during Transport in the Sediments under Hyperalkaline Conditions." *Environmental Science & Technology* 37, no. 16:3640-3646.
- Qafoku N., P.E. Dresel, J.P. McKinley, C. Liu, S.M. Heald, C.C. Ainsworth, and J.L. Phillips, et al. 2009. "Pathways of aqueous Cr(VI) attenuation in a slightly alkaline oxic subsurface." *Environmental Science & Technology* 43, no. 4:1071-1077.
- Qafoku N., P.E. Dresel, E.S. Ilton, J.P. McKinley, and C.T. Resch. 2010. "Chromium transport in an acidic waste contaminated subsurface medium: The role of reduction." *Chemosphere* 81, no. 11:1492-1500. doi:10.1016/j.chemosphere.2010.08.043
- Qafoku N., P.E. Dresel, J.P. McKinley, E.S. Ilton, W. Um, C.T. Resch, and R.K. Kukkadapu, et al. 2011. *Geochemical Characterization of Chromate Contamination in the 100 Area Vadose Zone at the Hanford Site - Part 2*. PNNL-17865. Pacific Northwest National Laboratory, Richland, Washington.

- Richmond M, W Perkins, and Y Chien. 2000. *Numerical Model Analysis of System-Wide Dissolved Gas Abatement Alternatives*. Prepared for the U.S. Army Corps of Engineers, Walla Walla District under Contract DACW68-96-D-0002, Battelle Pacific Northwest Division, Richland, Washington.
- Schroeder GC 1966. Discharge of Sodium Dichromate Solution. Compliance with executive order 11258. Douglas United Nuclear Inc., Richland, Washington.
- Shuai P, X Chen, X Song, GE Hammond, J Zachara, P Royer, H Ren, WA Perkins, MC Richmond, and M Huang. 2019. "Dam Operations and Subsurface Hydrogeology Control Dynamics of Hydrologic Exchange Flows in a Regulated River Reach." *Water Resources Research* 55(4):2593-2612. doi:10.1029/2018wr024193.
- Song X, X Chen, JM Zachara, JD Gomez-Velez, P Shuai, H Ren, and GE Hammond. 2020. River dynamics control transit time distributions and biogeochemical reactions in a dam-regulated river corridor. *Water Resour. Res.* 56, e2019WR026470. <https://doi.org/10.1029/2019WR026470>.
- Szecsody, J. E., Truex, M. J., Qafoku, N. P., McKinley, J. P., Ivarson, K. A., and Di Pietro, S. (2019). Persistence of chromate in vadose zone and aquifer sediments in Hanford, Washington. *Science of the Total Environment* 676, 482-492.
- Vermeul VR, MD Williams, JE Szecsody, JS Fruchter, CR Cole, and JE Amonette. 2002 "Creation of a Subsurface Permeable Reactive Barrier using In Situ Redox Manipulation." Ch. 6 in *Handbook of Groundwater Remediation using Permeable Reactive Barriers*, Elsevier Science, USA.
- Vignati DAL, J Dominik, ML Beye, M Pettine, BJD Ferrari. 2010. Chromium(VI) is more toxic than chromium(III) to freshwater algae: A paradigm to revise? *Ecotoxicology and Environmental Safety*. 73(5):743-749.
- WAC 173-201A-240, "Water Quality Standards for Surface Waters of the State of Washington," Washington Administrative Code.
- Waichler SR, WA Perkins, and MC Richmond. 2005. *Hydrodynamic Simulation of the Columbia River, Hanford Reach, 1940–2004*, PNNL-15226, Pacific Northwest National Laboratory. Richland, Washington.
- WCH. 2012a. *Remaining Sites Verification Package for the 100-D-56:2, South Portion of the Sodium Dichromate Underground Supply Lines*, WSRF-2009-16, Rev. 1, Washington Closure Hanford, Richland Washington.
- WCH. 2012b. *Remaining Sites Verification Package for the 100-D-56:1, North Portion of the Sodium Dichromate Underground Supply Lines*, WSRF-2008-44, Rev. 0, Washington Closure Hanford, Richland, Washington.
- WCH. 2015a. *Remaining Sites Verification Package for the 100-D-30, Sodium Dichromate Soil Contaminant Waste Site and the 100-D-104*, WSRF-2009-049, Rev. 0, Washington Closure Hanford, Richland, Washington.
- WCH. 2015b. *Unplanned Release Near 185-D Sodium Dichromate Storage Tank and Acid Neutralization French Drain Waste Site*, WSRF-2014-119, Rev. 0, Washington Closure Hanford, Richland, Washington.

Whipple JC. 1953. Design Planning of a Dichromate System for the 100-K Areas. HW-26913, Richland, Washington.

Zachara, J. M., Ainsworth, C. C., Cowan, C. E., and Resch, C. T. (1989). Adsorption of chromate by subsurface soil horizons. *Soil Sci. Soc. Am. J.* 53, 418-428.

Zachara J.M., X. Chen, X. Song, P. Shuai, C.J. Murray, and C.T. Resch. 2020. "Kilometer-scale hydrologic exchange flows in a gravel bed river corridor and their implications to solute migration." *Water Resources Research* 56, no. 2: Article No. e2019WR025258. doi:10.1029/2019WR025258.

Appendix A

A.1 Mann-Kendall Trend Analysis

The Mann-Kendall (M-K) test is a simple, non-parametric statistical test for trends in a data set. The non-parametric nature of the M-K test allows for fewer dependencies relative to other standard parametric statistical test, which allows it to be used with data sets that have missing data, irregular sampling periods, or deviations from normal distributions. Hexavalent chromium data sampling in the Hanford 100 Areas does not occur at regular intervals and occurs at different times for different sites. The data also tend to not be normally distributed. Therefore, the M-K test was considered to be appropriate and was applied to evaluate trends in the data.

The M-K tests were performed using the “trend” package in the R programming language (<https://cran.r-project.org/web/packages/trend/index.html>; last accessed 22-Aug-2020). One limitation of the M-K test is that seasonal effects should not be present in the data. Given that the Columbia River has seasonal effects (low and high river stages), the data was separated into low river stage (LRS) and high river stage (HRS) groups (LRS August 1 to December 31). A minimum of 10 samples is required, so sites with fewer than 10 measurements were excluded from analysis. The date range for which samples were analyzed is January 2010 to February 2020.

Data preparation for the M-T test requires ordering by time values. Mann-Kendall S, z and p-values are statistical parameters that are calculated according to the following equations:

$$S = \sum_{i=1}^{n-1} \sum_{j=i+1}^n \text{sign}(x_j - x_i) \quad (\text{A.1})$$

$$\text{var} = \frac{1}{18} \left[n(n-1)(2n+5) - \sum_t f_t(f_t-1)(2f_t+5) \right] \quad (\text{A.2})$$

n : number of data points
 f_t : frequency that rank appears

$$se = \sqrt{\text{var}} \quad (\text{A.3})$$

$$z = \begin{cases} \frac{(S-1)}{se}, & S > 0 \\ 0, & S = 0 \\ \frac{(S+1)}{se}, & S < 0 \end{cases} \quad (\text{A.4})$$

Positive and negative “S” values indicate increasing and decreasing trends, respectively, and p-values larger than the selected 0.05 value are considered to have no significant trend. Results for the LRS and HRS groups are shown in Table A.1 and Table A.2, respectively.

Table A.1. Mann-Kendall Trend Analysis Results For 100 Area Wells and Aquifer Tubes at LRS

Sampling Site	n	Minimum Value	Maximum Value	Mann-Kendall Statistic (S)	Normal Statistic (Z)	p-value	Trend
199-B4-14	18	0.0059	0.0408	-104	-3.904	0.000	Decreasing
199-D5-104	13	0.0335	0.469	-68	-4.103	0.000	Decreasing
199-D5-123	11	0.0042	0.307	-42	-3.202	0.001	Decreasing
199-D5-125	13	0.0103	2.04	-68	-4.124	0.000	Decreasing
199-D5-145	14	0.0121	0.15	-45	-2.409	0.016	Decreasing
199-D5-146	12	0.00767	0.065	-31	-2.075	0.038	Decreasing
199-D5-34	21	0.0267	0.57	-150	-4.503	0.000	Decreasing
199-D5-39	12	0.00373	0.112	-55	-3.712	0.000	Decreasing
199-D8-102	11	0.0215	0.046	-38	-2.907	0.004	Decreasing
199-H3-2C	13	0.024	0.079	-65	-3.912	0.000	Decreasing
199-H3-9	14	0.0272	0.11	-87	-4.708	0.000	Decreasing
199-H4-12A	11	0.0015	0.0225	-30	-2.283	0.022	Decreasing
199-H4-12C	15	0.0022	0.14	-67	-3.285	0.001	Decreasing
199-H4-75	11	0.00811	0.063	-51	-3.892	0.000	Decreasing
199-K-166	31	0.0026	39.7	-207	-3.501	0.000	Decreasing
199-K-173	21	0.0015	0.966	-67	-1.996	0.046	Decreasing
199-K-224	47	0.0039	14.4	-479	-4.388	0.000	Decreasing
199-K-235	70	0.0013	9.6	-722	-3.675	0.000	Decreasing
699-97-61	11	0.063	0.16	-33	-2.506	0.012	Decreasing
C7641	13	0.0013	0.0037	-45	-3.114	0.002	Decreasing
C7643	15	0.00148	0.002	-62	-3.439	0.001	Decreasing
C8841	12	0.0013	0.008	-39	-2.667	0.008	Decreasing
C8847	67	0.011	12.6	-512	-2.786	0.005	Decreasing
C9442	11	0.0036	0.024	-28	-2.108	0.035	Decreasing
199-B2-16	14	0.002	0.031	45	2.416	0.016	Increasing
199-B5-11	17	0.002	0.045	52	2.101	0.036	Increasing
199-B5-13	23	0.002	0.017	79	2.193	0.028	Increasing
199-K-106A	12	0.0015	0.012	34	2.274	0.023	Increasing
199-K-111A	17	0.05	0.44	57	2.317	0.021	Increasing
199-K-189	11	0.0017	0.00896	33	2.491	0.013	Increasing
199-K-205	107	0.021	44.7	854	2.296	0.022	Increasing
199-K-236	71	0.0015	16.1	856	4.244	0.000	Increasing
199-K-31	12	0.0054	0.00895	39	2.612	0.009	Increasing
199-K-36	11	0.018	0.27	37	2.803	0.005	Increasing
C6237	11	0.0031	0.00541	33	2.506	0.012	Increasing
C8852	40	0.002	0.019	243	2.941	0.003	Increasing
C8855	55	0.014	21.6	333	2.422	0.015	Increasing

Sampling Site	n	Minimum Value	Maximum Value	Mann-Kendall Statistic (S)	Normal Statistic (Z)	p-value	Trend
199-B3-47	16	0.049	0.0632	-15	-0.633	0.527	No Trend
199-B4-18	19	0.002	0.0445	-23	-0.778	0.437	No Trend
199-B5-14	17	0.002	0.008	27	1.207	0.228	No Trend
199-B5-6	16	0.028	0.037	-35	-1.532	0.125	No Trend
199-B5-9	19	0.002	0.0398	54	1.875	0.061	No Trend
199-D4-14	12	0.0086	0.0193	-25	-1.660	0.097	No Trend
199-D5-103	21	0.0222	0.73	26	0.756	0.450	No Trend
199-D5-14	12	0.0051	0.0966	-26	-1.714	0.086	No Trend
199-D5-155	27	0.0114	0.242	19	0.376	0.707	No Trend
199-D5-156	27	0.0165	1.65	-12	-0.229	0.819	No Trend
199-D5-157	25	0.008	1.12	39	0.888	0.375	No Trend
199-D5-158	26	0.0159	0.059	-28	-0.598	0.550	No Trend
199-D5-160	12	0.069	0.36	26	1.722	0.085	No Trend
199-D8-53	11	0.0015	0.0157	-23	-1.713	0.087	No Trend
199-D8-68	11	0.0082	0.021	-19	-1.422	0.155	No Trend
199-H3-4	11	0.0054	0.0649	-4	-0.234	0.815	No Trend
199-H4-63	11	0.0049	0.015	1	0.000	1.000	No Trend
199-H4-84	16	0.002	0.083	17	0.721	0.471	No Trend
199-H4-88	13	0.0023	0.02	1	0.000	1.000	No Trend
199-K-107A	17	0.0059	0.0148	-30	-1.199	0.230	No Trend
199-K-108A	14	0.002	0.007	29	1.573	0.116	No Trend
199-K-132	22	0.011	0.0219	8	0.199	0.842	No Trend
199-K-137	19	0.014	0.104	37	1.268	0.205	No Trend
199-K-138	12	0.00487	0.0211	-20	-1.303	0.193	No Trend
199-K-139	12	0.0063	0.0383	21	1.375	0.169	No Trend
199-K-140	11	0.007	0.0387	-8	-0.551	0.582	No Trend
199-K-165	24	0.0046	0.356	-3	-0.050	0.960	No Trend
199-K-168	14	0.0083	0.0751	-9	-0.439	0.660	No Trend
199-K-184	11	0.002	0.0103	23	1.713	0.087	No Trend
199-K-185	11	0.0041	0.0256	-13	-0.934	0.350	No Trend
199-K-19	11	0.0021	0.0078	-10	-0.703	0.482	No Trend
199-K-190	11	0.0037	0.0096	-22	-1.640	0.101	No Trend
199-K-192	26	0.002	0.0708	-83	-1.809	0.070	No Trend
199-K-200	16	0.00142	0.00629	-32	-1.402	0.161	No Trend
199-K-201	14	0.0025	0.083	-16	-0.822	0.411	No Trend
199-K-204	13	0.0015	0.00783	-6	-0.306	0.759	No Trend
199-K-207	16	0.0023	0.325	-8	-0.316	0.752	No Trend
199-K-223	45	0.00213	4.8	-122	-1.184	0.236	No Trend

Sampling Site	n	Minimum Value	Maximum Value	Mann-Kendall Statistic (S)	Normal Statistic (Z)	p-value	Trend
199-K-34	16	0.0058	0.011	-24	-1.038	0.299	No Trend
199-N-71	11	0.002	0.0346	4	0.234	0.815	No Trend
AT-K-1-D	12	0.0013	0.008	0	0.000	1.000	No Trend
C6238	11	0.0024	0.0055	16	1.171	0.241	No Trend
C7642	12	0.0015	0.0038	-17	-1.207	0.227	No Trend
C8842	12	0.0023	0.008	-11	-0.687	0.492	No Trend
C8843	72	0.0026	0.017	-331	-1.640	0.101	No Trend
C8844	51	0.0077	0.031	145	1.175	0.240	No Trend
C8848	54	0.017	0.033	-231	-1.722	0.085	No Trend
C8851	47	0.019	19.5	-193	-1.768	0.077	No Trend
C8853	12	0.0115	0.023	-27	-1.787	0.074	No Trend
C8856	63	0.0047	0.021	51	0.297	0.766	No Trend
C8860	13	0.008	0.0337	-20	-1.164	0.245	No Trend
C8861	13	0.015	0.049	28	1.653	0.098	No Trend

Table A.2. Mann-Kendall Trend Analysis Results for 100 Area Wells and Aquifer Tubes at HRS

Sampling Site	n	Minimum Value	Maximum Value	Mann-Kendall Statistic (S)	Normal Statistic (Z)	p-value	Trend
199-B4-14	20	0.0069	0.0366	-78	-2.4982	0.0125	Decreasing
199-D4-15	23	0.00194	0.835	-187	-4.9158	0.0000	Decreasing
199-D4-95	18	0.012	0.169	-64	-2.3995	0.0164	Decreasing
199-D4-96	17	0.0104	0.503	-72	-2.9363	0.0033	Decreasing
199-D4-97	16	0.00602	0.438	-74	-3.2933	0.0010	Decreasing
199-D5-101	17	0.00561	0.156	-113	-4.6175	0.0000	Decreasing
199-D5-102	12	0.0639	0.435	-61	-4.1241	0.0000	Decreasing
199-D5-104	29	0.0337	8.91	-370	-6.9274	0.0000	Decreasing
199-D5-106	13	0.0092	0.0391	-46	-2.7454	0.0060	Decreasing
199-D5-122	16	19.4	63.2	-84	-3.7369	0.0002	Decreasing
199-D5-123	18	0.0088	0.489	-137	-5.1514	0.0000	Decreasing
199-D5-125	18	0.026	2.31	-112	-4.2074	0.0000	Decreasing
199-D5-127	16	0.0037	0.312	-92	-4.1054	0.0000	Decreasing
199-D5-130	13	0.0118	0.236	-76	-4.5757	0.0000	Decreasing
199-D5-131	17	0.0138	1.79	-128	-5.2404	0.0000	Decreasing
199-D5-14	11	0.0098	1.1	-53	-4.0482	0.0001	Decreasing
199-D5-145	27	0.019	0.191	-166	-3.4405	0.0006	Decreasing
199-D5-146	16	0.00714	0.0697	-71	-3.1548	0.0016	Decreasing
199-D5-154	11	0.0178	0.0687	-51	-3.9163	0.0001	Decreasing

Sampling Site	n	Minimum Value	Maximum Value	Mann-Kendall Statistic (S)	Normal Statistic (Z)	p-value	Trend
199-D5-159	11	0.0207	0.0977	-47	-3.6030	0.0003	Decreasing
199-D5-37	11	0.002	0.0485	-37	-2.8026	0.0051	Decreasing
199-D5-39	18	0.00681	5.79	-140	-5.2688	0.0000	Decreasing
199-D5-43	15	0.0039	0.532	-77	-3.7610	0.0002	Decreasing
199-D5-97	19	0.0023	0.475	-143	-4.9822	0.0000	Decreasing
199-D5-99	11	0.465	9.22	-37	-2.8026	0.0051	Decreasing
199-D7-3	15	0.0025	0.0769	-93	-4.5528	0.0000	Decreasing
199-D8-4	18	0.00599	0.264	-122	-4.5865	0.0000	Decreasing
199-D8-69	12	0.0018	0.0645	-30	-1.9886	0.0467	Decreasing
199-D8-71	11	0.015	0.13	-48	-3.6701	0.0002	Decreasing
199-D8-73	12	0.0022	0.26	-44	-2.9486	0.0032	Decreasing
199-D8-88	16	0.0016	0.271	-88	-3.9356	0.0001	Decreasing
199-D8-89	19	0.0036	0.12	-121	-4.2034	0.0000	Decreasing
199-D8-90	14	0.0038	0.0409	-77	-4.1606	0.0000	Decreasing
199-D8-91	14	0.0057	0.038	-64	-3.4541	0.0006	Decreasing
199-D8-95	21	0.0216	0.784	-195	-5.8609	0.0000	Decreasing
199-D8-96	17	0.022	1.45	-122	-4.9843	0.0000	Decreasing
199-D8-97	16	0.0185	0.569	-117	-5.2386	0.0000	Decreasing
199-D8-98	16	0.011	0.142	-78	-3.4667	0.0005	Decreasing
199-H1-1	13	0.0088	0.0392	-48	-2.8674	0.0041	Decreasing
199-H1-2	13	0.027	0.047	-44	-2.6332	0.0085	Decreasing
199-H1-36	12	0.0189	0.051	-57	-3.8491	0.0001	Decreasing
199-H3-2C	17	0.0258	0.0635	-104	-4.2818	0.0000	Decreasing
199-H3-4	14	0.0056	0.0626	-42	-2.2479	0.0246	Decreasing
199-H3-9	12	0.0037	0.111	-40	-2.6743	0.0075	Decreasing
199-H4-12C	15	0.0581	0.13	-55	-2.6877	0.0072	Decreasing
199-H4-15A	12	0.0015	0.0168	-40	-2.7305	0.0063	Decreasing
199-H4-75	12	0.0189	0.0549	-58	-3.9271	0.0001	Decreasing
199-H4-80	11	0.013	0.023	-47	-3.6328	0.0003	Decreasing
199-H4-92	14	0.0038	0.0265	-82	-4.4410	0.0000	Decreasing
199-H4-93	14	0.0053	0.0605	-84	-4.5507	0.0000	Decreasing
199-K-117A	11	0.0015	0.0101	-40	-3.2425	0.0012	Decreasing
199-K-141	12	0.019	0.0463	-50	-3.3975	0.0007	Decreasing
199-K-168	15	0.00851	0.095	-94	-4.6080	0.0000	Decreasing
199-K-173	43	0.0015	0.965	-493	-5.1496	0.0000	Decreasing
199-K-18	13	0.0023	0.203	-74	-4.4703	0.0000	Decreasing
199-K-20	12	0.0013	0.003	-32	-2.2649	0.0235	Decreasing
199-K-235	58	0.0013	0.0141	-1132	-7.5984	0.0000	Decreasing

Sampling Site	n	Minimum Value	Maximum Value	Mann-Kendall Statistic (S)	Normal Statistic (Z)	p-value	Trend
199-K-236	64	0.00663	1.61	-1057	-6.1182	0.0000	Decreasing
C8841	15	0.0015	0.008	-44	-2.3647	0.0180	Decreasing
199-B8-9	20	0.002	0.0243	84	2.6929	0.0071	Increasing
199-D5-121	15	0.0264	0.106	93	4.5528	0.0000	Increasing
199-D5-149	12	0.001	0.022	31	2.0718	0.0383	Increasing
199-F5-4	11	0.0047	0.036	33	2.4912	0.0127	Increasing
199-H4-69	11	0.0018	0.014	41	3.1140	0.0018	Increasing
199-H4-70	11	0.0015	0.013	38	2.9130	0.0036	Increasing
199-K-111A	11	0.0316	0.368	35	2.6631	0.0077	Increasing
199-K-185	28	0.0015	0.0094	154	3.5438	0.0004	Increasing
199-K-186	12	0.002	0.03	30	2.0714	0.0383	Increasing
199-K-187	22	0.002	0.0301	75	2.3531	0.0186	Increasing
199-K-188	12	0.002	0.0416	34	2.2736	0.0230	Increasing
C8845	11	0.002	0.0181	45	3.4749	0.0005	Increasing
C8849	11	0.002	0.025	36	2.7555	0.0059	Increasing
C8853	11	0.0036	0.0206	33	2.5272	0.0115	Increasing
C8855	18	0.002	0.0259	75	2.8070	0.0050	Increasing
199-B3-47	12	0.0055	0.063	3	0.1375	0.8907	No Trend
199-B4-16	12	0.002	0.0186	23	1.5441	0.1226	No Trend
199-B5-11	16	0.002	0.0422	-14	-0.5853	0.5584	No Trend
199-B5-2	11	0.0143	0.055	-8	-0.5466	0.5846	No Trend
199-B5-6	15	0.002	0.041	24	1.1396	0.2545	No Trend
199-D2-11	19	0.0015	0.0088	-41	-1.4029	0.1607	No Trend
199-D4-14	14	0.002	0.142	-12	-0.6031	0.5464	No Trend
199-D4-98	15	0.0015	0.0689	-38	-1.8393	0.0659	No Trend
199-D4-99	15	0.0015	0.0094	-38	-1.8333	0.0668	No Trend
199-D5-103	46	0.0352	0.8	-18	-0.1610	0.8721	No Trend
199-D5-119	12	3.3	5.26	28	1.8515	0.0641	No Trend
199-D5-126	17	0.015	2.05	-45	-1.8140	0.0697	No Trend
199-D5-150	12	-0.004	0.196	-29	-1.9246	0.0543	No Trend
199-D5-151	19	0.001	0.16	41	1.3994	0.1617	No Trend
199-D5-152	19	0.0045	0.016	15	0.4904	0.6239	No Trend
199-D5-155	17	0.008	0.112	1	0.0000	1.0000	No Trend
199-D5-156	16	0.031	0.847	-11	-0.4507	0.6522	No Trend
199-D5-157	16	0.022	0.347	-2	-0.0450	0.9641	No Trend
199-D5-158	16	0.008	0.247	-9	-0.3615	0.7177	No Trend
199-D5-160	22	-0.005	0.263	8	0.1981	0.8429	No Trend
199-D5-32	17	0.0058	0.0737	-23	-0.9070	0.3644	No Trend

Sampling Site	n	Minimum Value	Maximum Value	Mann-Kendall Statistic (S)	Normal Statistic (Z)	p-value	Trend
199-D5-33	11	0.0015	0.0499	-4	-0.2428	0.8082	No Trend
199-D5-34	24	0.023	0.611	-48	-1.1665	0.2434	No Trend
199-D5-92	12	0.0015	0.0296	-28	-1.8515	0.0641	No Trend
199-D8-102	23	0	0.036	61	1.5894	0.1120	No Trend
199-D8-68	14	0.002	0.04	-12	-0.6031	0.5464	No Trend
199-H1-34	11	0.0019	0.0193	19	1.4013	0.1611	No Trend
199-H1-43	12	0.0015	0.0918	-23	-1.5122	0.1305	No Trend
199-H1-45	11	0.0015	0.05	-13	-0.9342	0.3502	No Trend
199-H2-1	11	0.0037	0.02	10	0.7221	0.4702	No Trend
199-H4-12A	13	0.0015	0.014	-23	-1.3670	0.1716	No Trend
199-H4-4	12	0.0015	0.0059	-23	-1.5218	0.1281	No Trend
199-H4-5	14	0.0017	0.01	-30	-1.5964	0.1104	No Trend
199-H4-63	13	0.0015	0.0173	-28	-1.6472	0.0995	No Trend
199-H4-84	27	0.0037	0.13	92	1.8991	0.0575	No Trend
199-H4-88	22	0.004	0.039	70	1.9464	0.0516	No Trend
199-H4-90	11	0.0102	0.024	2	0.0781	0.9378	No Trend
199-K-106A	13	0.002	0.00968	21	1.2286	0.2192	No Trend
199-K-107A	15	0.0069	0.0158	-26	-1.2428	0.2140	No Trend
199-K-108A	14	0.002	0.00968	6	0.2786	0.7805	No Trend
199-K-125A	12	0.0017	0.0043	2	0.0689	0.9451	No Trend
199-K-13	15	0.0013	0.00489	-23	-1.1098	0.2671	No Trend
199-K-132	21	0.014	0.0247	-53	-1.5974	0.1102	No Trend
199-K-137	26	0.013	0.232	-75	-1.6361	0.1018	No Trend
199-K-165	35	0.009	0.337	14	0.1850	0.8532	No Trend
199-K-166	18	0.0039	0.0818	-33	-1.2121	0.2255	No Trend
199-K-181	11	0.006	0.0152	5	0.3114	0.7555	No Trend
199-K-191	21	0.002	0.0353	16	0.6107	0.5414	No Trend
199-K-205	10	0.013	0.715	-23	-0.0609	0.9514	No Trend
199-K-220	5	0.0015	0.0223	-6	-0.3445	0.7305	No Trend
199-K-223	12	0	0.045	-102	-1.2225	0.2215	No Trend
199-K-224	39	-0.012	0.45	-125	-1.3947	0.1631	No Trend
199-K-230	41	0.0015	0.029	-2	-0.0802	0.9360	No Trend
199-K-34	11	0.0041	0.0354	-14	-0.4551	0.6490	No Trend
199-K-35	19	0.227	0.695	-17	-1.2456	0.2129	No Trend
699-97-43C	11	0.0015	0.00239	-11	-0.9245	0.3552	No Trend
699-97-60	13	0.0015	0.0737	-5	-0.2445	0.8069	No Trend
699-97-61	16	0.015	0.188	-1	0.0000	1.0000	No Trend

Sampling Site	n	Minimum Value	Maximum Value	Mann-Kendall Statistic (S)	Normal Statistic (Z)	p-value	Trend
699-98-51	16	0.0015	0.014	-15	-0.6437	0.5198	No Trend
C8840	14	0.0028	0.008	-2	-0.0552	0.9560	No Trend
C8842	14	0.003	0.008	5	0.2205	0.8255	No Trend
C8843	19	0.003	0.015	-45	-1.5431	0.1228	No Trend
C8844	15	0.0015	0.0182	34	1.6583	0.0973	No Trend
C8847	21	0.008	0.027	-41	-1.2125	0.2253	No Trend
C8848	18	0.0019	0.0214	-11	-0.3801	0.7039	No Trend
C8851	21	0.008	0.035	-51	-1.5105	0.1309	No Trend
C8852	17	0.0015	0.0144	-2	-0.0416	0.9668	No Trend
C8856	18	0.0015	0.0159	4	0.1143	0.9090	No Trend
C8859	11	0.002	0.0238	16	1.1713	0.2415	No Trend
C8860	13	0.0145	0.0236	7	0.3667	0.7138	No Trend
C8861	12	0.013	0.0293	3	0.1375	0.8907	No Trend

A.2 Cluster Analysis

This section describes some of the details of the agglomerative, hierarchical clustering method that was used in this study. As noted in the report, this type of clustering depends on two factors: 1) a distance metric, and 2) a linkage criterion that specifies the dissimilarity of clusters as function of distance. Dynamic time warping (DTW; Keogh and Ratanamahatana 2005; Berndt and Clifford 1994) was used for calculating the distance metrics, and the Ward method (Ward 1963) was used to define the linkage criterion. Additional details on these methods are provided below.

A.2.1 Dynamic Time Warping

The DTW method was developed to measure the difference (or so-called distance/proximity) between time series. The result of the DTW is a matrix D that contains the distance of each pair of time series of data. There are various metrics that can be used to measure the difference between two time series; for example, one of the most commonly used metrics is Euclidean distance (EU), which measures the absolute difference between two time series at corresponding times. A well-known disadvantage of the EU-like methods is that they cannot handle the phase lag between time series very well, as shown in Figure A.1 (Keogh and Ratanamahatana 2005). A better way to deal with phase lag is lagged correlation or covariance analysis, but this method still relies on the assumption that the phase lag is constant during the entire time period. To accommodate irregular phase lags, the DTW (Berndt and Clifford 1994) was developed. DTW allows an elastic shifting of the time axis, so that time series with similar trends can still be grouped to one cluster even they have irregular phase lags, as shown in Figure A.1 (Keogh and Ratanamahatana 2005).

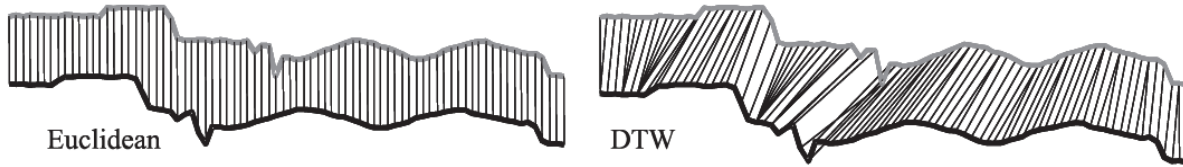


Figure A.1. Examples of Euclidean Distance and DTW (Keogh and Ratanamahatana 2005). The time series have an overall similar shape, but they are not aligned in the time axis. Euclidean distance, which assumes the i^{th} point in one sequence is aligned with the i^{th} point in the other, will produce a pessimistic dissimilarity measure. The nonlinear dynamic time warped alignment allows a more intuitive distance measure to be calculated.

DTW can also be described as follows. Suppose we have two time series, S and T, of length n and m, respectively, where

$$\begin{aligned} S &= s_1, s_2, \dots, s_i \dots s_n \\ T &= t_1, t_2, \dots, t_j \dots S_m \end{aligned} \tag{A.5}$$

The DTW method finds the best alignments between each point in S and T, so the total difference between the points in S and T can be minimized. Details are given by Keogh and Ratanamahatana (2005).

A.2.1.1 Test of DTW Algorithm

A Python script was written to calculate the DTW distance metrics. In this section, two groups of synthetic time series data were used to test the DTW algorithm. In addition to the DTW distance metrics, two other metrics were calculated, the mean absolute error (MAE) and root mean squared error (RMSE).

$$MAE = \frac{1}{n} \sum_{i=1}^n |y_m - y_n| \tag{A.6}$$

$$RMSE = \sqrt{\frac{1}{n} \sum_{i=1}^n (y_m - y_n)^2} \tag{A.7}$$

Four time series are compared in Test 1 (Figure A.2). Series #1 is a sine curve with an increasing trend. Series #2 is similar to #1 except with a time lag. Series #3 has the same trend as series #1 and #2, but no periodicity. Series #4 is a constant value with no trend or periodicity.

Table A.3 lists the computed DTW and two other distance metrics. The DTW metrics indicate that series #2 is the closest or most similar to series #1, and series #4 is the least similar to series #1. However, the MAE and RMSE metrics suggest that series #2 is the least similar to series #1. From Table A.2 it is clear that series #2 is actually the most similar to series #1, and series #4 is the least similar. This comparison shows that DTW algorithm finds the best match between these time series, and the use of other metrics may be misleading. Figure A.3 shows the pairings of data from DTW for time series #1 and #2 that result in the best alignment.

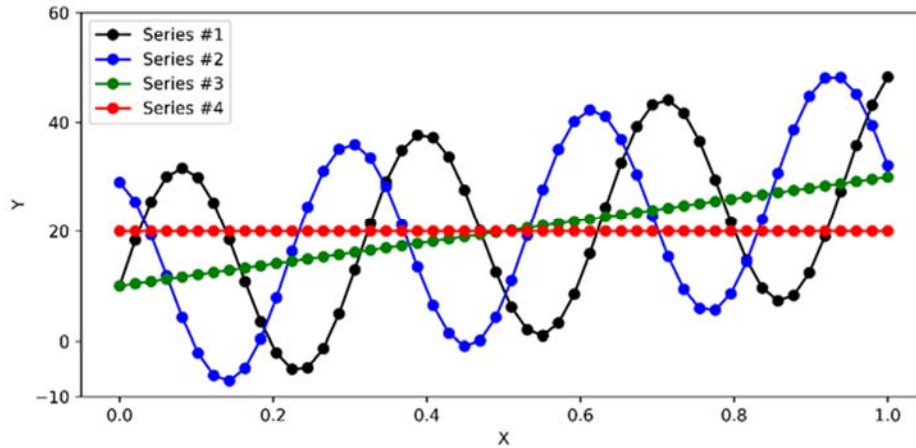


Figure A.2. Times Series Data Used for DTW Test Case 1

Table A.3. Results of DTW Test Case 1

	DTW	MAE	RMSE
#2 vs. #1	4.1	19.93	22.3
#3 vs. #1	9.7	12.53	14
#4 vs. #1	14.45	12.48	14.45

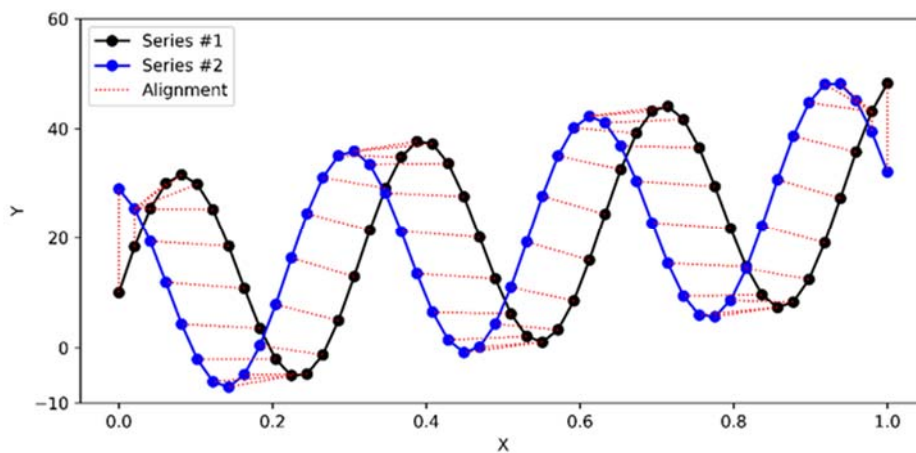


Figure A.3. Illustration of Alignments Between Series 1 and Series 2 Based on the Test 1 DTW Results

Test Case 2 was constructed by randomly sampling 30% of the data points from test case1, which mimics the irregular sampling that often occurs with field data. Table A.4 shows that the DTW method still correctly identifies the correct order of similarities between the four-time series, illustrating its superiority relative to the other two metrics.

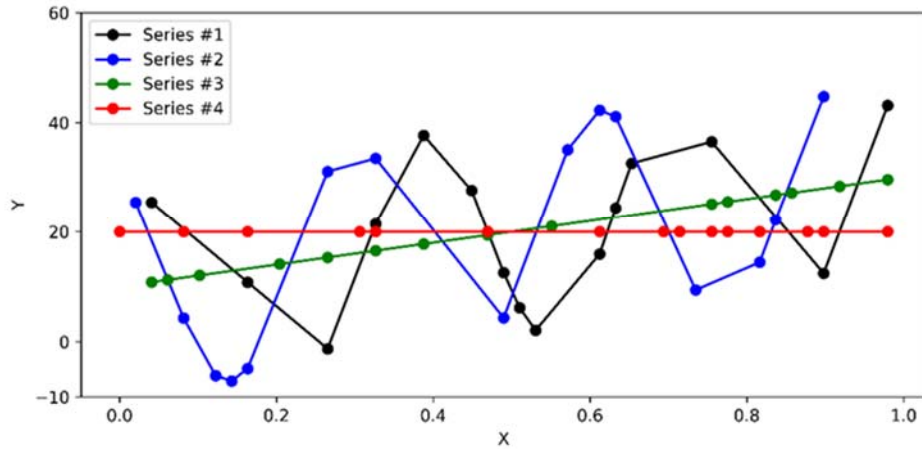


Figure A.4. Times Series Data Used for DTW Test Case 2

Table A.4. Results of DTW Test Case 2

	DTW	MAE	RMSE
#2 vs. #1	6.13	16.09	20.52
#3 vs. #1	9.57	10.76	12.31
#4 vs. #1	13.07	11.33	13.07

Figure A.5 shows the pairings of data from DTW for time series #1 and #2 that result in the best alignment for test case 2.

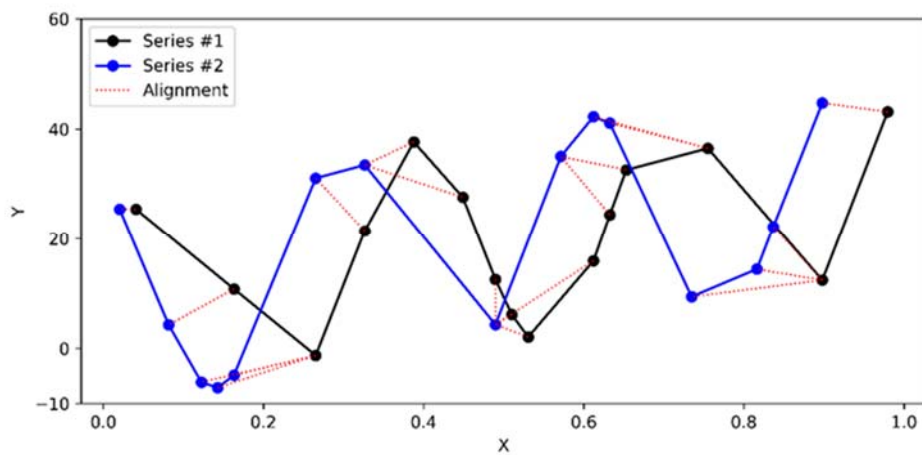


Figure A.5. Illustration of Alignments Between Series 1 and Series 2 Based on the Test 2 DTW Results

A.2.2 Ward's Minimum Variance Method

Various linkage criteria can be applied to specify the dissimilarity of sets as a function of the distance. Some of the common linkage criteria are defined below.

Single linkage: The similarity of two clusters (C_1 and C_2) is equal to the minimum of the similarity between observations O_i and O_j such that O_i belongs to C_1 and O_j belongs to C_2 . In each step, the two clusters with the smallest similarity will be merged.

Complete linkage: The similarity of two clusters (C_1 and C_2) is equal to the maximum of the similarity between observations O_i and O_j such that O_i belongs to C_1 and O_j belongs to C_2 . In each step, the two clusters with the smallest similarity will be merged.

Average linkage: Take all the pairs of points and compute their similarities and calculate the average of the similarities. In each step, the two clusters with the smallest similarity will be merged.

Centroids linkage: Compute the centroids of two clusters (C_1 and C_2) and take the similarity between the two centroids as the similarity between two clusters. In each step, the two clusters with the smallest similarity will be merged.

Ward's linkage: This approach minimizes the total within-cluster variance in each cluster level. At each step, the pair of clusters that leads to the minimum increase in total within-cluster variance will be merged.

Ward's linkage method was used in this study because it is the only one among the agglomerative clustering methods that is based on a classical sum-of-squares criterion and produces clusters that minimize within-cluster variations (Murtagh and Legendre 2014).

References

- Berndt D and J Clifford. 1994. "Using dynamic time warping to find patterns in time series." *AAAI-94 Workshop on Knowledge Discovery in Databases*. pp. 229-248.
- Keogh E and CA Ratanamahatana. 2005. "Exact indexing of dynamic time warping." *Knowledge and Information Systems* 7:358-386. doi: 10.1007/s10115-004-0154-9
- Murtagh F and P Legendre. 2014. "Ward's Hierarchical Agglomerative Clustering Method: Which Algorithms Implement Ward's Criterion?" *Classification* 31:274-295.
- Ward JH. 1963. "Hierarchical grouping to optimize an objective function." *Journal of the American Statistical Association* 58:236-244.

Pacific Northwest National Laboratory

902 Battelle Boulevard
PO Box 999
Richland, WA 99354
1-888-375-PNNL (7665)

www.pnnl.gov